Surface Plasmon Resonance Sensing of Small-Molecule Metabolites

by

Yong Cao

A thesis submitted in partial fulfillment of the requirements for the degree of

Doctor of Philosophy

Department of Chemistry
University of Alberta

Abstract

Small-molecule metabolites (MW < 1,000 Da) are now emerging as an important type of biomarkers, thanks to the rapid development of systems biology such as metabolomics. Compared to nucleic acids and protein, metabolite is closer to the phenotype. Rapid detection and quantification of metabolites can potentially provide an effective way to link the metabolite profile to disease state. A sensor based approach for the measurement of metabolites can fulfill the simplicity and portability required for widespread use. Surface plasmon resonance (SPR) combined with molecular recognition elements to deliver high specificity is a sensing platform that has been widely applied for a large range of biomolecules. However, direct detection of small molecules such as metabolites with SPR challenges the refractive-index based detection mechanism due to their low molecular weights. To this regard, sensing strategies that can tackle this challenge are highly demanded.

In this thesis, I successfully developed a series of indirect sensing strategies (competition, inhibition, displacement), some of which are using either small molecule or aptamer functionalized gold nanoparticle labels, to detect a few single metabolite targets. All the strategies have shown great analytical performance with good sensitivity and specificity. In each assay, either periplasmic binding protein, or antibody, or DNA aptamer, was served as the recognition element, which accounts for the high specificity observed. More importantly, the multiplexed detection of a panel of metabolites through a single SPR measurement was accomplished for the first time, based on the small molecule (micro)arrays patterned on our homemade SPR imaging chip. Compared to

SPR sensing of nucleic acids and proteins, the power of this technique was underestimated in metabolites sensing. I hope this thesis can provide some insights to the SPR community and inspire more work to be done in terms of small molecule sensing, thus having more impact in the fields of medical diagnostics, therapeutic drug discovery, food safety control, and environmental monitoring.

Preface

Some of the research conducted for this thesis forms part of a university research collaboration, led by Professor David S. Wishart at the University of Alberta, with Professor Mark T. McDermott being involved in the Metabolomics Devices project.

Chapter 2 of this thesis has been published as Y. Cao, B. Griffith, P. Bhomkar, D. S. Wishart, and M. T. McDermott, "Functionalized Gold Nanoparticle-Enhanced Competitive Assay for Sensitive Small-Molecule Metabolite Detection Using Surface Plasmon Resonance", *Analyst*, **2018**, 143, 289-296. I was responsible for the design of experiments and the data collection and analysis as well as the manuscript composition. B. Griffith and P. Bhomkar provided the folic acid binding protein and glutamine binding protein solutions. M. T. McDermott was the supervisory author and was involved with concept formation and manuscript composition.

Chapter 3 of this thesis has been submitted to *Analytical Biochemistry* as "A Surface Plasmon Resonance Based Inhibition Immunoassay for Sensitive and Selective Detection of Steroid Hormones". Chapter 1, Chapter 4 and Chapter 5 are being in preparation for publications. All the work contained in Chapters 1, 3, 4, and 5 are original work by Yong Cao under the supervision of Professor Mark T. McDermott.

Acknowledgements

It has been five years since my wife and I first landed in Canada on August 14, 2012. As an international student pursuing a PhD degree and part of my academic career, it is a great honor to have this great opportunity to study in such a beautiful, friendly, and a little bit cold country with support from both the government and the Chemistry department at University of Alberta. Many thanks should give to quite a few people.

First of all, I would like to thank my grandparents, Zuxin Dou and Mingyu Wang, my parents, Xiaoming Dou and Shiyi Cao, my uncles and aunts, Xiaobing Dou, Xiaolan Dou, Bo Gao, Yuanying Tan, my two little brothers, Hao Dou and Dian Gao, my beautiful wife and great parents-in-law, Dr. Zuoqiao Wu, Xiangdong Wu, Libin Ren for being always so supportive, encouraging and helpful out there! Without your support and love, this adventure would not be possible and achieved.

Secondly, special and many thanks should go to my great supervisor, Dr. Mark T. McDermott, for his kindness and patient guidance. Also, I would really appreciate the help from Dr. Rongbing Du, Dr. Lars Laurentius, Dr. Greg Kaufman, all the previous and current members of the McDermott Lab, as well as my supervisory committee members: Dr. Julianne Gibbs-Davis and Dr. Liang Li. Meanwhile, I would like to thank Dr. Gregory Kiema, Dr. Christie McDermott, Dr. Charles Lucy and Dr. Eric Flaim for sharing your great and professional teaching philosophy, because teaching is always as important as research in my mind.

Lastly but not least, I am very grateful for the help from our collaborators, the facility training and use at the National Institute for Nanotechnology as well as the nanoFAB of University of Alberta.

Table of Contents

Chapter 1 Introduction **1**

1.1 SURFACE PLASMON RESONANCE: A GENERAL INTRODUCTION AND CHRONOLOGICAL HISTORY 1

1.2 A THEORETICAL ANALYSIS OF THE CHALLENGE ASSOCIATED WITH SPR SENSING OF SMALL MOLECULES 16

1.3 STRATEGIES TO OVERCOME THE CHALLENGE 19

1.3.1 Indirect detection formats 19

1.3.2 Nanomaterials (NMs) enhanced sensing strategies 25

1.3.3 Other strategies 27

1.4 SUMMARY 28

1.5 REFERENCES 29

Chapter 2 Functionalized Gold Nanoparticle Enhanced Competitive Assay for Sensitive Detection of Metabolite Using Surface Plasmon Resonance Imaging **37**

2.1 INTRODUCTION 37

3.2 EXPERIMENTAL 39

2.3 RESULTS AND DISCUSSION 47

2.4 CONCLUSION 59

2.5 REFERENCES 60

Chapter 3 A Universal Inhibition Surface Plasmon Resonance Immunosensor for Sensitive and Selective Detection of Small-Molecule Metabolite **66**

3.1 INTRODUCTION 66

3.2 EXPERIMENTAL 68

3.3 RESULTS AND DISCUSSION 72

3.4 CONCLUSION 83

3.5 REFERENCES 84

Chapter 4 Aptamer-Gold Nanoparticle Conjugate for Small-Molecule Metabolite Analysis Using Surface Plasmon Resonance Imaging **88**

4.1 INTRODUCTION 88
4.2 EXPERIMENTAL 90
4.3 RESULTS AND DISCUSSION 94
4.4 CONCLUSION 107
4.5 REFERENCES 108

Chapter 5 Small-Molecule (Micro)Arrays for the Multiplexed Detection of Metabolites by Surface Plasmon Resonance Imaging **112**

5.1 INTRODUCTION 112
5.2 EXPERIMENTAL 114
5.3 RESULTS AND DISCUSSION 117
5.4 CONCLUSION 129
5.5 REFERENCES 129

Chapter 6 Conclusions and Future Outlook **132**

6.1 CHAPTER CONCLUSIONS 132
6.2 FUTURE OUTLOOK 135
6.3 REFERENCES 136

Bibliography/References **137**

List of Tables

Table 3.1 Curve-Fitting Parameters for E2-Ab Binding Curves Shown in Figure 3.3B 78

List of Figures

Figure 1.1 Schematic illustration of the excitation of surface plasmon polariton (SPP) by light on metal film using the attenuated total reflection (ATR) setup. The SPP is depicted in red. 2

Figure 1.2 A graphical illustration of the dispersion relations ω(k) of the incident light (k_x) and the SPPs (k_{sp}). 4

Figure 1.3 Schematic illustration of the occurrence of surface plasmon resonance (SPR) based on Kretschmann-Raether configuration. 6

Figure 1.4 A graphical illustration of the dispersion relations of the light and the SPPs based on Kretschmann-Raether configuration. The dispersion relation line of the light is shifted to the right side (red) and intersects with the dispersion line of the SPPs. 7

Figure 1.5 A typical SPR curve (light reflectivity R vs. angle of incidence θ) with a big dip occurred at the resonance angle (θ_r). 8

Figure 1.6 The shift of the SPR curve and the resonance angle to the right side due to the adsorption of molecules and an increase of the refractive index of the medium 2. 9

Figure 1.7 A representative SPR sensorgram (SPR signal vs. time) showing the association (on) and dissociation (off) of molecules to/from the metal film. The SPR signal can be angle shift, wavelength shift, or reflectivity change based on the specific SPR instrumentation. 11

Figure 1.8 The web of science searching results (a plot of # of publications vs. year) with "surface plasmon resonance" in title by May 15th, 2017. The year 1990 launched the first commercially available SPR product, the Biacore instrument. 13

Figure 1.9 The web of science searching results (a plot of # of publications vs. year) with "surface plasmon resonance and small molecule" in title by May 15th, 2017. 14

Figure 1.10 A comparison among the web of science searching results for "SPR+Protein" in title, "SPR+nucleic acid/DNA/RNA" in title, and "SPR+small molecule/metabolite) in title by May 15th, 2017. The black bars are general results, while the grey bars represent the sensing (with additional "detection/measurement/analysis") in title. 15

Figure 1.11 Schematic illustrations of 4 indirect detection formats (competition, inhibition, displacement, and sandwich) for SPR sensing of small molecules. 20

Figure 1.12 Typical SPR sensorgrams (a, c) and calibration curves (b, d) for the indirect detection formats: (a) competiton and inhibition, (b) competition, inhibition, and displacement using method 1 as signal output, (c) displacement, (d) displacement using method 2 as signal output and sandwich. 22

Figure 2.1 Schematic illustration of the folic acid (FA) functionalized gold nanoparticle (FA-AuNP) enhanced competitive assay for the detection of FA. Polyhistidine tagged folic acid binding protein (FBP) is immobilized to chip surface via Ni^{2+}-NTA coordination chemistry. FA-AuNP and FA compete for surface binding sites provided by FBP. 48

Figure 2.2 Results tracking the immobilization of polyhistidine tagged folic acid binding protein (FBP) to SPRi chip surface. (A) Typical continuous SPRi sensorgrams for FBP adsorption for different concentrations (91.5 nM, 183 nM, 366 nM, 915 nM, and 1830 nM) to NTA SAMS (red) and a BSA control surface (blue). The arrows indicate the injection of each concentration. (B) A plot of SPR signal vs. FBP solution concentration

for adsorption to NTA SAM. The symbols are the data points and the dashed line is the least-squares fit of the Langmuir adsorption isotherm equation ($R^2 = 0.9803$). 49

Figure 2.3 UV-Vis and Raman characterization of 10 nm AuNPs. (A) Extinction spectra for as-purchased 10 nm citrate capped AuNP (blue), the AuNP after modification with DTSP-AuNP (green), and FA-AuNP (red). The axes are expanded around the maximum extinction for clarity and λmax values for the three spectra are listed. (B) Raman spectra of FA in solution (100 μM in water, blue) and a solution of 9.47 nM of FA-AuNP (red, signal ×6). The scale bar is equivalent to 40,000 counts. 51

Figure 2.4 Representative difference images of three SPRi chip surfaces after exposure to 1 nM (A), 2 nM (B), and 2.5 nM (C) FA-AuNP solutions, respectively. Each chip surface was modified with FBP (five spots in the middle) and GBP (four spots at the corners) before exposure to FA-AuNP solution. 53

Figure 2.5 Binding of 10 nm FA-AuNP to FBP. (A) Typical continuous SPRi sensorgrams for the adsorption of FA-AuNPs at seven concentrations (94.7 pM – 4.74 nM) to FBP surface (red) and GBP control surface (blue). The arrows indicate the injection of each concentration. (B) A plot of SPR signal vs. FA-AuNP solution concentration for adsorption to FBP. The symbols are the data points and the dashed line is the least-squares fit of the Langmuir adsorption isotherm equation ($R^2 = 0.9648$). 54

Figure 2.6 Scanning electron micrographs of SPRi Au chip surfaces with (A, B) FBP (× 60.0 k, × 300 k) and (C) GBP (× 60.0 k) after exposure to 94.7 pM of the as-prepared 10 nm FA-AuNPs. 55

Figure 2.7 Representative sensorgrams for analysis of FA in the (A) micromolar (μM) range and (B) nanomolar (nM) range. The concentrations of 10 nm FA-AuNPs in the competitive assays are (A) 9.47 nM and (B) 189 pM. 57

Figure 2.8 Calibration curves for the determination of FA using the AuNP based competitive assay. (A) Plot of SPRi signal vs concentration of free FA for the assay where the concentration of FA-AuNPs was 4.74 nM. (B) Plot of SPRi signal vs concentration of free FA for the assay where the concentration of FA-AuNPs was 189 pM. In both plots, the symbols represent the mean of at least 3 repetitive measurements and the error bars are the standard deviation. The dashed line through the data is the linear least-squares fit. 58

Figure 3.1 Schematic illustration of the analytical principle of the indirect inhibition immunosensor for 17β-estradiol (E2) analysis using surface plasmon resonance imaging. A SH-NHS monolayer containing ethylene glycol group was first formed on the gold chip surface, then BSA-E2 conjugates were immoblized via NHS coupling. BSA-E2 conjugates and free E2 molecules in solution compete for binidng sites provided by anti-E2 monocolonal antibody. A calibration curve with negative slope can be obtained due to the inhibition mechanism. 73

Figure 3.2 Results tracking the adsorption of BSA-E2 conjugate to SH-NHS monolayer on gold chip surface. (A) A representative sensorgram for continuous adsorption of 7 BSA-E2 conjugate solutions with different concentrations. The arrows indicate the injection of each concentration. (B) A plot of SPR signal vs. BSA-E2 conjugate solution concentration for adsorption to SH-NHS monolayer. The symbols are the data points and

the dashed line is the least-squares fit of the Langmuir adsorption isotherm equation (R^2 = 0.9691). The error bars represent standard deviation of triplicate measurements. 75

Figure 3.3 Binding of E2-Ab to BSA-E2 conjugate under different surface coverage (S.C.) on gold chip surface. (A) Representative sensorgrams for the binding of 5 μg/mL E2-Ab to BSA control (blue) and BSA-E2 conjugate at three S.C.: 0.21 (red), 0.49 (green), and 0.82 (purple). (B) Plots of SPR signal vs. E2-Ab concentrations (5 μg/mL, 10 μg/mL, 25 μg/mL, 50 μg/mL, and 200 μg/mL). The symbols are the data points and the solid lines are the least-squares fits of the Langmuir isotherm adsorption equation. The error bars represent standard deviation of triplicate measurements. (C) A representative difference image of the chip after E2-Ab binding to BSA (control) and BSA-E2 conjugate with 0.21 S.C. (four spots in the middle) and 0.82 S.C. (four spots at the corners). 77

Figure 3.5 Specificity study of the inhibition immunosensor using estrone (E1) as a potential interference. Binding results for mixed solutions of E2-Ab with E2 (circle) and E1 (triangle) are shown, respectively. The symbols are the mean of at least 3 repetitive measurements and the error bars are the standard deviation. 82

Figure 4.1 Schematic illustration of the DNA aptamer-gold nanoparticle conjugate enhanced sensing strategy for dopamine (DA) analysis using SPR imaging. Amine-terminated single-stranded complementary DNA (cDNA) to DNA aptamer is immobilized on gold chip surface via polydopamine surface chemistry. In the absence and presence of DA, the conjugate is in its 'ON' and 'OFF' states respectively. 'ON' state means the conjugate can bind to the immobilized cDNA, thus generate a big SPR

signal. On the contrary, 'OFF' state means no binding will occur between the conjugate and the cDNA due to the blocking of DNA aptamer by the binding of DA. 95

Figure 4.2 UV-vis characterization of the as-prepared 10 nm dopamine aptamer-gold nanoparticle (DAAPT-AuNP) conjugate in H_2O and buffers. (A) Extinction spectra for as-purchased 10 nm citrate-AuNP in H_2O (blue) and as-prepared 10 nm DAAPT-AuNP conjugate in H_2O (red), PBS (green), and TBS (purple). (B) Amplified portion around the maximum extinction for clarity. The dashed line marks the maximum extinction of 10 nm citrate-AuNP. 97

Figure 4.3 Extinction spectra for 20 nm (A), 30 nm (B), and 40 nm (C) citrate-AuNPs in H_2O (blue) and DAAPT-AuNP conjugates in H_2O (red), PBS (green), and TBS (purple). 98

Figure 4.4 (A) SPRi sensorgrams for the adsorption of 10.5 mM PDA solution to bare gold spots surface; (B) quantitative analysis of the signal response as a function of time after PDA solution exposure. Error bars represent standard deviation for triplicate measurements. 100

Figure 4.5 Binding of 10 nm DAAPT-AuNP conjugate to cDNA probe on gold chip surface. (A) Typical SPRi sensorgrams for the binding of 10 nm DAAPT-AuNP at six concentrations: 0.095 nM (blue), 0.24 nM (red), 0.47 nM (green), 0.95 nM (purple), 2.5 nM (cyan), and 4.7 nM (orange). (B) A plot of SPR signal vs. DAAPT-AuNP solution concentration for adsorption to cDNA. The symbols are the data points and the dashed line is the least-squares fit of Langmuir adsorption isotherm equation ($R^2 = 0.9669$). The error bars represent standard deviation for triplicate measurements. 101

Figure 4.6 Detection of DA using the inhibition assay from higher micromolar (μM) range to lower milimolar (mM) range. (A) Representative SPRi sensorgrams for mixed solutions (1:1 volume ratio) of 10 nm DAAPT-AuNP solution at fixed concentration (9.5 nM) and DA standard solutions at different concentrations: blank (no DA, blue), 200 μM (red), 300 μM (green), 500 μM (purple), 1 mM (cyan), and 2 mM (orange). (B) Calibration curve (SPR signal vs. DA concentration) for the determination of DA in the corresponding concentration range. The error bars represent standard deviation for triplicate measurements. 104

Figure 4.7 Detection of DA using the inhibition assay from higher femtomolar (fM) range to lower picomolar (pM) range. (A) Representative SPRi sensorgrams for mixed solutions (1:1 volume ratio) of 10 nm DAAPT-AuNP solution at fixed concentration (1.9 nM) and DA standard solutions at different concentrations: blank (no DA, blue), 200 fM (red), 300 fM (green), 500 fM (purple), 20 pM (cyan), 20 nM (dark blue), and 2 μM (orange). (B) Calibration curve (SPR signal vs. DA concentration) for the determination of DA in the corresponding concentration range. The error bars represent standard deviation for triplicate measurements. 105

Figure 4.8 Specificity study of the inhibition assay using DA analogs (DOPA, DOPAC, catechol, epinephrine, homovanillic acid, ascorbic acid) and other metabolites (estradiol and folic acid) as potential interferences. The error bars represent standard deviation for at least triplicate measurements of each small molecule. 106

Figure 5.1 Schematic illustration of the fabrication of the small-molecule arrays (SMAs) on the SRPi chip surface with 9 gold spots. Mixed thiolate self-assembled monolayers

(SAMs) terminated with carboxyl (-COOH) group and hydroxyl (-OH) group are formed on chip surface via gold-thiol interaction. Metabolites containing primary amino ($-NH_2$) group are immobilized to chip surface via EDC/NHS chemistry. The pattern of the SMA and the number of metabolites can be controlled accordingly. The binding of the primary antibody (Ab) and secondary Ab can be measured by SPRi. Poly(ethylene glycol groups) introduced by the formation of thiolate SAMs are highlighted in the red rectangles. 118

Figure 5.2 SPRi measurement of the continuous binding of dopamine primary antibody (DA-Ab) and goat-anti-mouse secondary antibody (G-a-M Ab) to dopamine chip surface with different COOH/OH ratios (i.e. different DA surface densities). (A) SPRi sensorgrams for the binding of 10.0 μg/mL (67 nM) DA-Ab, and then 22.4 μg/mL (150 nM) G-a-M Ab to a single chip surface patterned with 0, 0.2, 0.5, 0.8, and 1.0 ratios of COOH/OH. The arrows indicate the injection of the primary antibody and the secondary antibody. (B) Plots of SPRi signal vs. COOH/OH ratio. The data points are the mean of triplicate measurements, and the error bars are the standard deviation. 121

Figure 5.3 SPRi measurement of the binding of folic acid primary antibody (FA-Ab) to folic acid chip surface with different COOH/OH ratios (i.e. different FA surface densities). (A) Corrected SPRi sensorgrams for the binding of 5.0 μg/mL (33 nM) FA-Ab to a single chip surface patterned with 0.2, 0.5, 0.8, and 1.0 ratios of COOH/OH. (B) Plot of SPRi signal vs. COOH/OH ratio. The data points are the mean of triplicate measurements, and the error bars are the standard deviation. 122

Figure 5.4 SPRi measurement of the continuous binding of cysteine primary antibody (Cys-Ab) and goat-anti-mouse secondary antibody (G-a-M Ab) to cysteine chip surface with different COOH/OH ratios (i.e. different Cys surface densities). (A) Corrected SPRi

sensorgrams for the binding of 5.0 μg/mL (33 nM) DA-Ab, and then 22.4 μg/mL (150 nM) G-a-M Ab to a single chip surface patterned with 0.2, 0.5, 0.8, and 1.0 ratios of COOH/OH. The arrows indicate the injection of the primary antibody and the secondary antibody. (B) Plots of SPRi signal vs. COOH/OH ratio. The data points are the mean of triplicate measurements, and the error bars are the standard deviation. 123

Figure 5.5 Characterization of the primary antibodies' (Abs) cross-reactivity using the small-molecule arrays (SMAs) patterned with dopamine (DA), folic acid (FA), and cysteine (Cys) with optimal surface densities. SPRi sensorgrams for the binding of 10 μg/mL (67 nM) (A) FA-Ab, (B) DA-Ab, (C) Cys-Ab. (D) Cross-reactivity of the Abs to different metabolites surfaces on the same chip. The bar height represents the mean SPRi signal of triplicate measurements, and the error bars are the standard deviation. 125

Figure 5.6 The inhibition of dopamine (DA) on antibody binding. SRPi sensorgrams for the continuous binding of (A) 20.0 μg/mL (133 nM) DA-Ab and 22.4 μg/mL (150 nM) G-a-M Ab; (B) mixed 20.0 μg/mL DA-Ab with 100 μM DA and 22.4 μg/mL G-a-M Ab. Insets are 3D difference images showing the chip surface after SPRi measurements of (A) and (B) respectively. The spot in the center of the chip is the negative control with 0 COOH/OH ratio, while the four spots at the corners and that in the middles have 1.0 and 0.8 COOH/OH ratios, respectively. (C) The inhibition effect after primary Ab binding and secondary Ab binding. The bars height represents the mean signal intensity of triplicate measurements, and the error bars are standard deviations. 127

Figure 5.7 Multiplexed detection of dopamine (DA), folic acid (FA), and cysteine (Cys) using the SMAs. (A) Representative SPRi sensorgrams for the binding of a mixed solution of Abs (30.0 μg/mL of DA-Ab, 30.0 μg/mL of FA-Ab, and 30.0 μg/mL of Cys-

Ab), then a mixed solution of metabolites (10 μM FA, 200 μM DA, and 200 μM Cys) to DA surface (red), FA surface (blue), and Cys surface (green) on a single SPRi chip. Calibration curves (plots of SPRi signal vs. metabolite concentration) for the determination of (B) DA, (C) FA, and (D) Cys. In all plots, the symbols represent the mean of triplicate measurements, and the error bars are the standard deviation. 128

List of Symbols

ω	Angular frequency
k	Wave vector
k_x	Wave vector of light
k_{sp}	Wave vector of surface plasmon
c	Speed of light
ε_d	Dielectric constant of a medium
ε_m	Real part of the dielectric constant of a metal
θ	Angle of incidence
θ_r	Angle of surface plasmon resonance
$h\nu$	Plank's constant times frequency
n	Refractive index
h	Hour
min	Minute
s	Second
mM	Mili molar
μM	Micro molar
nM	Nano molar
pM	Pico molar
fM	Femto molar
mg	Mili gram
μg	Micro gram

ng	Nano gram
mm	Mili metre
nm	Nano metre
mW	Mili Watt
v/v	Volume/Volume
L	Litre
mL	Mili litre
μL	Micro litre
mm^2	Mili metre squared
C	Surface concentration in mass/volume
∂n/∂C	Refractive index increment
kDa	Kilo Dalton
Da	Dalton
kV	Kilo Volt
MΩ	Mega Ohm
°C	Degree Celsius
K_d	Dissociation constant
α	Factor converting refractive index change to resonance unit
rpm	Revolutions per minute
ppb	Part per billion
ppt	Part per trillion
Δ%R	Change in percent reflectivity
Θ	Surface coverage

[SM]	Concentration of small molecule
[FA]	Concentration of folic acid
[E2]	Concentration of 17β-estradiol
[BSA-E2]	Concentration of bovine serum albumin-estradiol conjugate

List of Abbreviations

AA	Ascorbic Acid
Ab	Antibody
Ag	Silver
Ar	Argon
ATP	Adenosine Triphosphate
ATR	Attenuated Total Reflection
Au	Gold
AuNP	Gold Nanoparticle
AuNPs	Gold Nanoparticles
AuNR	Gold Nanorod
AuNS	Gold Nanostar
BSA	Bovine Serum Albumin
BSA-E2	Bovine Serum Albumin-17β-Estradiol Conjugate
CCD	Charge-Coupled Device
cDNA	Complementary DNA
COOH	Carboxyl Group
Cys	Cysteine
DA	Dopamine
DAAPT	Dopamine DNA Aptamer
DI	Deionized
DMSO	Dimethyl Sulfoxide

DNA	Deoxyribonucleic Acid
DNP	2,4-Dinitrophenol
DOPA	L-3,4-dihydroxyphenylalanine
DOPAC	3,4-dihydroxyphenylacetic Acid
DTSP	3, 3'-dithiodipropionic acid di(N-hydroxysuccinimide ester)
E1	Estrone
E2	17β-Estradiol
E2-Ab	Estradiol Antibody
EDC	3-(Ethyliminomethyleneamino)-*N*,*N*-dimethylpropan-1-amine
EDCs	Endocrine Distrupting Compounds
EG	Ethylene Glycol
EP	Epinephrine
FA	Folic Acid
FA-AuNP	Folic Acid Functionalized Gold Nanoparticle
FBP	Folic Acid Binding Protein
G-a-M	Goat-anti-Mouse
GBP	Glutamine Binding Protein
HBS-P	HEPES-Buffered Saline with P20 (surfactant)
HCl	Hydrochloric Acid
HCR	Hybridization Chain Reaction
HeNe	Helium Neon
HEPES	2-[4-(2-hydroxyethyl)piperazin-1-yl]ethanesulfonic acid
HIS_6	Polyhistidine Tag

HPLC	High-Performance Liquid Chromatography
HSA	Human Serum Albumin
H_2SO_4	Sulfuric Acid
HVA	Homovanillic Acid
IgG	Immunoglobulin G
K-R	Kretschmann-Raether
LSPR	Localized Surface Plasmon Resonance
M	Metabolite
MIPs	Molecularly Imprinted Polymers
MNP	Magnetic Nanoparticle
MS	Mass Spectrometry
MW	Molecular Weight
NA	Nucleic Acid
NaCl	Sodium Chloride
NHS	N-Hydroxysuccinimide
NH_2	Amino Group
Ni	Nickel
$NiCl_2$	Nickel Chloride
NMs	Nanomaterials
NMR	Nuclear Magnetic Resonance
NP	Nanoparticle
NTA	Nitrilotriacetic Acid
OD	Optical Density

OH	Hydroxyl Group
PBS	Phosphate-Buffer Saline
PDA	Polydopamine
PSP	Propagating Surface Plasmon
RII	Refractive Index Increment
RNA	Ribonucleic Acid
RU	Resonance Unit
SAM	Self-Assemble Monolayer
Γ	Surface Coverage
SDS-PAGE	Sodium Dodecyl Sulfate Polyacrylamide Gel Electrophoresis
SEM	Scanning Electron Microscopy
SERS	Surface-Enhanced Raman Spectroscopy
SMAs	Small-Molecule Arrays
SMM	Small-Molecule Microarray
SP	Surface Plasmon
SPPs	Surface Plasmon Polaritons
SPR	Surface Plasmon Resonance
SPRi	Surface Plasmon Resonance Imaging
ss	Single-stranded
SM	Small Molecule
TBS	Tris-Buffered Saline
TM	Transverse Mode
Tris	2-Amino-2-(hydroxymethyl)propane-1,3-diol

UV-Vis	Ultraviolet-Visible
vs	versus

Chapter 1 Introduction

1.1 Surface Plasmon Resonance: A General Introduction and Chronological History

Surface plasmon polaritons (SPPs) represent transverse mode (TM) electromagnetic waves propagating along a metal-dielectric interface (Figure 1.1), which have a maximum intensity on the surface and exponentially decaying fields perpendicular to it. The existence of SPPs is a physical phenomenon first observed by Wood back to 1902[1,2]. In theory, SPPs can be excited by either electrons or photons radiated to the metal-dielectric interface. However, the excitation of SPPs by electrons is out of scope of this thesis, and can refer to these books[3,4]. Herein, we will mainly focus on SPPs excited by light/photons in an optical device using the attenuated total reflection (ATR) setup shown in Figure 1.1, other optical excitation methods will also be briefly discussed.

In Figure 1.1, the light strikes the metal-dielectric 1 interface, there exists an evanescent wave with an exponentially decaying field perpendicular to the interface with a characteristic penetration depth, which is of the order of half a wavelength.

Surface plasmon resonance (SPR) is a resonance phenomenon occurred between SPPs and the incident light under particular conditions, and cannot always occur in the metal-dielectric interface due to the fact that energy and momentum conversation between SPPs and light is not fulfilled at all times. There are three ways to match the energy and momentum simultaneously: Otto configuration, Kretschmann-Raether configuration, and gratings. A. Otto first described the excitation of nonradiative surface plasma waves in silver by the method of frustrated total reflection, and proposed the Otto

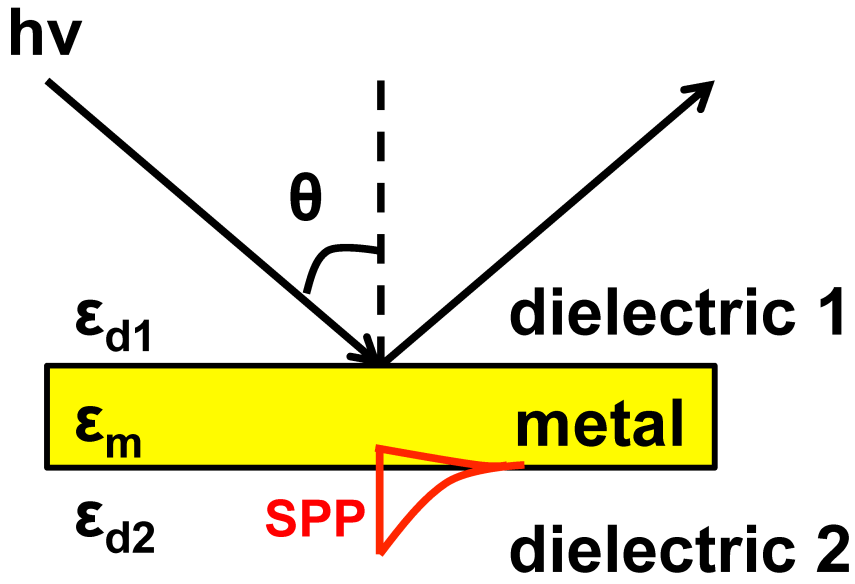

Figure 1.1 Schematic illustration of the excitation of surface plasmon polariton (SPP) by light on metal film using the attenuated total reflection (ATR) setup. The SPP is depicted in red.

configuration in 1968.[5] At the same year, E. Kretschmann and H. Raether proposed the K-R configuration based on attenuated total reflection.[6] R. H. Ritchie et al studied surface plasmon resonance effect in grating diffraction and proposed the use of gratings to excite SPPs and couple them to the light almost at the same time.[7] Moreover, two books[4,8] by H. Raether published in the 1980s systematically study the excitation of SPPs by electrons and photons respectively. All these work mentioned above summarize the very basic principle of SPPs excitation via different ways and the occurrence of SPR in the early days, thus lay a solid foundation for the future SPR sensing applications. In the next paragraph, we will discuss more detailed principle about dispersion relations of light and SPPs, the energy and momentum mismatch, and how the mismatched is addressed.

The dispersion relations ω(k) of the incident light and the SPPs are expressed in equation 1 and equation 2 respectively, where k_x is the wave vector of the incident light parallel to the surface, k_{sp} is the wave vector of the SPPs, ω is the angular frequency of light, c is the speed of light in vacuum, ε_m is the real part of the dielectric constant of the metal at the given frequency, ε_{d1} and ε_{d2} are the dielectric constant of dielectric medium 1 and medium 2 on both sides of the metal respectively, θ is the angle of incidence of the light. A graphical illustration of the dispersion relations based on equation 1 and equation 2 is given in Figure 1.2.

$$\mathbf{k_x = \frac{\omega}{c}\sqrt{\varepsilon_{d1}}\sin\theta} \qquad \mathbf{(1)}$$

$$\mathbf{k_{sp} = \frac{\omega}{c}\sqrt{\frac{\varepsilon_m \varepsilon_{d2}}{\varepsilon_m + \varepsilon_{d2}}}} \qquad \mathbf{(2)}$$

According to the dispersion relations, if both dielectric media 1 and 2 are air and for a negative ε_m of a metal, it is realized that at any given frequency (ω) and incidence angle (θ) of light, the parallel wave vector of light (k_x) is less than that of SPPs (k_{sp}). In other

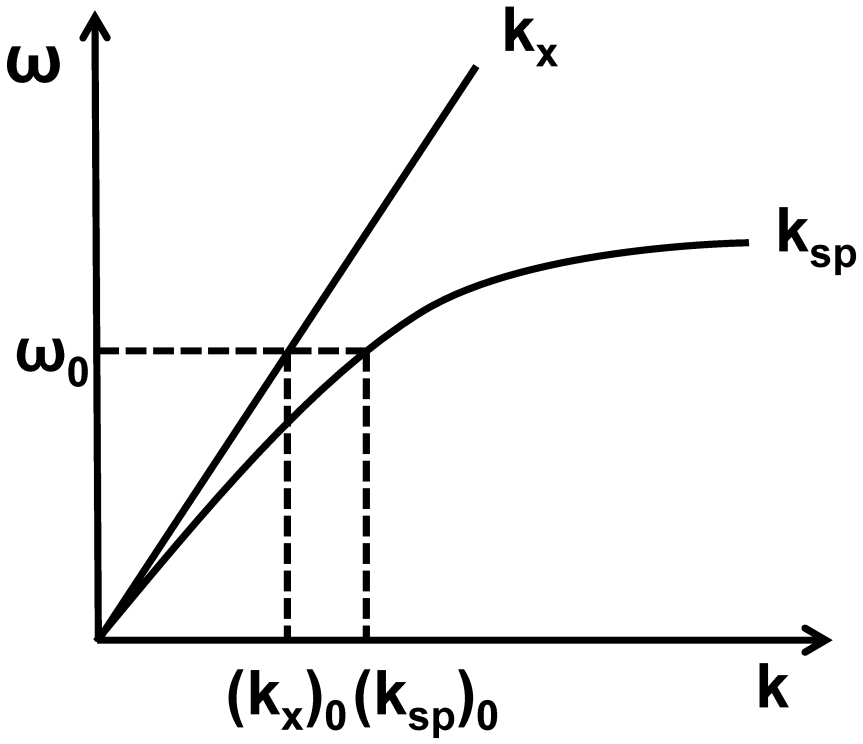

Figure 1.2 A graphical illustration of the dispersion relations ω(k) of the incident light (k_x) and the SPPs (k_{sp}).

words, the two wave vectors are not coupled to each other for any values of ω and θ. However, the mismatch was cleverly addressed by putting a prism with a high refractive index close enough (~ 100 nm) to one side of the metal by A. Otto[5]. E. Kretschmann and H. Raether went further to attach the prism to the metal, which creates the well known K-R configuration[9] (Figure 1.3). The K-R configuration has been widely utilized by most modern instrumentations since then. From a theoretical point of view, the introduction of a prism with a high refractive index increases ε_{d1} in equation 1, which will shift the dispersion relation line of the light to the right side (Figure 1.4). While the dispersion line of the SPPs remains the same as previous, the shift of the light dispersion line makes the two curves intersect with each other as shown in Figure 1.4. Now k_x is equal to k_{sp} at ω_1 and a resulting θ, and the coupling between the parallel wave vector of light and that of SPPs results in the occurrence of surface plasmon resonance (SPR) that can be experimentally observed by a big dip in light reflectivity of the SPR curve. Figure 1.5 shows a typical SPR curve (a plot of light reflectivity R versus angle of incidence θ) with a big dip occurred at the resonance angle (θ_r). This minimum reflectivity is due to a complete transformation of the incoming light into SPPs. Here we will focus on SPR instrumentation based on K-R configuration, since it is mostly used by modern instrumentations, SPR instrumentations based on Otto configuration and grating coupling are referred to these literatures[5,7,8,10,11].

For SPR-based sensing mechanism, any change of the dielectric constant (or refractive index) of the dielectric medium 2 due to adsorption/desorption of molecules to/from the thin metal film surface will affect the wave vector of SPPs, thus shift the SPR curve to the right/left side in order to re-fulfill the coupling conditions. Figure 1.6 shows

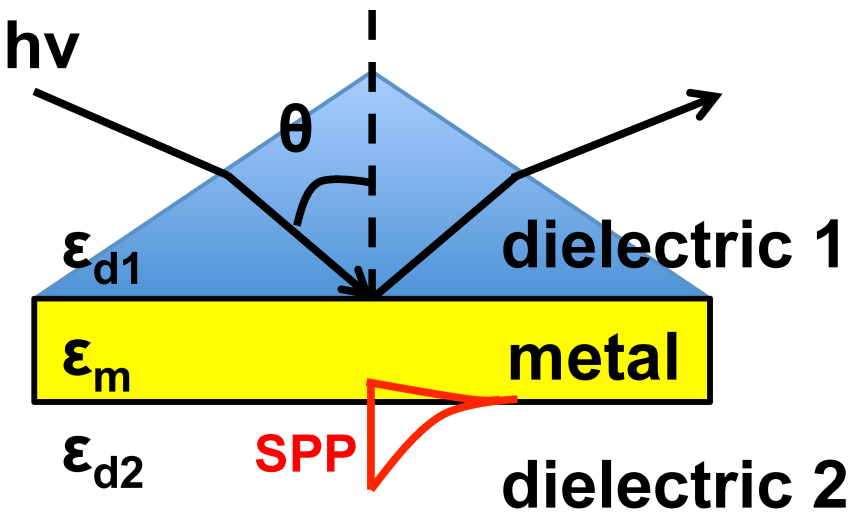

Figure 1.3 Schematic illustration of the occurrence of surface plasmon resonance (SPR) based on Kretschmann-Raether configuration.

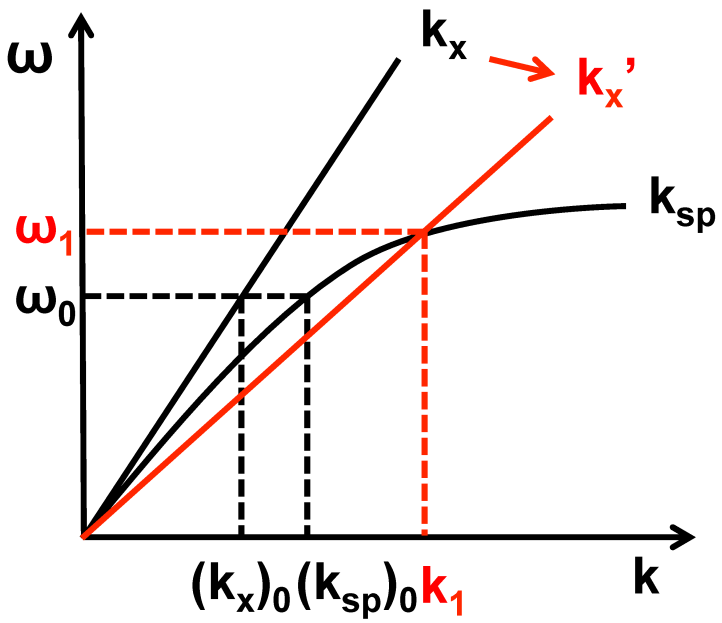

Figure 1.4 A graphical illustration of the dispersion relations of the light and the SPPs based on Kretschmann-Raether configuration. The dispersion relation line of the light is shifted to the right side (red) and intersects with the dispersion line of the SPPs.

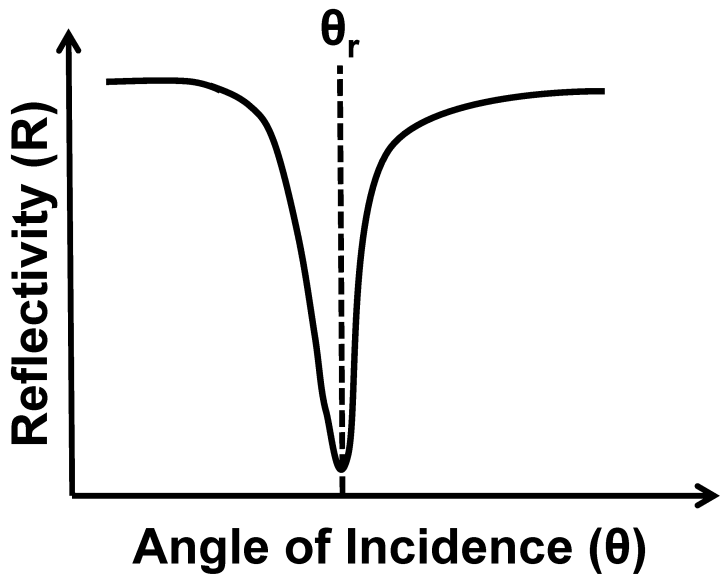

Figure 1.5 A typical SPR curve (light reflectivity R vs. angle of incidence θ) with a big dip occurred at the resonance angle (θ_r).

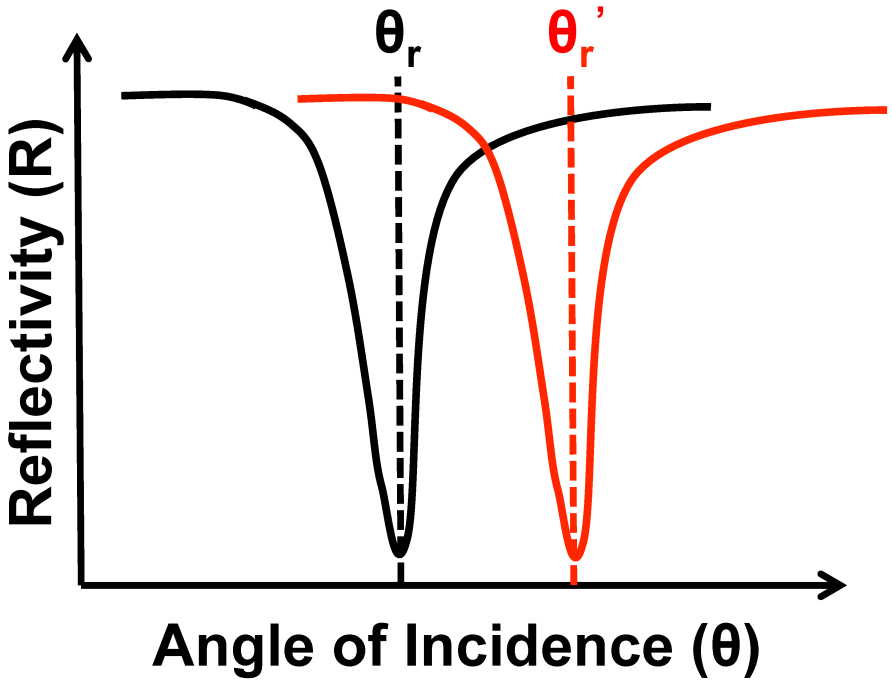

Figure 1.6 The shift of the SPR curve and the resonance angle to the right side due to the adsorption of molecules and an increase of the refractive index of the medium 2.

the shift of SPR curve to the right side due to the adsorption of molecules and an increase of refractive index of medium 2. Therefore, the shift of the resonance angle from θ_r to θ_r' resulting from the refractive index change of medium 2 is indicative of the surface concentration of adsorbed species, which constitutes the basic principle for SPR-based sensing. Figure 1.7 contains a representative SPR sensorgam (SPR signal vs. time) showing the association (on) and dissociation (off) of molecules to/from the metal film. It should be pointed out that the SPR signal of a SPR sensorgam could be angle shift, wavelength shift, or reflectivity change based on the specific interrogation of the SPR instrumentation.

Since SPR is extremely sensitive to the refractive index change of the dielectric medium 2 on one side of the thin metal film, people have been using this technique to sense a variety of chemical and biological species. The very first work in terms of SPR sensing was related to gas sensing by this technique. In 1982, Lieberg et al used SPR to detect the anaesthetic halothane gas down to the ppm range, where a silicon oil film was uniformly deposited on the 56 nm silver film surface to reversibly adsorb the gas molecules.[12] A year later, they published another work[13] regarding gas detection and biosensing using SPR. To our knowledge, this is the first time SPR was used to detect biomolecules. Human IgG molecules were first physisorbed to the silver film surface, and then anti-human IgG antibodies down to nanomolar (nM) range were exposed to the IgG surface. The specific interaction between antibody-antigen leads to a detectable SPR angle shift. In 1984, Pantell et al developed a similar immunosensor based on SPR to detect anti-human serum albumin (HSA), and mentioned the importance of employing a covalent chemical linkage for the first time to immobilize the HSA protein layer to the

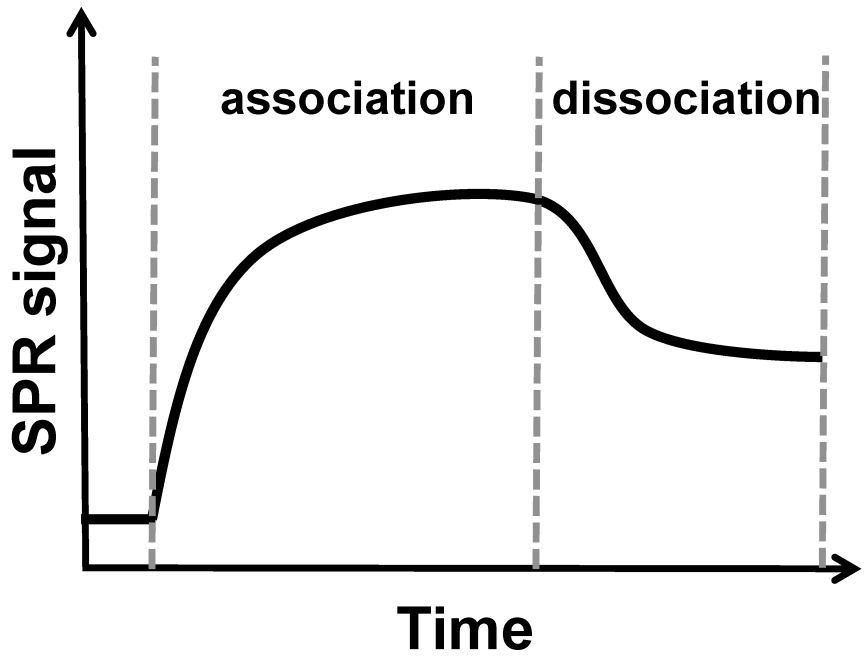

Figure 1.7 A representative SPR sensorgram (SPR signal vs. time) showing the association (on) and dissociation (off) of molecules to/from the metal film. The SPR signal can be angle shift, wavelength shift, or reflectivity change based on the specific SPR instrumentation.

substrate.[14] In 1987, C. R. Lowe et al first reported the detection of immune-complex formation via SPR on gold-coated diffraction gratings.[10] In 1988, the first SPR sensing of liquid chemical (acetone) based on wavelength shift of SPR curve was published.[15] The same year witnessed a few other SPR-based immunosensing applications.[16,17] It is noteworthy that there was still no commercially available SPR instrument until 1988, all the work mentioned above were using a homemade instrumentation.

The year of 1990 was the "golden" year in SPR history, since it arose the first commercialization of the Biacore SPR instrument released by Pharmacia Biosensor AB (the initial name before the company changed its name to Biacore AB Corporation). Ever since the golden year, we can see an explosive development in SPR research and applications. Figure 1.8 is a plot of # of publications vs. year, showing the web of science searching results with "surface plasmon resonance" in title. Apparently, an exponential growth trend is observed from 1990 to 2016, coinciding with the power of commercialization of a technique. This indicates commercialization has a profound impact on the development of a technique and its corresponding field. Thus, SPR have found widespread applications in studying all sorts of biomolecular interactions[18-38], sensing chemical species[39-41] and biomolecules[21,42-64] (specifically proteins and nucleic acids) during the first decade (1990-1999) after commercialization. However, if we narrow down the searching condition to "surface plasmon resonance and small molecule" in title using the same database, we will get the results shown in Figure 1.9. By comparing Figure 1.9 to Figure 1.8, we can make a few points: first, there exists a more than ten-year time lag for small molecule study using SPR, since the first small molecule study came out around 2000[65]; second, there is a huge gap in the # of publications

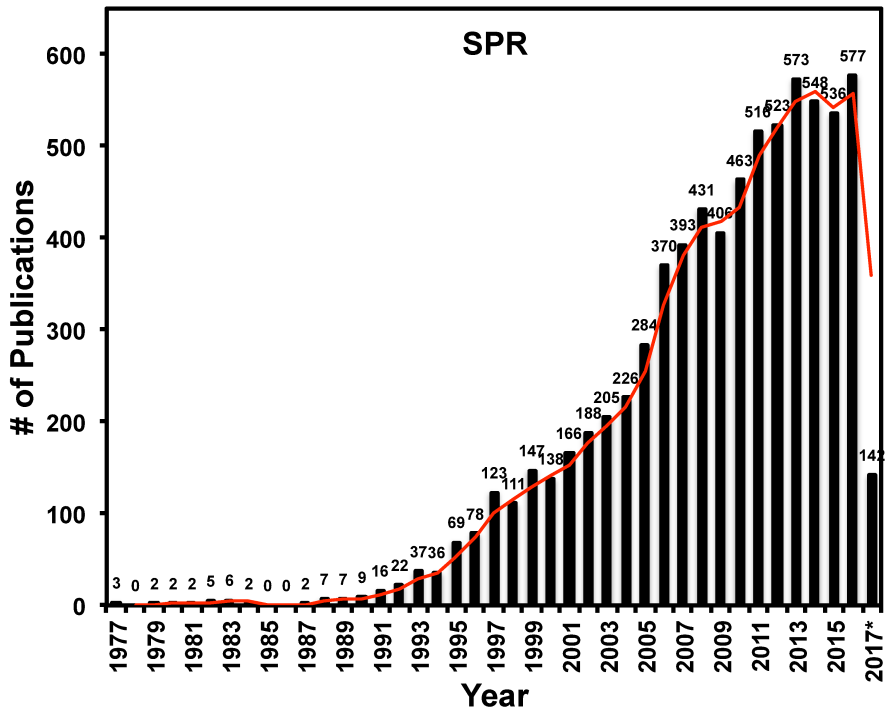

Figure 1.8 The web of science searching results (a plot of # of publications vs. year) with "surface plasmon resonance" in title by May 15th, 2017. The year 1990 launched the first commercially available SPR product, the Biacore instrument.

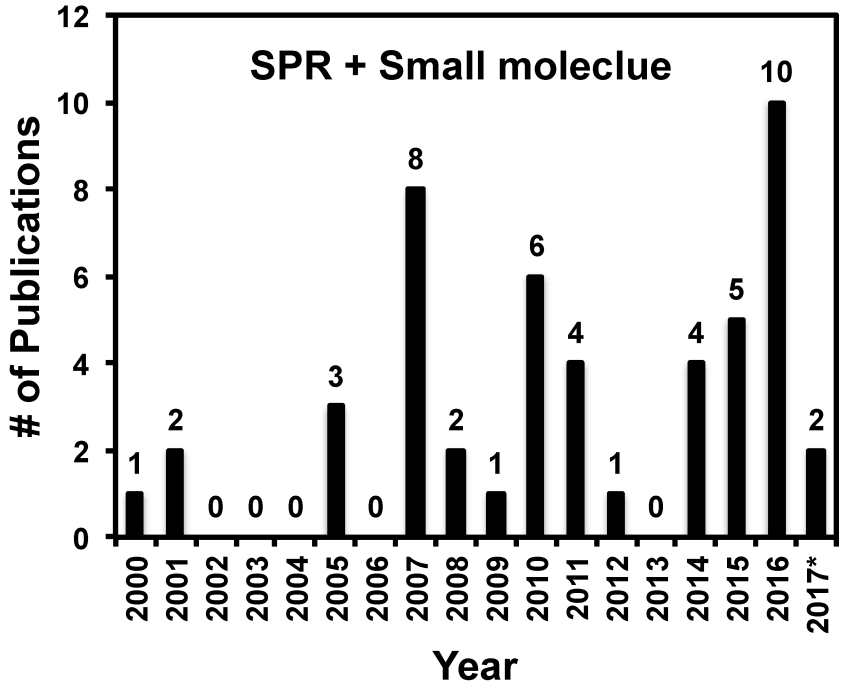

Figure 1.9 The web of science searching results (a plot of # of publications vs. year) with "surface plasmon resonance and small molecule" in title by May 15th, 2017.

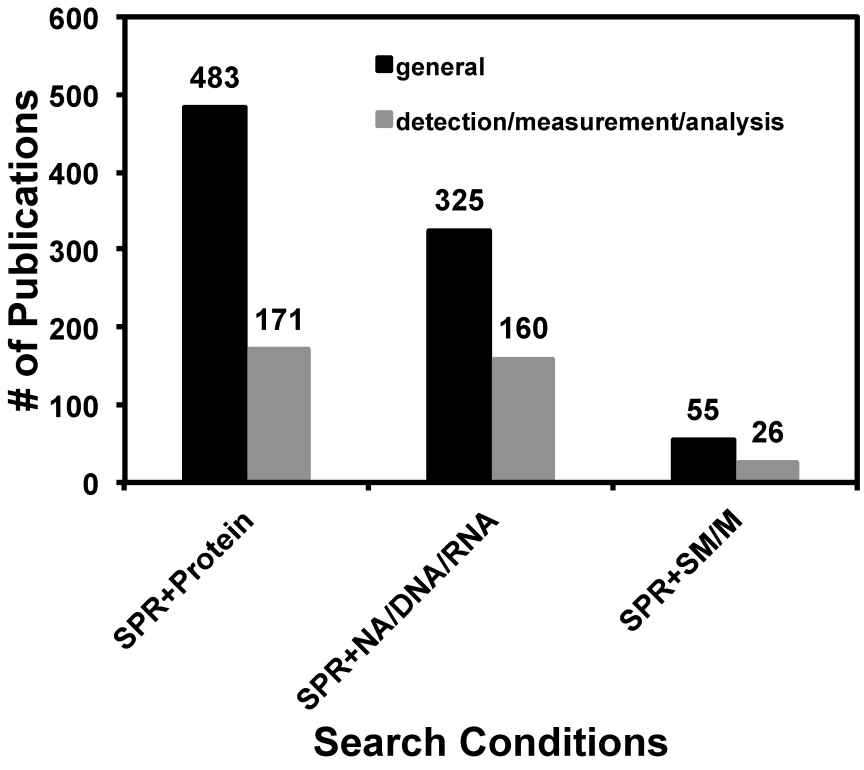

Figure 1.10 A comparison among the web of science searching results for "SPR+Protein" in title, "SPR+nucleic acid/DNA/RNA" in title, and "SPR+small molecule/metabolite) in title by May 15th, 2017. The black bars are general results, while the grey bars represent the sensing (with additional "detection/measurement/analysis") in title.

between SPR (7371) and SPR + small molecule (49); last but not least, SPR-based small molecule study is not continuous and very sporadic. In addition, a direct comparison among SPR-based protein, nucleic acid (NA)/DNA/RNA, and small molecule (SM)/metabolite (M) searching results is made in Figure 1.10, the # of publications for SPR-based SM/M is the least among the three and less than 17% of that for SPR-based NA/DNA/RNA and SPR-based protein results, whether it is for general study or sensing (detection/measurement/analysis) study. All the observations suggest it may be challenging to study small molecule and/or metabolite compared to protein and nuclei acids using SPR and more work need to be done to bride the gap between small molecule and the other two.

1.2 A Theoretical Analysis of the Challenge Associated with SPR Sensing of Small Molecules

Small molecule (SM) is another type of important target besides protein and nucleic acid in bioanalytical chemistry, for example, metabolites, therapeutic drugs, food additives, environmental contaminants, etc. SM sensing thus is of great significance in the fields of human health, therapeutic drug discovery, food safety, and environmental monitoring. Compared to proteins and nucleic acids, SM typically has a molecular weight (MW) less than 1000 Da, which are orders of magnitude smaller. This most obvious difference among them introduces a lot of difficulties for SM sensing. As discussed above, SPR have found a wide variety of applications in proteins and nucleic acids sensing since the first commercialization of this technique, but this is not the truth for SM sensing by SPR. Why is this happening? Can we explain where the challenge of sensing

SMs by this technique comes from? To answer these questions, we will discuss the origin of this particular challenge associated with SM sensing from a theoretical analysis.

In a Biacore system, the SPR angle shift is depending on the refractive index change at the surface, and the change in concentration of molecules at a biospecific surface is measured through this dependency, which can be described in equation 3[65,66] as:

$$\mathbf{RU_{meas} = \Delta n \times \alpha = [(\partial n/\partial C)_{ligand} \times C] \times \alpha} \qquad \mathbf{(3)}$$

where RU_{meas} is the measured instrument response in resonance units, Δn is the refractive index change at the surface which increases as ligand binds to immobilized macromolecule, α is a factor that converts Δn to RU_{meas}. $(\partial n/\partial C)_{ligand}$ is the refractive index increment (RII) of the bound ligand, and C is the concentration of ligand bound at the biospecific surface in mass/volume. In the equation, the most important parameter is the RII – $(\partial n/\partial C)_{ligand}$, and RII can be determined from the slope of Δn versus concentration of ligand in mass/volume. Generally, 1000 RU with a Biacore system correspond to an angle shift of approximately 0.1°, which is equivalent to roughly 1 ng/mm^2 of surface protein concentration.[67]

The simplest one-site binding model can be described as follow:

$$\mathbf{P + T \rightarrow C}$$

where P is a probe molecule with a specific binding site, T is a target molecule that can bind to that site, C is the resulting complex. Suppose P is a big macromolecule probe immobilized on the chip, T is a small molecule target, and then equation 4 can be deduced from equation 3:

$$\mathbf{(RU_{SM})_{max} = \alpha \times C_P \times (MW_{SM}/MW_P) \times (\partial n/\partial C)_{SM}} \qquad \mathbf{(4)}$$

since $\mathbf{RU_P = \alpha \times [(\partial n/\partial C)_P \times C_P]}$, then

$$\mathbf{(RU_{SM})_{max} = RU_P \times (MW_{SM}/MW_P) \times [(\partial n/\partial C)_{SM}/(\partial n/\partial C)_P]} \quad \mathbf{(5)}$$

where $(RU_{SM})_{max}$ is the predicted maximum instrument response in resonance units for small molecule binding at a single site, RU_P is the experimental amount of macromolecule probe on the chip surface in resonance units, MW_{SM} and MW_P are molecular weights of the small molecule target and the macromolecule probe respectively, $(\partial n/\partial C)_{SM}$ is the RII of the small molecule, $(\partial n/\partial C)_P$ is the RII of the macromolecule, C_P is the surface concentration of the macromolecule in mass/volume.

From equation 4, we know that the signal response for small molecule binding to a surface macromolecule probe is related to the surface concentration (i.e. surface coverage/density) of the macromolecule, molecular weights for both parts of the binding pair, as well as RII for the small molecule. Once the target and the macromolecule probe binding pair is chosen for a detection system, the signal response is simply proportional to the surface concentration (C_P) of the macromolecule probe, as all the remaining parameters on the right side of the equation are constant for a chosen binding pair. Meanwhile, equation 5 explains why small molecule binding has a much lower signal response than that for macromolecule binding, because the signal response is related to the molecular weight ratio of SM over P. It has been reported that small molecules RII values can be very similar as those of protein and nucleic acid receptors, but can also be significantly different than those of receptors, depending on refractive index and chemical structure of the small molecule.[65,68,69] For example, the small molecule RII ratios versus BSA reported in the literature[65] range from 0.9 to 2.0. Therefore, the limiting factors that cause a much smaller signal response for SM detection are the molecular weight of the small molecule target itself and the surface concentration of the

macromolecule probe. For these two factors, researcher can only play with the latter if they would like to detect SM directly, since molecular weight is an unchangeable factor.

Indeed, the situation in the real world coincides with the theoretical prediction. The number of reports of direct measurement of small molecule is very small and the distribution is sporadic.[67,70-74] Till now, most of the work reported in terms of direct detection of small molecule were based on Biacore SPR systems, and in some cases the saturated signal response in RU for small molecule binding is as low as ~22 RU. This suggests that direct detection of small molecule targets generally suffers from low signal and poor sensitivity, which agrees well with our theoretical analysis of small molecule sensing. Except for the surface probe capacity, researchers do not have much room to play with to detect small molecule directly. This leads to a strong motivation to develop other strategies. In order to enhance the signal and improve the sensitivity, various strategies have been developed by different groups (including our group) to sense small molecules by SPR. In the next section, we will divide these strategies into three different categories and discuss them separately.

1.3 Strategies to Overcome the Challenge of Detection SM by SPR

1.3.1 Indirect detection formats

Researchers have been using a few indirect detection strategies that have found success in small molecule sensing by SPR. The schematic illustrations of four indirect detection formats, namely 1) competition, 2) inhibition, 3) displacement, and 4) sandwich, are shown in Figure 1.11. Ideally, by using either of these indirect detection formats,

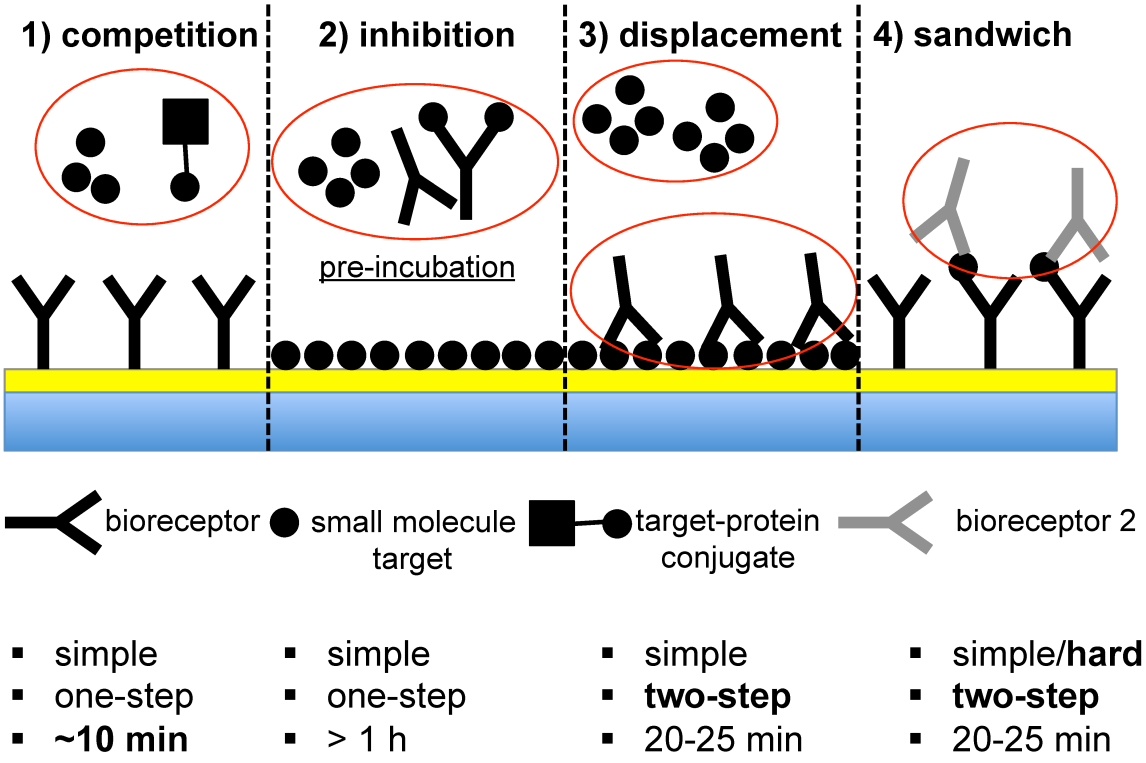

Figure 1.11 Schematic illustrations of 4 indirect detection formats (competition, inhibition, displacement, and sandwich) for SPR sensing of small molecules.

researchers are converting the task of detecting small molecules directly into detecting relatively large protein molecules instead. As a result, the challenge of low signal and poor sensitivity with direct small molecule detection is eliminated by this smart conversion from detecting small molecule to detecting protein binding.

Specifically, in the competition format, the small molecule target is pre-mixed with a small molecule-protein conjugate. Since both species can bind to the bioreceptor on the chip surface, they will compete for the binding site of the bioreceptor. If the concentration of small molecule-protein conjugate is kept constant in the pre-mixed solution, the signal response generated from the small molecule-protein conjugate binding to the surface can be tuned by varying the concentration of small molecule in the pre-mixed solution. A higher concentration of small molecule will lead to a lower signal response, and a lower concentration of small molecule will lead to a higher signal response (Figure 1.12a). To this regard, the signal response generated from the small molecule-protein conjugate binding is inversely related to the concentration of the small molecule target (Figure 1.12b). However, in an inhibition format, the bioreceptor is not on the chip surface, instead, the small molecule is immobilized on the surface. The bioreceptor will be pre-incubated with small molecule target, if more small molecule targets are present in the pre-incubated solution, less bioreceptor will bind to the small molecule on the surface, and thus a low signal response will be generated. Similar to a competition format, the signal response is inversely related to the concentration of the small molecule target as well. Typically, for both competition and inhibition formats, the calibration curve (Figure 1.12b) demonstrates a sigmoidal shape with a negative slope. More importantly, the dynamic range and limit of detection can usually be lowered by

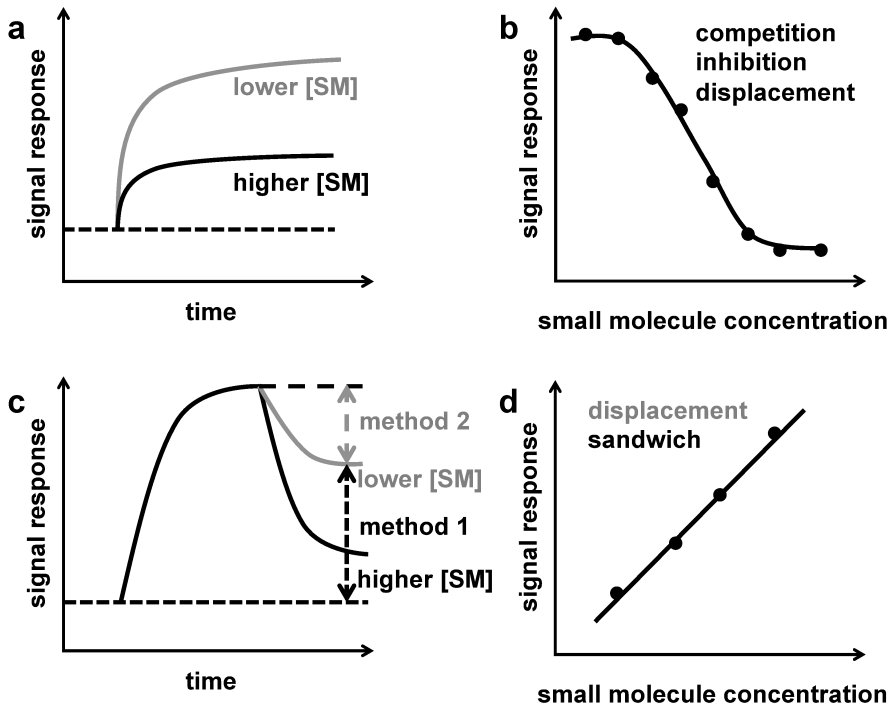

Figure 1.12 Typical SPR sensorgrams (a, c) and calibration curves (b, d) for the indirect detection formats: (a) competiton and inhibition, (b) competition, inhibition, and displacement using method 1 as signal output, (c) displacement, (d) displacement using method 2 as signal output and sandwich.

decreasing the small molecule-protein conjugate concentration in the pre-mixed solution in the competition format or the bioreceptor concentration in the pre-incubated solution in the inhibition format.

The story of displacement detection format is a bit different due to the fact that this format involves two steps: i) binding of the bioreceptor to the small molecule immobilized on chip surface; ii) displacement of the bound bioreceptor from the surface by exposing the surface to the small molecule target solution. Based on this mechanism, we have two methods (Figure 1.12c) to relate the signal response to the concentration of small molecule target. The first method is to use the signal difference between signal after displacement and the baseline, and the signal response measured through this method is inversely related to the concentration of small molecule target (Figure 1.12b). The second method is to only use the signal decrease part due to the displacement of bound bioreceptor molecules from the surface. This method will generate a direct correlation between the signal decrease intensity and the small molecule target concentration (Figure 1.12d), because the higher the small molecule target concentration, the more bound bioreceptor will be displaced (i.e. a higher signal decrease).

When we make a comparison among the three indirect detection formats in terms of assay time, competition will give the best performance, displacement will hold a position somewhere in the middle, and inhibition will be the last choice, because competition is the most straightforward one-step format, displacement introduces another step to displace the bound bioreceptor molecules, while inhibition involves an extra pre-incubation step that will usually take a longer time ($\geq$ 1 h) than that spent on the extra step in displacement format. More importantly, all three formats do have another strength

in terms of further signal enhancement, where a secondary bioreceptor that can bind to the first bioreceptor in inhibition and displacement formats or the small molecule-protein conjugate in the competition format can be employed to further enhance the signal in some circumstances. For example, Aizawa et al have developed a SPR-based competition immunosensor to detect 2,4-dinitorophenol (DNP) in the concentration range 1 ppt to 1 ppb, where a secondary anti-DNP antibody was used to further enhance the SPR signal by a factor of three.[75] Kawazumi et al have developed a compact SPR immunosensor using the indirect inhibition format to analyze benzopyrene and 2-hydroxybiphenyl simultaneously.[76] Keegan et al have reported the successful detection of eleven benzimidazole carbamate (BZT) and four amino-benzimidazole metabolites in liver tissue from animals treated with benzimidazole drugs based on two SPR inhibition assays.[77] We have developed an inhibition assay based on SPR imaging to detect 17β-estradiol, where BSA-estradiol conjugate is immobilized on our homemade chip surface and monoclonal antibody against 17β-estradiol is used as the bioreceptor. The assay exhibits high sensitivity, specificity, and a dynamic range from 10 picomolar to 2 nanomolar.

Sandwich assay is another type of indirect detection format that is most commonly used in protein biomarker detection. However, it is not a commonly used format for small molecule detection. Typically, for a sandwich assay, at least two bioreceptor or bio-recognition elements are needed, and this requires the target to have two different epitopes in its structure. While it is not uncommon for protein biomarkers to have two epitopes, small molecule has been rarely reported to have multiple epitopes that allow the generation of a pair of bio-recognition elements due to it small molecular size.

The only exception till now is the split aptamer, where one complete bio-recognition element (aptamer) is cut into two small fragments, and only in the presence of the small molecule target can the two fragments come together to form this sandwich structure.[78,79] Researchers are trying hard enough to develop more aptamers with high affinity and specificity for more small molecules, despite the intrinsic difficulties associated with low-epitope small molecule targets.[80,81]

1.3.2 Nanomaterials (NMs) enhanced sensing strategies

Nanomaterials (NMs) with different shapes and compositions have been tremendously incorporated into SPR sensing strategies as signal amplifiers to detect biomolecules. By now, the nanomaterials that have been used in SPR sensing of small molecules include gold nanoparticle[82-85] (AuNP), gold nanostar[86] (AuNS), and magnetic nanoparticle[87,88] (MNP). The range of NMs used in small molecule SPR sensing is much narrower than that used in protein and nucleic acid sensing. Besides these used in small molecule SPR sensing, gold nanorods[89] (AuNR), carbon nanostructures[90-94] (carbon nanotubes and graphene), quantum dots[95,96], magnetic-gold nanoparticle composite[97] have been used in SPR sensing of proteins and nucleic acids. Liposome nanoparticles[98] have been used to enhance the signal in SPR sensing as well.

Two major effects account for the success of using different nanomaterials as signal amplifiers in SPR sensing: mass effect and/or plasmonic coupling effect.[99-103] For metal nanomaterials, both effects could exist; while for other nanomaterials (magnetic, carbon-based, quantum dots), the signal enhancement mechanism is primarily due to the mass effect. Mass effect is fairly easy to understand, because nanomaterials can introduce

a much higher surface concentration in mass/volume and refractive index increment than biomolecules themselves on the right side of equation (3), thus a stronger signal enhancement. Plasmonic coupling effect occurs between the localized surface plasmon resonance (LSPR) of metal nanomaterials and the propagating surface plasmon (PSP) on Au film, which can lead to a big signal enhancement due to the coupling. Wang et al developed an aptamer-based AuNP-enhanced SPR sensing strategy to detect adenosine from 1 nanomolar to 1 micromolar.[84] The DNA aptamer is immobilized on SPR gold film, which can hybridize with AuNP-tagged complementary ss-DNA and lead to a large SPR signal. However, the presence of adenosine will trigger a conformational change of the DNA aptamer from ss-DNA to tertiary structure, hindering the hybridization between AuNP tag and surface DNA aptamer, thus the SPR signal change is decreased. The same group published another two similar work later on, in which the position of the complementary ss-DNA and the DNA aptamer is switched[82], and AuNP is changed to magnetic NP[87]. We have developed a competitive assay to easily detect folic acid in the nanomolar range, where folate-binding protein with a polyhistidine tag is immobilized on homemade SPR chip surface via Ni^{2+}-NTA surface chemistry and folic acid functionalized AuNP is used as a competitor as well as signal amplifier. Wang et al have developed a split aptamer fragments based sandwich sensing strategy to detect adenosine with a limit of detection of 1.5 pM. In their strategy, one ss-DNA fragment is immobilized on Au film, the other is attached to the AuNP, only in the presence of adenosine can the two parts come together, form a sandwich structure, and generate a big detectable signal response. Kim et al recently developed a gold nanostar enhanced antibody-aptamer sandwich assay to detect tetracycline at 10 attomolar.[86] All the above

examples have demonstrated that nanomaterials in conjunction with indirect detection formats can be very effective tools to achieve an extremely high sensitivity and overcome the challenge associated with small molecule sensing by SPR. However, more work can be achieved and highly required to expand the types of nanomaterials with a broad range of shapes and compositions in SPR sensing of small molecule, compared to that used in protein and nucleic acid sensing.

1.3.3 Other strategies

Besides these indirect detection formats and nanomaterials enhanced sensing strategies, researchers are still developing other strategies to enrich the toolbox of addressing the challenge with SPR sensing of small molecules. For example, Wang et al developed a method to detect ascorbic acid in the concentration range of 20 micromolar to 1 millimolar using catalyzed deposition of metal ions on gold substrate.[104] Silver ions were reduced by ascorbic acid to form silver atom on assembly of gold nanoparticles on SPR gold film, which resulted in a decrease of depth in SPR reflectance intensity curve as well as a shift of SPR angle. Other efforts were made on the use of molecularly imprinted polymers[105-112] (MIPs) as a highly specific selector for small molecule target. Also, dextran hydrogel[113] was used to coat the SPR gold sensor chip to enhance surface immobilization capacity. The protein immobilization capacity of the hydrogel was reported to be 10 times greater than the bare gold surface and 20 times greater than the 11-mercaptoundecanoic acid surface. A monolayer of graphene-coated gold film[94] was reported to be more sensitive than the traditional bare gold film. Li et al coupled hybridization chain reaction (HCR) with SPR, which achieved multiple signal

amplification on SPR chip surface and detection of ATP down to 1 nanomolar with high specificity.[88] Another work using the similar idea achieved detection of ATP from 0.1-10 micromolar.[114]

1.4 Summary and Objective

This chapter gives a brief introduction to SPR sensing principles, a chronological history of the development of this technique, and a theoretical analysis of the origin of the challenge associated with small molecule sensing by this technique. A variety of sensing strategies developed by researchers to overcome the challenge and achieve sensitive detection of small molecules are summarized. Compared to SPR sensing of proteins and nucleic acids, the power of this technique was underestimated in small molecule sensing. To overcome the sensitivity challenge associated with direct SPR detection of small molecules, we have developed a series of indirect sensing strategies: competition, inhibition, and displacement. In all scenarios, either functionalized AuNPs (Chapter 2 and 4) or antibodies (Chapter 3 and 5) are used to enhance the signal. By these indirect sensing strategies, we are converting the direct detection of small molecules to indirect detection of relatively large AuNPs and protein molecules, thus overcome the sensitivity challenge. All the work contained in this thesis were conducted with a SPR imaging (SPRi) system, which allows for the multiplexed detection of multiple metabolites simultaneously. We believe the work included in this thesis will give some insights to the SPR community and inspire more work to be done in terms of small molecule sensing, thus having more impact in the fields of medical diagnosis of small molecule biomarkers, therapeutic drug discovery, food safety control, and environmental monitoring.

1.5 References

(1) Wood, R. W. *Philos. Mag.* **1902**, *4*, 396-402.

(2) Wood, R. W. *Philos. Mag.* **1912**, *23*, 310-317.

(3) Pick, H.; Raether, H.; Bennemann, K. H. *Springer Tracts in Modern Physics*, vol. 38; Springer-Verlag, 1965.

(4) Raether, H. *Excitation of Plasmons and Interband Transitions by Electrons*; Springer-Verlag, 1980.

(5) Otto, A. *Z. Phys.* **1968**, *216*, 398-410.

(6) Kretschmann, E.; Raether, H. *Z. Naturforsch., Teil A,* **1968**, *23*, 2135-2136.

(7) Ritchie, R.; Arakawa, E.; Cowan, J.; Hamm, R. *Phys. Rev. Lett.* **1968**, *21*, 1530-1533.

(8) Raether, H. *Surface Plasmons on Smooth and Rough Surfaces and on Gratings*; Springer-Verlag, 1986.

(9) Bruns, R.; Raether, H. *Z. Phys.* **1970**, *237*, 98-106.

(10) Cullen, D. C.; Brown, R. G. W.; Lowe, C. R. *Biosensors* **1987**, *3*, 211-225.

(11) Raether, H. *Thin Solid Films* **1975**, *28*, 119-124.

(12) Nylander, C.; Liedberg, B.; Lind, T. *Sens. Actuators* **1982**, *3*, 79-88.

(13) Liedberg, B.; Nylander, C.; Lundstrom, I. *Sens. Actuators* **1983**, *4*, 299-304.

(14) Flanagan, M. T.; Pantell, R. H. *Electron. Lett.* **1984**, *20*, 968-970.

(15) Zhang, L. M.; Uttamchandani, D. *Electron. Lett.* **1988**, *24*, 1469-1470.

(16) Daniels, P. B.; Deacon, J. K.; Eddowes, M. J.; Pedley, D. G. *Sens. Actuators* **1988**, *15*, 11-18.

(17) Kooyman, R. P. H.; Kolkman, H.; Vangent, J.; Greve, J. *Anal. Chim. Acta* **1988**, *213*, 35-45.

(18) Johnsson, B.; Lofas, S.; Lindquist, G. *Anal. Biochem.* **1991**, *198*, 268-277.

(19) Jonsson, U.; Fagerstam, L.; Ivarsson, B.; Johnsson, B.; Karlsson, R.; Lundh, K.; Lofas, S.; Persson, B.; Roos, H.; Ronnberg, I.; Sjolander, S.; Stenberg, E.; Stahlberg, R.; Urbaniczky, C.; Ostlin, H.; Malmqvist, M. *Biotechniques* **1991**, *11*, 620-627.

(20) Jost, J. P.; Munch, O.; Andersson, T. *Nucleic Acids Res.* **1991**, *19*, 2788-2788.

(21) Lofas, S.; Malmqvist, M.; Ronnberg, I.; Stenberg, E.; Liedberg, B.; Lundstrom, I. *Sens. Actuators, B.* **1991**, *5*, 79-84.

(22) Altschuh, D.; Dubs, M. C.; Weiss, E.; Zederlutz, G.; Vanregenmortel, M. H. V. *Biochemistry* **1992**, *31*, 6298-6304.

(23) Brighamburke, M.; Edwards, J. R.; Oshannessy, D. J. *Anal. Biochem.* **1992**, *205*, 125-131.

(24) Dubs, M. C.; Altschuh, D.; Vanregenmortel, M. H. V. *Immunol. Lett.* **1992**, *31*, 59-64.

(25) Hasegawa, Y.; Okazaki, I.; Endo, T.; Kawasaki, T.; Kobata, A. *Glycoconjugate J.* **1993**, *10*, 283-283.

(26) Terrettaz, S.; Stora, T.; Duschl, C.; Vogel, H. *Langmuir* **1993**, *9*, 1361-1369.

(27) Natsume, T.; Koide, T.; Yokota, S.; Hirayoshi, K.; Nagata, K. *J. Biol. Chem.* **1994**, *269*, 31224-31228.

(28) OConnorMcCourt, M. D.; Segarini, P.; Grothe, S.; Tsang, M. L. S.; Weatherbee, J. A. *Ann. N. Y. Acad. Sci.* **1995**, *766*, 300-302.

(29) Englebienne, P. *Analyst* **1998**, *123*, 1599-1603.

(30) Mayer, M.; Lederer, F.; Le, K. H. D. *J. Inorg. Biochem.* **1999**, *74*, 227-227.

(31) Saenko, E.; Sarafanov, A.; Greco, N.; Shima, M.; Loster, K.; Schwinn, H.; Josic, D. *J. Chromatogr. A* **1999**, *852*, 59-71.

(32) Zakhary, D. R.; Bond, M. *Biophys. J.* **1999**, *76*, 100-100.

(33) Bondeson, K.; Frostellkarlsson, A.; Fagerstam, L.; Magnusson, G. *Anal. Biochem.* **1993**, *214*, 245-251.

(34) Polymenis, M.; Stollar, B. D. *J Immunol.* **1995**, *154*, 2198-2208.

(35) Yang, W. P.; Wu, H.; Barbas, C. F. *J. Immunol. Methods* **1995**, *183*, 175-182.

(36) Seimiya, M.; Kurosawa, Y. *FEBS Lett.* **1996**, *398*, 279-284.

(37) Haruki, M.; Noguchi, E.; Kanaya, S.; Crouch, R. J. *J. Biol. Chem.* **1997**, *272*, 22015-22022.

(38) Hendrix, M.; Priestley, E. S.; Joyce, G. F.; Wong, C. H. *J. Am. Chem. Soc.* **1997**, *119*, 3641-3648.

(39) Vukusic, P. S.; Brown, G. P. B.; Sambles, J. R. *Sensors* **1991**, 145-149.

(40) Ideta, K.; Arakawa, T. *Sens. Actuators, B* **1993**, *13*, 384-386.

(41) Jorgenson, R. C.; Yee, S. S. *Sens. Actuators, B* **1993**, *12*, 213-220.

(42) Stenberg, E.; Persson, B.; Roos, H.; Urbaniczky, C. *J. Colloid Interface Sci.* **1991**, *143*, 513-526.

(43) Oshannessy, D. J.; Odonnell, K. C.; Martin, J.; Brighamburke, M. *Anal. Biochem.* **1995**, *229*, 119-124.

(44) Uda, T.; Hifumi, E.; Kubota, N.; Shimizu, K.; Ogino, K. *Denki Kagaku* **1995**, *63*, 1160-1166.

(45) Kunz, U.; Katerkamp, A.; Reinhard, R.; Spener, F.; Cammann, K. *Sens. Actuators, B* **1996**, *32*, 149-155.

(46) Saito, K.; Yokota, H.; Yanagida, T. *Biophys. J.* **1996**, *70*, 300-300.

(47) Salamon, Z.; Wang, Y.; Soulages, J. L.; Brown, M. F.; Tollin, G. *Biophys. J.* **1996**, *71*, 283-294.

(48) Sigal, G. B.; Bamdad, C.; Barberis, A.; Strominger, J.; Whitesides, G. M. *Anal. Chem.* **1996**, *68*, 490-497.

(49) Sota, H.; Hasegawa, Y.; Iwakura, M. *Anal. Chem.* **1998**, *70*, 2019-2024.

(50) Stockley, P. G.; Baron, A. J.; Wild, C. M.; Parsons, I. D.; Miller, C. M.; Holtham, C. A. M.; Baumberg, S. *Biosens. Bioelectron.* **1998**, *13*, 637-650.

(51) Wink, T.; van Zuilen, S. J.; Bult, A.; van Bennekom, W. P. *Anal. Chem.* **1998**, *70*, 827-832.

(52) Brockman, J. M.; Frutos, A. G.; Corn, R. M. *J. Am. Chem. Soc.* **1999**, *121*, 8044-8051.

(53) Caide, X.; Sui, S. F. *Eur. Biophys. J.* **1999**, *28*, 151-157.

(54) Green, R. J.; Davies, M. C.; Roberts, C. J.; Tendler, S. J. B. *Biomaterials* **1999**, *20*, 385-391.

(55) Rebois, R. V.; VanRyk, D.; Schuck, P. *Faseb J.* **1999**, *13*, 1510-1510.

(56) Schlereth, D. D. *J Electroanal. Chem.* **1999**, *464*, 198-207.

(57) Schwarz, T.; Yeung, D.; Hawkins, E.; Heaney, P.; Mcdougall, A. *Trends Biotechnol.* **1991**, *9*, 339-340.

(58) Devries, E. F. A.; Schasfoort, R. B. M.; Vanderplas, J.; Greve, J. *Biosens. Bioelectron.* **1994**, *9*, 509-514.

(59) Jordan, C. E.; Frutos, A. G.; Thiel, A. J.; Corn, R. M. *Anal. Chem.* **1997**, *69*, 4939-4947.

(60) Peterlinz, K. A.; Georgiadis, R. M.; Herne, T. M.; Tarlov, M. J. *J. Am. Chem. Soc.* **1997**, *119*, 3401-3402.

(61) Thiel, A. J.; Frutos, A. G.; Jordan, C. E.; Corn, R. M.; Smith, L. M. *Anal. Chem.* **1997**, *69*, 4948-4956.

(62) Kuhn, C.; Muller, F.; Melle, C.; Nasheuer, H. P.; Janus, F.; Deppert, W.; Grosse, F. *Oncogene* **1999**, *18*, 769-774.

(63) Kukanskis, K.; Elkind, J.; Melendez, J.; Murphy, T.; Miller, G.; Garner, H. *Anal. Biochem.* **1999**, *274*, 7-17.

(64) Wink, T.; de Beer, J.; Hennink, W. E.; Bult, A.; van Bennekom, W. P. *Anal. Chem.* **1999**, *71*, 801-805.

(65) Davis, T. M.; Wilson, W. D. *Anal. Biochem.* **2000**, *284*, 348-353.

(66) Hall, D. *Handbook of Surface Plasmon Resonance* **2008**, 81-122.

(67) Wilson, W. D. *Science* **2002**, *295*, 2103-2105.

(68) Al Mubarak, Z. H.; Ramesh, R.; Liu, L.; Krishnan, S. *J. Colloid Interface Sci.* **2015**, *460*, 209-213.

(69) Mehand, M. S.; Srinivasan, B.; De Crescenzo, G. *Sci. Rep.* **2015**, *5*.

(70) Myszka, D. G. *Anal. Biochem.* **2004**, *329*, 316-323.

(71) Yakes, B. J.; Kanyuck, K. M.; DeGrasse, S. L. *Anal. Chem.* **2014**, *86*, 9251-9255.

(72) Kennedy, A. E.; Sheffield, K. S.; Eibl, J. K.; Murphy, M. B.; Vohra, R.; Scott, J. A.; Ross, G. M. *J. Biomol. Screening* **2016**, *21*, 96-100.

(73) Munoz, E. M.; Lorenzo-Abalde, S.; Gonzalez-Fernandez, A.; Quintela, O.; Lopez-Rivadulla, M.; Riguera, R. *Biosens. Bioelectron.* **2011**, *26*, 4423-4428.

(74) Nakamoto, K.; Kurita, R.; Sekioka, N.; Niwa, O. *Chem. Lett.* **2008**, *37*, 698-699.

(75) Aizawa, H.; Tozuka, M.; Kurosawa, S.; Kobayashi, K.; Reddy, S. M.; Higuchi, M. *Anal. Chim. Acta* **2007**, *591*, 191-194.

(76) Kawazumi, H.; Gobi, K. V.; Ogino, K.; Maeda, H.; Miura, N. *Sens. Actuators, B* **2005**, *108*, 791-796.

(77) Keegan, J.; O'Kennedy, R.; Crooks, S.; Elliott, C.; Brandon, D.; Danaher, M. *Anal. Chim. Acta* **2011**, *700*, 41-48.

(78) Zuo, X. L.; Xiao, Y.; Plaxco, K. W. *J. Am. Chem. Soc.* **2009**, *131*, 6944-6945.

(79) Sharma, A. K.; Heemstra, J. M. *J. Am. Chem. Soc.* **2011**, *133*, 12426-12429.

(80) Ruscito, A.; DeRosa, M. C. *Front. Chem.* **2016**, *4*, 14.

(81) Yang, K. A.; Barbu, M.; Halim, M.; Pallavi, P.; Kim, B.; Kolpashchikov, D. M.; Pecic, S.; Taylor, S.; Worgall, T. S.; Stojanovic, M. N. *Nat. Chem.* **2014**, *6*, 1003-1008.

(82) Wang, J. L.; Munir, A.; Zhou, H. S. *Talanta* **2009**, *79*, 72-76.

(83) Wang, Q.; Huang, J. H.; Yang, X. H.; Wang, K. M.; He, L. L.; Li, X. P.; Xue, C. Y. *Sens. Actuators, B* **2011**, *156*, 893-898.

(84) Wang, J. L.; Zhou, H. S. *Anal. Chem.* **2008**, *80*, 7174-7178.

(85) Zou, F.; Wu, B. P.; Wang, X. X.; Chen, Y. Y.; Koh, K.; Wang, K. M.; Chen, H. X. *Sens. Actuators, B* **2017**, *241*, 160-167.

(86) Kim, S.; Lee, H. J. *Anal. Chem.* **2017**, *89*, 6624-6630.

(87) Wang, J. L.; Munir, A.; Zhu, Z. Z.; Zhou, H. S. *Anal. Chem.* **2010**, *82*, 6782-6789.

(88) Li, X. M.; Wang, Y.; Wang, L. L.; Wei, Q. L. *Chem. Commun.* **2014**, *50*, 5049-5052.

(89) Law, W. C.; Yong, K. T.; Baev, A.; Prasad, P. N. *ACS Nano* **2011**, *5*, 4858-4864.

(90) Lisi, S.; Scarano, S.; Fedeli, S.; Pascale, E.; Cicchi, S.; Ravelet, C.; Peyrin, E.; Minunni, M. *Biosens. Bioelectron.* **2017**, *93*, 289-292.

(91) Wang, Q.; Li, Q.; Yang, X. H.; Wang, K. M.; Du, S. S.; Zhang, H.; Nie, Y. J. *Biosens. Bioelectron.* **2016**, *77*, 1001-1007.

(92) Lee, E. G.; Park, K. M.; Jeong, J. Y.; Lee, S. H.; Baek, J. E.; Lee, H. W.; Jung, J. K.; Chung, B. H. *Anal. Biochem.* **2011**, *408*, 206-211.

(93) Zagorodko, O.; Spadavecchia, J.; Serrano, A. Y.; Larroulet, I.; Pesquera, A.; Zurutuza, A.; Boukherroub, R.; Szunerits, S. *Anal. Chem.* **2014**, *86*, 11211-11216.

(94) Singh, M.; Holzinger, M.; Tabrizian, M.; Winters, S.; Berner, N. C.; Cosnier, S.; Duesberg, G. S. *J. Am. Chem. Soc.* **2015**, *137*, 2800-2803.

(95) Ghrera, A. S.; Pandey, M. K.; Malhotra, B. D. *Biosens. Bioelectron.* **2016**, *80*, 477-482.

(96) Malic, L.; Sandros, M. G.; Tabrizian, M. *Anal. Chem.* **2011**, *83*, 5222-5229.

(97) Liang, R. P.; Yao, G. H.; Fan, L. X.; Qiu, J. D. *Anal. Chim. Acta* **2012**, *737*, 22-28.

(98) Fenzl, C.; Hirsch, T.; Baeumner, A. J. *Anal. Chem.* **2015**, *87*, 11157-11163.

(99) He, L.; Musick, M. D.; Nicewarner, S. R.; Salinas, F. G.; Benkovic, S. J.; Natan, M. J.; Keating, C. D. *J. Am. Chem. Soc.* **2000**, *122*, 9071-9077.

(100) Zeng, S.; Baillargeat, D.; Ho, H. P.; Yong, K. T. *Chem. Soc. Rev.* **2014**, *43*, 3426-3452.

(101) Hong, X.; Hall, E. A. H. *Analyst* **2012**, *137*, 4712-4719.

(102) Szunerits, S.; Spadavecchia, J.; Boukherroub, R. *Rev. Anal. Chem.* **2014**, *33*, 153-164.

(103) Yang, C. T.; Wu, L.; Bai, P.; Thierry, B. *J. Mater. Chem. C* **2016**, *4*, 9897-9904.

(104) Wang, J. L.; Wang, F.; Zou, X. Q.; Xu, Z. A.; Dong, S. J. *Electrochem. Commun.* **2007**, *9*, 343-347.

(105) Lai, E. P. C.; Fafara, A.; VanderNoot, V. A.; Kono, M.; Polsky, B. *Can. J. Chem.* **1998**, *76*, 265-273.

(106) Haupt, K.; Mosbach, K. *Chem. Rev.* **2000**, *100*, 2495-2504.

(107) Kugimiya, A.; Takeuchi, T. *Biosens. Bioelectron.* **2001**, *16*, 1059-1062.

(108) Matsui, J.; Akamatsu, K.; Hara, N.; Miyoshi, D.; Nawafune, H.; Tamaki, K.; Sugimoto, N. *Anal. Chem.* **2005**, *77*, 4282-4285.

(109) Zheng, R.; Cameron, B. D. *Proc. SPIE* **2010**, *7577*, 75770A.

(110) Xu, X. Y.; Tian, X. G.; Cai, L. G.; Xu, Z. L.; Lei, H. T.; Wang, H.; Sun, Y. M. *Anal. Methods* **2014**, *6*, 3751-3757.

(111) Cenci, L.; Andreetto, E.; Vestri, A.; Bovi, M.; Barozzi, M.; Iacob, E.; Busato, M.; Castagna, A.; Girelli, D.; Bossi, A. M. *J. Nanobiotechnol.* **2015**, *13*, 51.

(112) Gupta, B. D.; Shrivastav, A. M.; Usha, S. P. *Sensors* **2016**, *16*, 1381.

(113) Li, S. P.; Yang, M.; Zhou, W. F.; Johnston, T. G.; Wang, R.; Zhu, J. S. *Appl. Surf. Sci.* **2015**, *355*, 570-576.

(114) Ding, X. J.; Cheng, W.; Li, Y. J.; Wu, J. L.; Li, X. M.; Cheng, Q.; Ding, S. J. *Biosens. Bioelectron.* **2017**, *87*, 345-351.

Chapter 2 Functionalized Gold Nanoparticle Enhanced Competitive Assay for Sensitive Detection of Metabolite Using Surface Plasmon Resonance Imaging

2.1 Introduction

The development of sensor based approaches for the detection and quantitative measurement of small molecules (MW < 1000 Da) is impacting areas such as environmental monitoring[1,2] and human health[3,4]. For example, the measurement of small-molecule metabolites is a research area with increasing interest due to the promise of using the information for diagnostic purposes.[4-8] Currently, the major advances in the identification and quantification of metabolites are being driven by work that uses nuclear magnetic resonance[9-12] (NMR) and mass spectrometry[10,11,13,14] (MS). These powerful techniques are producing and will continue to produce metabolite profiles[8] that can be linked to disease state. It is expected that the diagnosis and treatment of an expanded number of diseases will be greatly aided by the determination of the quantities of metabolites in a panel. At that point, facile, rapid and quantitative multiplexed sensing platforms for small molecule metabolites will be important. The work presented here describes the development of a small molecule assay on a detection platform that satisfies the requirements noted above.

Surface plasmon resonance (SPR) is an optical sensing technique first developed in 1990s.[1,15] It can provide label-free, real-time, sensitive, and quantitative information of bio-molecular interactions.[1] The technique is based upon detection of a change in dielectric constant within a few hundreds nanometers[1] of a metal-solution interface and

has been broadly applied to measure larger biomolecules such as proteins[16-21] and nucleic acids[22-25]. It is widely known that the direct detection of low molecular weight species with SPR is very challenging due to the small refractive index change induced by the adsorption of a monolayer of small molecules. There have been reports of the direct detection of small molecules but such demonstrations are sporadic and these measurements generally suffer from low signal intensity and poor sensitivity.[26,27] The challenges of measuring small molecules with SPR may be addressed by the application of nanomaterials as labels.[28,29] For example, metal nanoparticles[16,25,30], magnetic nanoparticles[31,32], quantum dots[33], and carbon-based nanomaterials[22,34] have been used to amplify the signal in different assays, but most of time such demonstrations are limited to the detection of proteins and nucleic acids, not metabolites. In addition, studies have shown that an indirect detection format[35,36], either inhibition or competition, can be utilized to measure targets like steroid hormones[37,38], toxins[39], drugs[40], and explosive residues[41]. Based on the previous work, a pathway for the inclusion of SPR as a sensing platform for metabolites may be realized by employing metal nanoparticle reagents in a competitive format.

In this chapter, we have developed a gold nanoparticle (AuNP) enhanced competitive assay to detect and quantitate folic acid (FA) using SPR imaging (SPRi). Folic acid, which is used in the prevention and treatment of folate deficiency and megaloblastic anemia[42] has been used as the target for a wide range of sensing strategies. Electrochemical techniques[43], surface enhanced Raman scattering (SERS)[44] as well as SPR[45] have been used to measure FA. The physiological levels of FA in human blood range from a few nanomolar (nM) to less than 50 nM.[42,46] Our assay incorporates an

immobilized layer of folate binding protein (FBP) as the sensing surface and 10 nm FA-functionalized AuNPs (FA-AuNP) as a competitive reagent. The FBP was tagged with polyhistidine (HIS_6) for facile immobilization to the SPRi chip surface. The relatively large size of the AuNP as well as previously reported plasmonic coupling between the particle and the SPR substrate[47,48] enable the measurement of very low surface coverages of adsorbed AuNPs. We demonstrate the applicability of this competitive assay to detect and quantitate FA in both the micromolar and nanomolar concentration ranges.

3.2 Experimental

Chemicals and Reagents. BSA (bovine albumin serum), folic acid (meeting USP testing specifications), DTSP (3, 3'-dithiodipropionic acid di(N-hydroxysuccinimide ester)), and DMSO (dimethyl sulfoxide, ≥ 99.9%) were all purchased from Sigma-Aldrich and used as received. HBS-P buffer (0.01 M HEPES, pH 7.4, 0.15 M NaCl, 0.005% v/v surfactant P20) and nickel chloride ($NiCl_2$) solution (0.5 mM) were purchased from GE Healthcare. 10 nm citrate-capped gold nanoparticle (AuNP) stock solution (5.7×10^{12} particles/mL, 9.47 nM) was purchased from Ted Pella, Inc. Anhydrous ethyl alcohol was obtained from Commercial Alcohols. Deionized (DI) (18 MΩ•cm)/filtered H_2O was from a NANOpure water purification system (Barnstead International, Dubuque, IA). 2-{2-[2-(1-mercaptoundec-11-yloxy)-ethoxy]-ethoxy}-ethoxy-nitrilotriacetic acid ($HS-(CH_2)_{11}-EG_3-NTA$) was purchased from ProChimia Surfaces. (Tridecafluoro-1,1,2,2-tetrahydrooctyl)-1-dimethylchlorosilane was purchased from United Chemical Technologies, Inc. Polyhistidine-tagged folic acid binding protein (FBP) and polyhistidine-tagged periplasmic binding protein for glutamine (GBP) were

expressed in *E. Coli*. Purified proteins were received in stock solutions of 18.3 μM in phosphate buffered saline (PBS, pH 7.4) for FBP and 34.2 mM in PBS buffer for GBP.

Complete Amino-Acid Sequence for Polyhistidine-Tagged Folic Acid Binding Protein (FBP). MGSSHHHHHH SSGLVVPRGS HMAFTPFPPR QPTASARLPL TLMTLDDWAL ATITGADSEK YMQGQVTADV SQMAEDQHLL AAHCDAKGKM WSNLRLFRDG DGFAWIERRS VREPQLTELK KYAVFSKVTI APDDERVLLG VAGFQARAAL ANLFSELPSK EKQVVKEGAT TLLWFEHPAE RFLIVTDEAT ANMLTDKLRG EAELNNSQQW LALNIEAGFP VIDAANSGQF IPQATNLQAL GGISFKKGCY TGQEMVARAK FRGANKRALW LLAGSASRLP EAGEDLELKM GENWRRTGTV LAAVKLEDGQ VVVQVVMNND MEPDSIFRVR DDANTLHIEP LPYSLEE

Complete Amino-Acid Sequence for Polyhistidine-Tagged Periplasmic Binding Protein for Glutamine (GBP). MGSSHHHHHH SSGLVPRGSH MADKKLVVAT DTAFVPFEFK QGDKYVGFDV DLWAAIAKEL KLDYELKPMD FSGIIPALQT KNVDLALAGI TITDERKKAI DFSDGYYKSG LLVMVKANNN DVKSVKDLDG KVVAVKSGTG SVDYAKANIK TKDLRQFPNI DNAYMELGTN RADAVLHDTP NILYFIKTAG NGQFKAVGDS LEAQQYGIAF PKGSDELRDK VNGALKTLRE NGTYNEIYKK WFGTEPKGS

Bacterial Strains, Growth conditions and Chemicals. *E. coli* strains XL10-Gold (Stratagene, USA) and BL21 (DE3) (Novagen Inc, USA) were used for all plasmid construction and protein expression studies described in this work. For plasmid construction, *E.coli* cells were grown in Luria-Bertani (LB) medium at 37 °C and selected using 50 mg/L ampicillin. For protein expression and purification, *E.coli* cells

were grown in LB medium at 25 °C. Ampicillin and IPTG were procured from Gold Biotechnology (St.Louis, MO, USA), while LB medium was prepared using Difco^{TM} LB broth Miller (BD Biosciences, Canada). Restriction enzymes were obtained from New England Biolabs (Pickering ON, Canada) and primer sequences were commercially synthesized from Integrated DNA Technologies (San Diego, USA). All molecular cloning manipulations were performed according to standard protocols described in the Molecular Cloning Manual (Sambrook and Russell 2001).[49]

Plasmid Construction. The DNA sequences coding for the Folate Binding Protein (ygfZ, EcoGene Accession Number: EG12685) and the Glutamine Binding Protein (glnH, EcoGene Accession Number: EG10386) were cloned into the protein expression plasmid pET15b (obtained from Novagen Inc, USA) in a sequential manner. The *ygfZ* and *glnH* coding sequences were PCR amplified using *E. coli* genomic DNA as a template using the primer pairs, *ygfZ*-FW1, -RW1 and *glnH*-FW1, -RW1, ligated into PCR 2.1-TOPO (Thermofisher Scientific, K45002), and appropriate number of clones were sequence verified to obtain plasmids PCR 2.1- *ygfZ* and PCR 2.1- *glnH*. These plasmids were double-digested using *Nde*I and *BamH*I and the DNA fragments corresponding to *ygfZ* and *glnH* were inserted into *Nde*I-*BamH*I digested pET15b. The ligation mixture was transformed into chemically-competent XL10-Gold cells and selected on LB medium which was supplemented with 50 mg/L ampicillin to identify the recombinant plasmids harboring the *ygfZ* and *glnH* coding sequences. Selected colonies harbouring the recombinant plasmid were confirmed via plasmid isolation followed by an *Nde*I-*BamH*I digest. These plasmids are hitherto referred to as pET15b-*ygfZ* and pET15b-*glnH*.

Protein Expression. Chemically competent cells of the *E. coli* protein expression strain BL21 (DE3) were transformed with pET15b-*ygfZ* and pET15b- *glnH* and transformants were selected on LB medium supplemented with 50 mg/L ampicillin (LB amp_{50}). The starter culture was initiated by inoculating 25 mL of LB amp_{100} with a single colony and the cells were cultured overnight at 37 °C, 225 rpm. After this incubation period, all of the starter culture was added to 500 ml pre-warmed LB $amp_{100,}$ and the cells were shaken as before for 4-5 h (OD_{600}=0.4-0.8). At this point, expression of recombinant proteins was induced by addition of 2 mM IPTG and the cells were allowed to grow overnight at 25 °C, 250 rpm. Following overnight incubation, the cells were pelleted by centrifugation at 11,000 g for 30 minutes at 4 °C. The supernatant was discarded and cell pellets stored at -20 °C.

Protein Purification Using Ni-NTA Affinity Column. The cell pellet was thawed, resuspended in 50 mL of Lysis buffer (25 mM Tris, 100 mM NaCl, pH 6.5-7.5) and sonicated on ice (six times for 15 s at 42% amplitude). Following sonication, the cell lysate was centrifuged for 802000 g for 60 minutes at 10 °C and the protein supernatant was transferred to a clean tube. The protein supernatant was carefully loaded onto a Ni-NTA chromatography column (pre-cleaned by washing with lysis buffer) and allowed to flow-through under the influence of gravity. The chromatography column was washed sequentially with five volumes of wash buffer 1 (0.1% Triton X-100 with 25mM Tris 25 mM NaCl pH 6.5-7.5) and 5 volumes of wash buffer 2 (25 mM Tris 25 mM NaCl pH 6.5 to 7.5). The imidazole gradient was re-established by washing the column with approximately 50 mL of 25 mM Tris 25 mM NaCl pH 6.5 - 7.5. Following this final wash, the protein bound to Ni-NTA beads was eluted by setting up a gradient from 0 to

500mM imidazole in 25 mM Tris 25 mM NaCl pH 6.5 to 7.5, and running the gradient at a flow rate of 1.0 mL/minute for 90 minutes (BioLogic LP, BIORAD). The gradient was run for an additional 15 minutes at a flow rate of 1.0 mL/minute of 500mM imidazole 25mM Tris 25mM NaCl pH 6.5 to 7.5 to ensure all protein was eluted off the column. Protein fractions were collected at 1.2-minute intervals (BioLogic Biofrac Fraction Collector, BIORAD). The different fractions were checked on an SDS-PAGE gel (4% stacking, 14 % resolving), the relevant fractions enriched for purified protein were pooled and dialyzed into 100 mM sodium phosphate buffer (pH 7). Protein concentration was determined by the MicroBCA Protein assay kit (product number 23235, Thermo Scientific, Rockford, USA).

Fabrication of SPRi Chip with Multiple Au Spots. An SF-10 glass sheet (100 mm × 100 mm × 1 mm) was purchased from Schott Glass. The sheet was cut into small square substrates (18 mm × 18 mm). The substrates were cleaned using hot piranha solution (1:4 30% H_2O_2:H_2SO_4) followed by thorough rinsing with DI water. Substrates were blown dry using Ar gas. [*Warning: Piranha solution should be handled with extreme care; it is a strong oxidant and reacts violently with many organic materials. It also presents an explosion danger. All work should be performed under a fume hood with appropriate personal safety equipment*.] The cleaned and dried substrates were mounted to a mask that expose nine 2 mm diameter round spots and placed into the chamber of a thermal evaporator (Torr International Inc., New Windsor, NY). Metal films of chromium (2 nm) and gold (42 nm) were sequentially coated on the glass substrate through the mask. After removal from the evaporator, the substrates were then exposed to a vapor of (tridecafluoro-1,1,2,2-tetrahydrooctyl)-1-dimethylchlorosilane under reduced

pressure for 24 h to create a hydrophobic background on the glass surface. The SPRi chips were stored in a desiccator under vacuum at room temperature until use.

10 nm Folic Acid Conjugated Gold Nanoparticle (FA-AuNP) Preparation. We first added 10 μL of 10 mM DTSP in DMSO to 1 mL of 10 nm citrate-capped AuNP solution, and incubated the mixed solution for 30 min at room temperature. After incubation, 10 μL of 10 mM FA in DMSO solution was added to the mixed solution. The final solution was left overnight (~17 h) at room temperature. Then the solution was centrifuged for 45 min at 14000 rpm (Eppendorf a5417R microcentrifuge). The supernatant was carefully removed to avoid any loss of the particles. The AuNP pellet was re-dispersed in 1 mL DI water as a stock FA-AuNP solution (9.47 nM based on the initial AuNP concentration). The suspended FA-AuNP solution was stored at 4 °C until use.

UV-Vis Spectroscopy. Extinction spectra of 10 nm citrate-capped AuNP solution, DTSP-AuNP solution, and FA-AuNP solution were obtained by UV-Vis measurements. 500 μL of each AuNP solution was added to a quartz micro-cuvette for the measurement. All solutions were measured in transmission mode in a double-beam Perkin-Elmer Lambda 35 instrument. DI water was used as a reference for each measurement.

Raman Spectroscopy. Raman spectra were collected with Renishaw inVia Raman microscope fitted with a liquid cell accessory for solution samples. Spectra were collected using 633 nm excitation from a HeNe laser with 10 mW of power through a 50× objective. The integration time was 50 s. 500 μL of 100 μM folic acid solution and 500 μL of 9.47 nM FA-NPs solution were measured separately.

SPRi Measurement of FBP Immobilization. Prior to the modification, the homemade SPRi chip was rinsed with pure ethanol and DI water and dried under an argon gas flow. For the chip modification, the four spots at the corner of the square substrate were used as the control group and the remaining five spots in the middle were the experimental group. A 2.5 μL droplet of 1 mg/mL BSA solution was added to the control spots and a 2.5 μL droplet of 2 mM HS-$(CH_2)_{11}$-EG_3-NTA solution was added to the experimental spots. The chips with the solution droplets were stored in a humid petri dish for 7 h at room temperature. Then, the chip was rinsed with DI water and dried under argon gas flow. Each spot of the chip was next activated by adding 2.5 μL of 0.5 mM $NiCl_2$ solution for 1 h in the petri dish. After rinsing and drying, the chip was mounted to the SPRi instrument (Horizon SPRimager, GWC Technologies, Madison, MI) to measure the adsorption of FBP to the SH-NTA self-assembled monolayer (SAM). The apparatus has been described in detail elsewhere.[50,51] FBP solutions at five different concentrations (91.5 nM, 183 nM, 366 nM, 915 nM, and 1830 nM) were prepared from the stock FBP solution (18.3 μM). All FBP solutions were sequentially exposed to the chip surface from the most diluted solution to the least diluted solution, and the real-time SPRi sensorgram was recorded and analyzed.

SPRi Measurement of 10 nm FA-AuNP Binding. FBP and GBP were immobilized on the SPRi chip as described above to study the binding of the 10 nm FA-AuNPs. 2.5 μL of 3.42 μM GBP solution and 1.83 μM FBP solution were added to the corresponding control and experimental spots after the formation of SH-NTA SAMs and activation with Ni^{2+}. After overnight (~17 h) incubation, the chip was rinsed with DI water and dried under argon gas flow. Seven 10 nm FA-AuNP solutions with dilution

factors 1/2, 1/3, 1/5, 1/10, 1/25, 1/50, and 1/100 from the 9.47 nM 10 nm FA-AuNP stock solution were sequentially flowed into the instrument and a real-time SPRi sensorgram was obtained.

Competitive Assays. All Assays were carried out on chips containing FBP (target) and GBP (control) spots. As described below, two concentration ranges of FA were studies. For the higher (μM) range, a solution of 9.47 nM (before mixing) 10 nm FA-AuNPs was mixed with FA standard solutions of 2, 20, 50, and 100 μM) in a 1:1 volume ratio. The solutions were flowed into the instrument for measurements separately and SPRi sensorgram was obtained for each mixed solution. For the physiologically relevant concentration range (nM), we decreased the concentration of 10 nm FA-AuNP solution to 379 pM (before mixing). The NP solution was mixed with FA standard solutions 5, 10, 20, 30, 40, 50 nM concentrations. The solutions were flowed into the instrument continuously from the most concentrated to the least concentrated and the SPRi sensorgram was obtained.

Scanning Electron Microscopy (SEM). SPRi chip surfaces with FBP and GBP after exposure to the least concentrated (94.7 pM) 10 nm FA-AuNP solution were air-dried, mounted on specimen stubs and examined under Philip/FEI XL 30 SEM at 10.0 kV.

All Langmuir isotherms were obtained by fitting the experimental data using the one-site ligand-binding model included in SigmaPlot (Systat Software, Inc., San Jose, CA). All error bars shown here represent standard deviation of triplicate measurements.

2.3 Results and Discussion

A variety of assay formats have been developed for recognition based measurement of small molecules for SPR using antibodies and aptamers.[27,35-39] The competitive format for folic acid (FA) demonstrated in this work is shown in Figure 2.1. A layer of polyhistidine labeled folate-binding protein (FBP) is immobilized to the gold SPRi chip through complexation with Ni^{2+} and an NTA-terminated monolayer. A sample solution containing FA will be spiked with AuNPs conjugated to FA. The free FA in solution then competes with the AuNPs for FBP binding sites. The binding of the relatively large AuNP to the SPR chip can easily be measured. The relationship between the concentration of free FA and SPRi signal is expected to result in a calibration curve with a negative slope as shown in Figure 2.1.

The binding between FA and FBP has been previously characterized.[52-54] Thus, the location of the binding site is known, enabling the expression of FBP in *E. Coli.* with the HIS_6 tag in a region of the protein that ensures the optimum orientation upon immobilization. Nitrilotriacetic acid (NTA) functional groups combined with Ni^{2+} are commonly used to capture or immobilize histidine tagged proteins.[55] Thus, the SPRi chip was modified with a HS-$(CH_2)_{11}$-EG_3-NTA self-assembled monolayer (SAM). The immobilization of FBP to the chip was optimized by measuring the amount of FBP adsorbed with SPRi for five different solution concentrations (91.5 nM, 183 nM, 366 nM, 915 nM, and 1.83 μM). Figure 2.2A contains a continuous flow SPRi sensorgram for the adsorption of FBP to chip surface. FBP exhibits specific adsorption to the NTA-terminated monolayer (NTA SAM), while insignificant adsorption is observed for BSA

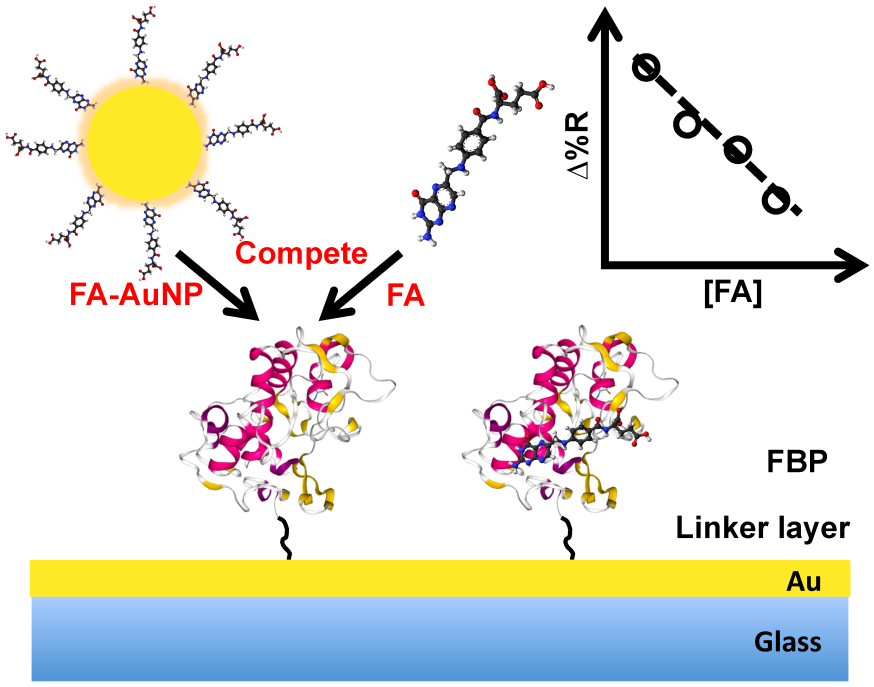

Figure 2.1 Schematic illustration of the folic acid (FA) functionalized gold nanoparticle (FA-AuNP) enhanced competitive assay for the detection of FA. Polyhistidine tagged folic acid binding protein (FBP) is immobilized to chip surface via Ni^{2+}-NTA coordination chemistry. FA-AuNP and FA compete for surface binding sites provided by FBP.

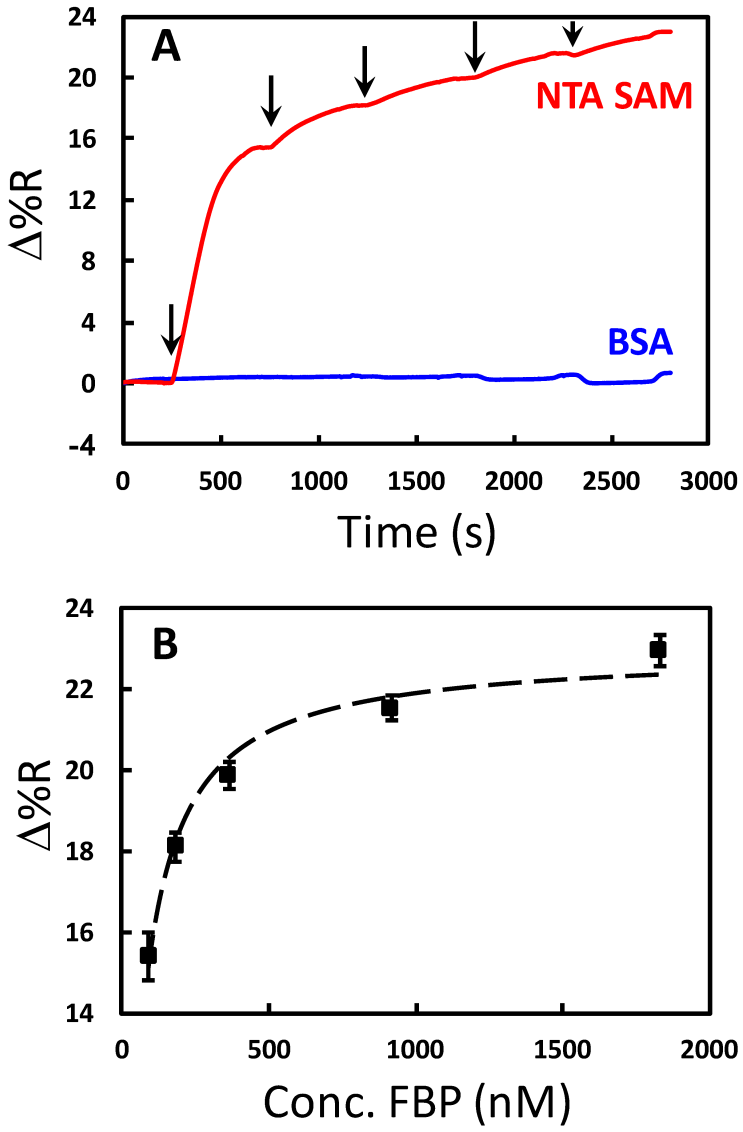

Figure 2.2 Results tracking the immobilization of polyhistidine tagged folic acid binding protein (FBP) to SPRi chip surface. (A) Typical continuous SPRi sensorgrams for FBP adsorption for different concentrations (91.5 nM, 183 nM, 366 nM, 915 nM, and 1830 nM) to NTA SAMS (red) and a BSA control surface (blue). The arrows indicate the injection of each concentration. (B) A plot of SPR signal vs. FBP solution concentration for adsorption to NTA SAM. The symbols are the data points and the dashed line is the least-squares fit of the Langmuir adsorption isotherm equation ($R^2 = 0.9803$).

control spots. A plot of the SPR signal vs. FBP solution concentration is shown in Figure 2.2B. These data are fit to a Langmuir adsorption isotherm with a reasonable correlation (R^2 = 0.9803). The dissociation constant (K_d) for the FBP adsorption was determined from this fit to be 47 ± 5 nM, which is a similar order of magnitude to the values reported in the literature (14 ± 1 nM).[55] The results of the experiment in Figure 2.2 allow us to conclude that the FBP is being immobilized via the expected complexation interaction and to control the surface density of FBP through solution concentration.

The FA conjugated AuNPs were prepared through a 2-step reaction. First, a monolayer of the bifunctional ligand DTSP was adsorbed to 10 nm AuNPs. This ligand has been used previously to conjugate anitibodies to AuNPs.[56] FA was then linked to the AuNP via an amide bond formed from the reaction of the free amine on the FA and the succinimide ester group on the DTSP. The FA conjugated AuNPs (FA-AuNPs) were characterized by UV-Vis spectroscopy and Raman spectroscopy. Figure 2.3A shows the extinction spectra of the initial 10 nm citrate-AuNP, the DTSP modified AuNP, and the FA-AuNP. All spectra exhibit typical localized surface plasmon resonance (LSPR) peaks characteristic of 10 nm AuNPs. The extinction maxima of the LSPR band red shifts from 518 nm (citrate-AuNP) to 520 nm (DTSP-AuNP) to 522 nm (FA-AuNP), indicative of a variation of the dielectric constant of the surface layer due to each modification step. Figure 2.3B contains Raman spectra of FA in solution and a solution of the FA-AuNPs. Bands characteristic of FA are clearly observed in the spectra of the FA-AuNPs consistent with the association of the FA with the AuNPs. The UV-Vis results combined with the Raman results confirm the successful conjugation of FA to the 10 nm AuNP surface. The FA-AuNPs showed colloidal stability when diluted in buffer solution, which

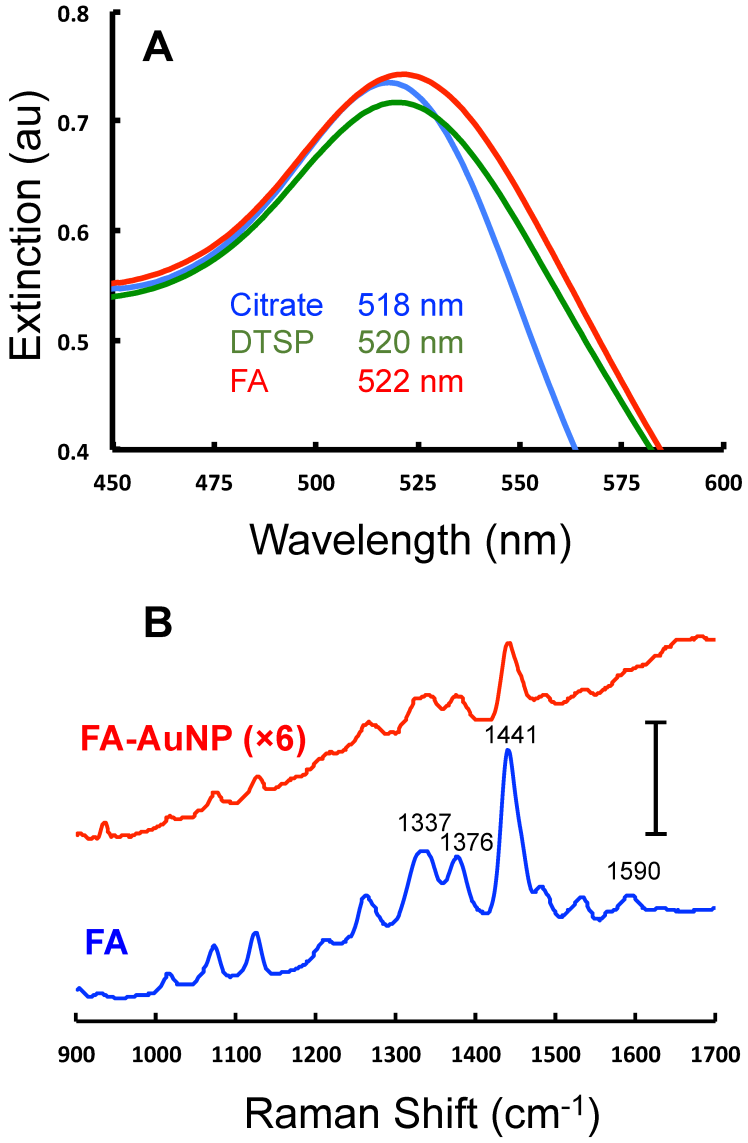

Figure 2.3 UV-Vis and Raman characterization of 10 nm AuNPs. (A) Extinction spectra for as-purchased 10 nm citrate capped AuNP (blue), the AuNP after modification with DTSP-AuNP (green), and FA-AuNP (red). The axes are expanded around the maximum extinction for clarity and λmax values for the three spectra are listed. (B) Raman spectra of FA in solution (100 μM in water, blue) and a solution of 9.47 nM of FA-AuNP (red, signal ×6). The scale bar is equivalent to 40,000 counts.

is critical for a useful reagent in a competitive assay format.

The binding of FA-AuNPs to FBP immobilized on the chip surface was studied to aid in the design of the competitive assay. The chip contained 9 spots modified with either FBP or the control protein (Figure 2.4). The control spots in this experiment were modified identically to the FBP spots with histidine tagged glutamine binding protein (GBP). Part A of Figure 2.5 contains a continuous SPRi sensorgram for various concentrations of FA-AuNPs interacting with the chip. An increase in the SPRi signal is observed at the FBP spots with each successive higher concentration. As shown in Figure 2.5A, insignificant adsorption of the FB-AuNPs was observed at the GBP spots. Thus, the FA-AuNPs bind specifically to the immobilized FBP. Figure 2.5B contains a plot of the baseline corrected SPRi signal vs the concentration of the modified AuNPs and the corresponding Langmuir fit. The K_d value determined from the fit is 0.8 ± 0.2 nM. The binding of large polymeric nanoparticles conjugated with FA to immobilized FBP was previously studied.[57] The density of the FA on the polymer particles was relatively low (< 15% of the surface covered) and the K_d for this system was reported as 800 nM. We estimate a coverage of FA of at least 80% speculate that the interaction between our FA-AuNPs and the immobilized FBP may involve multivalent interactions resulting in a tighter binding and a lower K_d, but this is not examined further in this work. Scanning electron microscopy (SEM) analysis of the chips following FA-AuNP adsorption reveals that very low coverages of the AuNPs are being detected at the lower concentrations (Figure 2.6). For example, we estimate a coverage of 1.3×10^9 particles/cm^2 resulting from the adsorption from 94.7 pM solutions. Coverages as low as 2×10^7 particles/cm^2 have been detected in the initial reports of

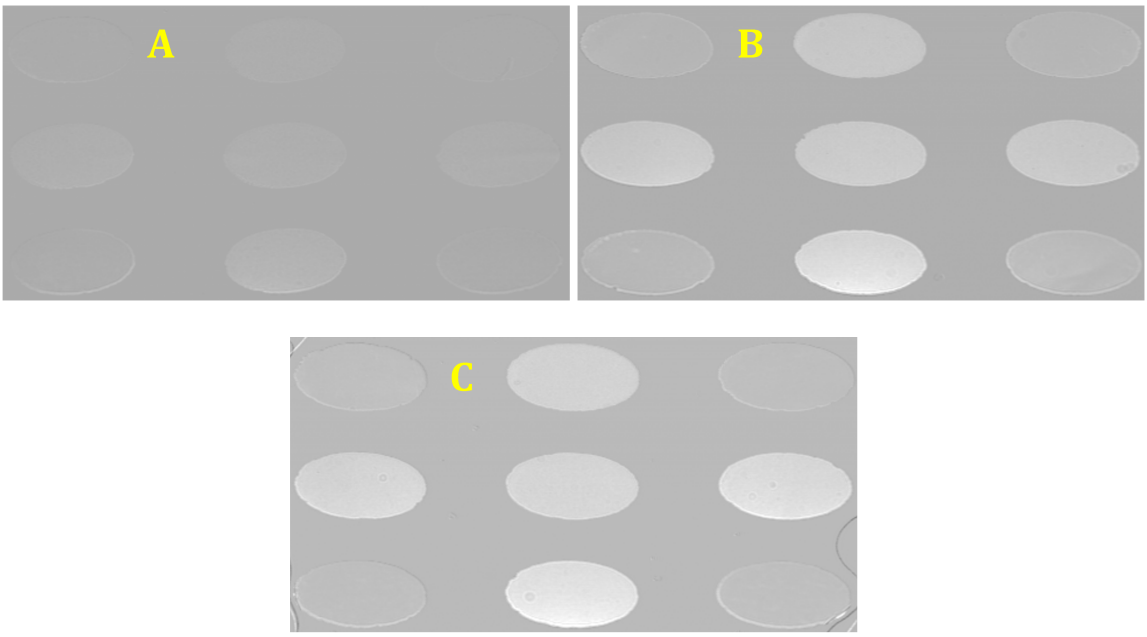

Figure 2.4 Representative difference images of three SPRi chip surfaces after exposure to 1 nM (A), 2 nM (B), and 2.5 nM (C) FA-AuNP solutions, respectively. Each chip surface was modified with FBP (five spots in the middle) and GBP (four spots at the corners) before exposure to FA-AuNP solution.

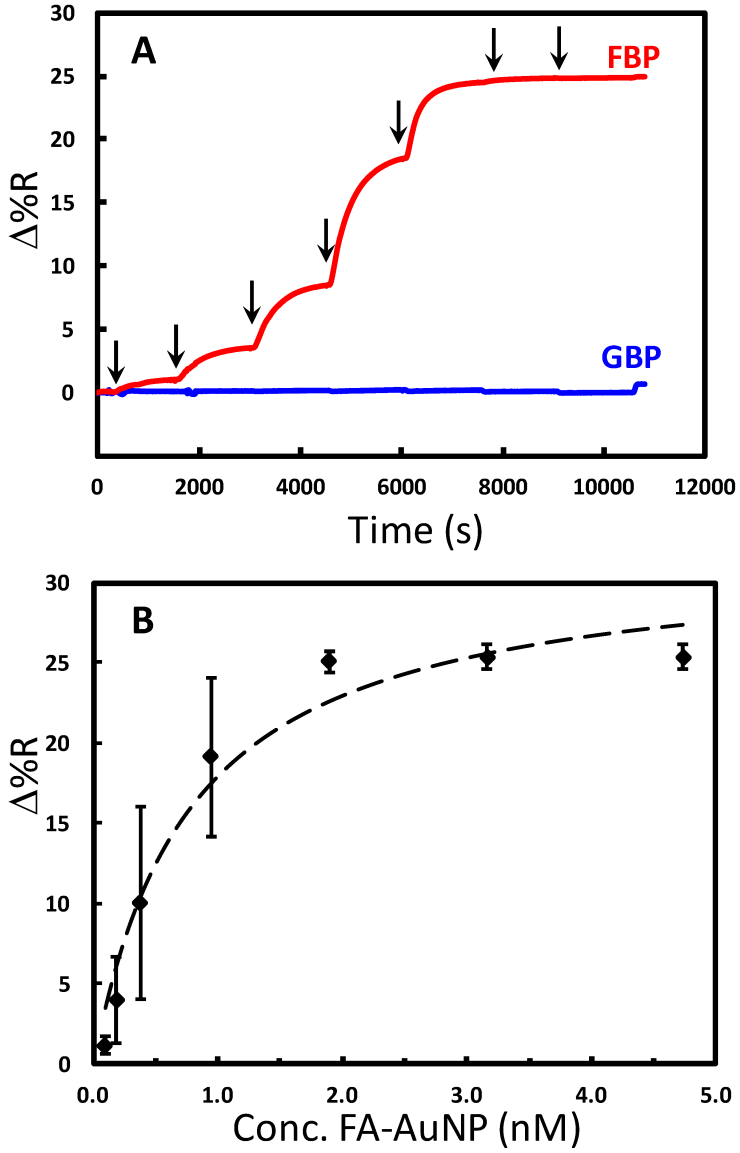

Figure 2.5 Binding of 10 nm FA-AuNP to FBP. (A) Typical continuous SPRi sensorgrams for the adsorption of FA-AuNPs at seven concentrations (94.7 pM – 4.74 nM) to FBP surface (red) and GBP control surface (blue). The arrows indicate the injection of each concentration. (B) A plot of SPR signal vs. FA-AuNP solution concentration for adsorption to FBP. The symbols are the data points and the dashed line is the least-squares fit of the Langmuir adsorption isotherm equation ($R^2 = 0.9648$).

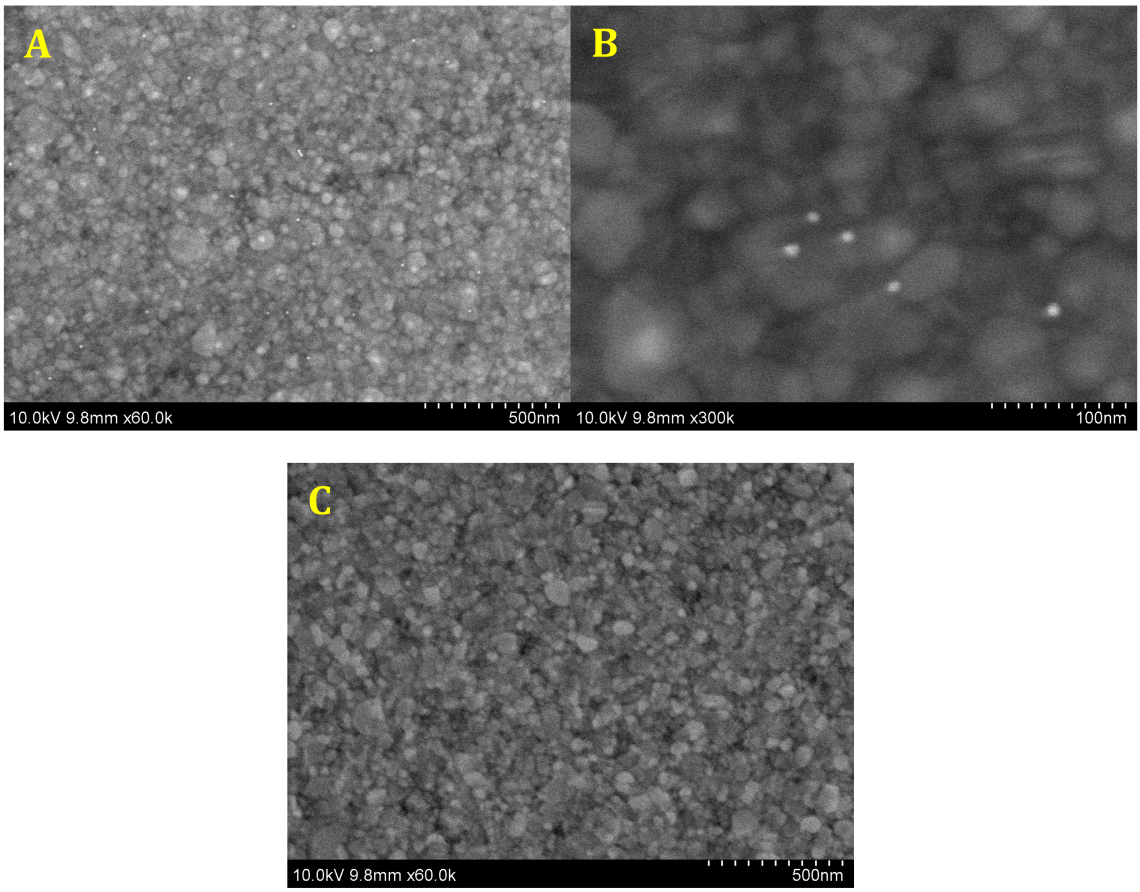

Figure 2.6 Scanning electron micrographs of SPRi Au chip surfaces with (A, B) FBP (× 60.0 k, × 300 k) and (C) GBP (× 60.0 k) after exposure to 94.7 pM of the as-prepared 10 nm FA-AuNPs.

AuNP enhanced SPR.[48] This lays a solid foundation for the following analytical performance of the competitive assay.

As noted above, FA has been the subject of many measurement studies. A variety of techniques have quantified FA in the concentration range of pM to hundreds of μM.[43-45] The physiological concentration range of FA is 10-50 nM in blood. The proposed competitive assay was first tested to detect and quantitate FA in the μM concentration range as a proof-of-principle. Solutions containing a fixed concentration of FA-AuNP (4.74 nM, after mixing) and various concentrations of free FA (2, 20, 50, 100 μM) were allowed to compete with the FBP on the chip. The SPRi sensorgrams for this experiment exhibit a maximum signal for solutions with no free FA present and lower signals for solutions of higher free FA concentration (Figure 2.7A). Figure 2.8A is a plot of SPRi signal vs free FA concentration in the concentration range that provided the highest sensitivity. This plot is analogous to a dose-response curve in drug screening or enzyme inhibition assays.[58] The plot is linear with the expected negative slope and serves as a calibration curve for free FA in solution. Figure 2.8A can be used to successfully quantitate FA in the range of 2 to 100 μM.

It is known from the application of other competitive assays that the dose-response curve can be shifted to lower target concentrations by decreasing the concentration of the competitor.[59,60] Thus, the quantitative concentration range can be varied in our competitive assay by changing the concentration of the FA-AuNP reagent. Qualitatively, considering Figure 2.5B, a concentration of 4.74 nM results in the saturation coverage of the AuNPs. Thus, a relatively high concentration of free FA would be required to compete for the FBP sites. Lowering the concentration of the FA-

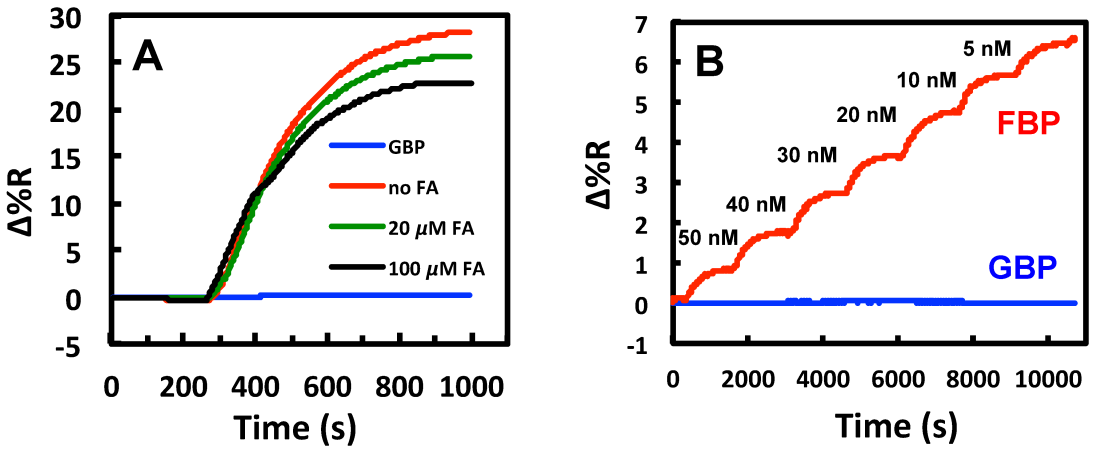

Figure 2.7 Representative sensorgrams for analysis of FA in the (A) micromolar (μM) range and (B) nanomolar (nM) range. The concentrations of 10 nm FA-AuNPs in the competitive assays are (A) 4.74 nM and (B) 189 pM.

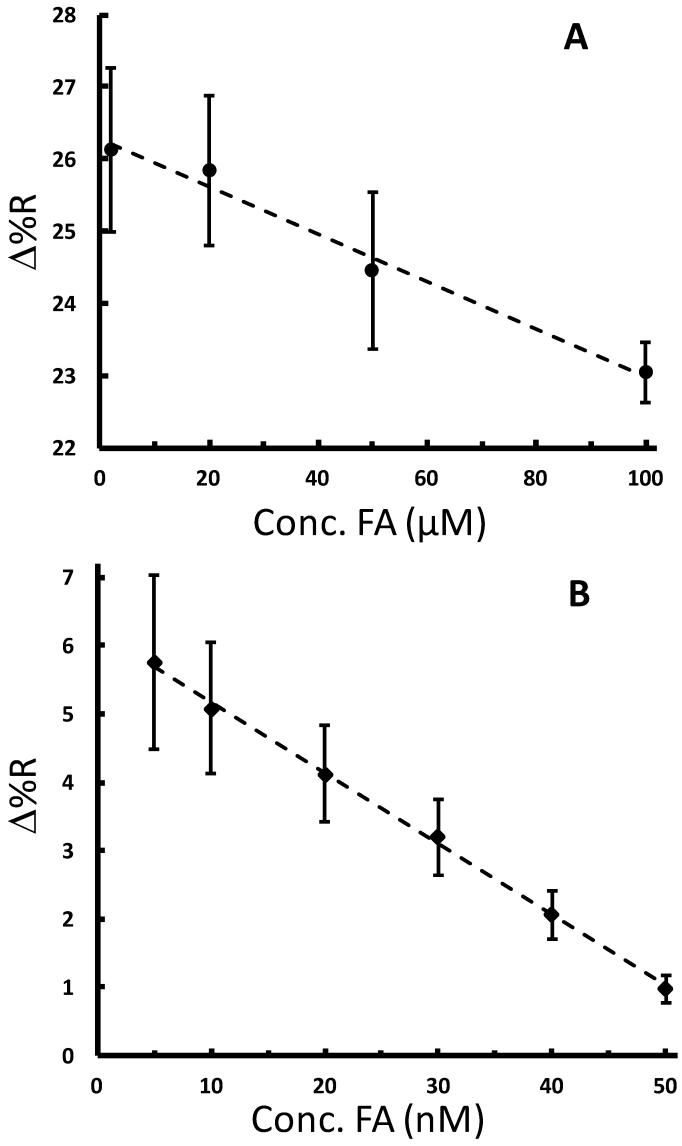

Figure 2.8 Calibration curves for the determination of FA using the AuNP based competitive assay. (A) Plot of SPRi signal vs concentration of free FA for the assay where the concentration of FA-AuNPs was 4.74 nM. (B) Plot of SPRi signal vs concentration of free FA for the assay where the concentration of FA-AuNPs was 189 pM. In both plots, the symbols represent the mean of at least 3 repetitive measurements and the error bars are the standard deviation. The dashed line through the data is the linear least-squares fit.

AuNPs to the sub-nM range should provide higher sensitivity as suggested by the isotherm in Figure 2.5B. Accordingly, we incorporated a fixed concentration of the FA-AuNP 189 pM (after mixing) into solutions with free FA concentrations in range of 5 to 50 nM. Analysis of the corresponding sensorgrams (Figure 2.7B) yields the plot in Figure 2.8B. A linear curve is obtained in the range of 5 to 50 nM, which contains the physiological concentration range of interest. A previous investigation that employed an antibody based competitive assay with SPR detection measured folic acid in fortified food from 16 nM to 1269 nM.[45] Our study shows that small molecule conjugated AuNPs are flexible reagents for competitive assays with tunable concentration range.

2.4 Conclusion

We have developed a SPRi-based competitive assay for detection and quantitation of FA. The assay is flexible and is able to quantitate FA at physiological concentrations. The introduction of FA-AuNPs overcomes the sensitivity challenge of detecting small molecules with SPR due to the higher mass of the functionalized AuNP. The FA-AuNPs are stable in buffer, and exhibit strong and specific binding to the FA binding protein, thanks to the chemistries used to immobilize the protein and conjugate FA to AuNP surface. The competitive assay shows excellent analytical performance to detect and quantitate FA in the physiological concentration range, with a linear range from 5 nM to 50 nM. In addition, the dynamic range can be adjusted by simply changing the concentration of the FA-AuNP solution used for the competition. Most importantly, this competitive assay can be applied to other small-molecule metabolites as well, which paves the way for future multiplexed detection of metabolites using SPRi platform.

2.5 References

(1) Homola, J. *Chem. Rev.* **2008**, *108*, 462-493.

(2) Long, F.; Zhu, A.; Shi, H. *Sensors* **2013**, *13*, 13928-13948.

(3) Lee, J. R.; Choi, J.; Shultz, T. O.; Wang, S. X. *Anal. Chem.* **2016**, *88*, 7457-7461.

(4) Hilvo, M.; de Santiago, I.; Gopalacharyulu, P.; Schmitt, W. D.; Budczies, J.; Kuhberg, M.; Dietel, M.; Aittokallio, T.; Markowetz, F.; Denkert, C.; Sehouli, J.; Frezza, C.; Darb-Esfahani, S.; Braicu, E. I. *Cancer Res.* **2016**, *76*, 796-804.

(5) Seviour, T.; Doyle, L. E.; Lauw, S. J.; Hinks, J.; Rice, S. A.; Nesatyy, V. J.; Webster, R. D.; Kjelleberg, S.; Marsili, E. *Chem. Commun.* **2015**, *51*, 3789-3792.

(6) Lam, C. W.; Law, C. Y.; Sze, K. H.; To, K. K. *Clin. Chim. Acta* **2015**, *438*, 24-28.

(7) Park, M. H.; Igarashi, K. *Biomol. Ther.* **2013**, *21*, 1-9.

(8) Fernie, A. R.; Trethewey, R. N.; Krotzky, A. J.; Willmitzer, L. *Nat. Rev. Mol. Cell Biol.* **2004**, *5*, 763-769.

(9) Ravanbakhsh, S.; Liu, P.; Bjorndahl, T. C.; Mandal, R.; Grant, J. R.; Wilson, M.; Eisner, R.; Sinelnikov, I.; Hu, X.; Luchinat, C.; Greiner, R.; Wishart, D. S. *PLoS One* **2015**, *10*, e0124219.

(10) Bouatra, S.; Aziat, F.; Mandal, R.; Guo, A. C.; Wilson, M. R.; Knox, C.; Bjorndahl, T. C.; Krishnamurthy, R.; Saleem, F.; Liu, P.; Dame, Z. T.; Poelzer, J.; Huynh, J.; Yallou, F. S.; Psychogios, N.; Dong, E.; Bogumil, R.; Roehring, C.; Wishart, D. S. *PLoS One* **2013**, *8*, e73076.

(11) Psychogios, N.; Hau, D. D.; Peng, J.; Guo, A. C.; Mandal, R.; Bouatra, S.; Sinelnikov, I.; Krishnamurthy, R.; Eisner, R.; Gautam, B.; Young, N.; Xia, J.; Knox, C.; Dong, E.; Huang, P.; Hollander, Z.; Pedersen, T. L.; Smith, S. R.; Bamforth, F.; Greiner,

R.; McManus, B.; Newman, J. W.; Goodfriend, T.; Wishart, D. S. *PLoS One* **2011**, *6*, e16957.

(12) Larive, C. K.; Barding, G. A., Jr.; Dinges, M. M. *Anal. Chem.* **2015**, *87*, 133-146.

(13) Chen, D.; Su, X.; Wang, N.; Li, Y.; Yin, H.; Li, L.; Li, L. *Sci. Rep.* **2017**, *7*, 40543.

(14) Zhao, S.; Luo, X.; Li, L. *Anal. Chem.* **2016**, *88*, 10617-10623.

(15) Couture, M.; Zhao, S. S.; Masson, J. F. *Phys. Chem. Chem. Phys.* **2013**, *15*, 11190-11216.

(16) Wu, B.; Jiang, R.; Wang, Q.; Huang, J.; Yang, X.; Wang, K.; Li, W.; Chen, N.; Li, Q. *Chem. Commun.* **2016**, *52*, 3568-3571.

(17) Patra, A.; Ding, T.; Engudar, G.; Wang, Y.; Dykas, M. M.; Liedberg, B.; Kah, J. C.; Venkatesan, T.; Drum, C. L. *Small* **2016**, *12*, 1174-1182.

(18) Bockova, M.; Chadtova Song, X.; Gedeonova, E.; Levova, K.; Kalousova, M.; Zima, T.; Homola, J. *Anal. Bioanal. Chem.* **2016**, *408*, 7265-7269.

(19) Jang, H. R.; Wark, A. W.; Baek, S. H.; Chung, B. H.; Lee, H. J. *Anal. Chem.* **2014**, *86*, 814-819.

(20) Maisonneuve, M.; Valsecchi, C.; Wang, C.; Brolo, A. G.; Meunier, M. *Biosensors & Bioelectronics* **2015**, *63*, 80-85.

(21) Martinez-Perdiguero, J.; Retolaza, A.; Bujanda, L.; Merino, S. *Talanta* **2014**, *119*, 492-497.

(22) Zagorodko, O.; Spadavecchia, J.; Serrano, A. Y.; Larroulet, I.; Pesquera, A.; Zurutuza, A.; Boukherroub, R.; Szunerits, S. *Anal. Chem.* **2014**, *86*, 11211-11216.

(23) Zhou, W. J.; Chen, Y.; Corn, R. M. *Anal. Chem.* **2011**, *83*, 3897-3902.

(24) Scarano, S.; Ermini, M. L.; Spiriti, M. M.; Mascini, M.; Bogani, P.; Minunni, M. *Anal. Chem.* **2011**, *83*, 6245-6253.

(25) He, L.; Musick, M. D.; Nicewarner, S. R.; Salinas, F. G.; Benkovic, S. J.; Natan, M. J.; Keating, C. D. *J. Am. Chem. Soc.* **2000**, *122*, 9071-9077.

(26) Li, S.; Yang, M.; Zhou, W.; Johnston, T. G.; Wang, R.; Zhu, J. *Appl. Surf. Sci.* **2015**, *355*, 570-576.

(27) Liang, W.; Wang, S.; Festa, F.; Wiktor, P.; Wang, W.; Magee, M.; LaBaer, J.; Tao, N. *Anal. Chem.* **2014**, *86*, 9860-9865.

(28) Zeng, S.; Baillargeat, D.; Ho, H. P.; Yong, K. T. *Chem. Soc. Rev.* **2014**, *43*, 3426-3452.

(29) Bolduc, O. R.; Masson, J. F. *Anal. Chem.* **2011**, *83*, 8057-8062.

(30) Jain, P. K.; Huang, X.; El-Sayed, I. H.; El-Sayad, M. A. *Plasmonics* **2007**, *2*, 107-118.

(31) Liang, R. P.; Yao, G. H.; Fan, L. X.; Qiu, J. D. *Anal. Chim. Acta* **2012**, *737*, 22-28.

(32) Wang, J.; Munir, A.; Zhu, Z.; Zhou, H. S. *Anal. Chem.* **2010**, *82*, 6782-6789.

(33) Malic, L.; Sandros, M. G.; Tabrizian, M. *Anal. Chem.* **2011**, *83*, 5222-5229.

(34) Singh, M.; Holzinger, M.; Tabrizian, M.; Winters, S.; Berner, N. C.; Cosnier, S.; Duesberg, G. S. *J. Am. Chem. Soc.* **2015**, *137*, 2800-2803.

(35) Mitchell, J. *Sensors* **2010**, *10*, 7323-7346.

(36) Wang, J.; Zhou, H. S. *Anal. Chem.* **2008**, *80*, 7174-7178.

(37) Yockell-Lelievre, H.; Bukar, N.; McKeating, K. S.; Arnaud, M.; Cosin, P.; Guo, Y.; Dupret-Carruel, J.; Mougin, B.; Masson, J. F. *Analyst* **2015**, *140*, 5105-5111.

(38) Miyashita, M.; Shimada, T.; Miyagawa, H.; Akamatsu, M. *Anal. Bioanal. Chem.* **2005**, *381*, 667-673.

(39) Meneely, J. P.; Sulyok, M.; Baumgartner, S.; Krska, R.; Elliott, C. T. *Talanta* **2010**, *81*, 630-636.

(40) Zhao, S. S.; Bukar, N.; Toulouse, J. L.; Pelechacz, D.; Robitaille, R.; Pelletier, J. N.; Masson, J. F. *Biosens. Bioelectron.* **2015**, *64*, 664-670.

(41) Shankaran, D. R.; Kawaguchi, T.; Kim, S. J.; Matsumoto, K.; Toko, K.; Miura, N. *Anal. Bioanal. Chem.* **2006**, *386*, 1313-1320.

(42) Greenberg, J. A.; Bell, S. J.; Guan, Y.; Yu, Y. H. *Rev. Obstet. Gynecol.* **2011**, *4*, 52-59.

(43) Akbar, S.; Anwar, A.; Kanwal, Q. *Anal. Biochem.* **2016**, *510*, 98-105.

(44) Ren, W.; Fang, Y. X.; Wang, E. K. *ACS Nano* **2011**, *5*, 6425-6433.

(45) Caselunghe, M. B.; Lindeberg, J. *Food Chem.* **2000**, *70*, 523-532.

(46) Lermo, A.; Fabiano, S.; Hernandez, S.; Galve, R.; Marco, M. P.; Alegret, S.; Pividori, M. I. *Biosens. Bioelectron.* **2009**, *24*, 2057-2063.

(47) Mock, J. J.; Hill, R. T.; Degiron, A.; Zauscher, S.; Chilkoti, A.; Smith, D. R. *Nano Lett.* **2008**, *8*, 2245-2252.

(48) Lyon, L. A.; Musick, M. D.; Natan, M. J. *Anal. Chem.* **1998**, *70*, 5177-5183.

(49) Sambrook, J.; Russell, D. W. *Molecular Cloning: A Laboratory Manual*; Cold Spring Harbor Laboratories Press: Cold Spring Harbor, New York, 2001.

(50) Nelson, B. P.; Frutos, A. G.; Brockman, J. M.; Corn, R. M. *Anal. Chem.* **1999**, *71*, 3928-3934.

(51) Kanda, V.; Kariuki, J. K.; Harrison, D. J.; McDermott, M. T. *Anal. Chem.* **2004**, *76*, 7257-7262.

(52) Campbell, I. G.; Jones, T. A.; Foulkes, W. D.; Trowsdale, J. *Cancer Res.* **1991**, *51*, 5329-5338.

(53) Elwood, P. C. *J. Biol. Chem.* **1989**, *264*, 14893-14901.

(54) Sadasivan, E.; Rothenberg, S. P. *J. Biol. Chem.* **1989**, *264*, 5806-5811.

(55) Knecht, S.; Ricklin, D.; Eberle, A. N.; Ernst, B. *J. Mol. Recognit.* **2009**, *22*, 270-279.

(56) Wang, G.; Lipert, R. J.; Jain, M.; Kaur, S.; Chakraboty, S.; Torres, M. P.; Batra, S. K.; Brand, R. E.; Porter, M. D. *Anal. Chem.* **2011**, *83*, 2554-2561.

(57) Stella, B.; Arpicco, S.; Peracchia, M. T.; Desmaele, D.; Hoebeke, J.; Renoir, M.; D'Angelo, J.; Cattel, L.; Couvreur, P. *J. Pharm. Sci.* **2000**, *89*, 1452-1464.

(58) Auld, D. S.; Farmen, M. W.; Kahl, S. D.; Kriauciunas, A.; McKnight, K. L.; Montrose, C.; Weidner, J. R. In *Assay Guidance Manual*, Sittampalam, G. S.; Coussens, N. P.; Brimacombe, K.; Grossman, A.; Arkin, M.; Auld, D.; Austin, C.; Baell, J.; Bejcek, B.; Chung, T. D. Y.; Dahlin, J. L.; Devanaryan, V.; Foley, T. L.; Glicksman, M.; Hall, M. D.; Hass, J. V.; Inglese, J.; Iversen, P. W.; Lal-Nag, M.; Li, Z.; McGee, J.; McManus, O.; Riss, T.; Trask, O. J., Jr.; Weidner, J. R.; Xia, M.; Xu, X., Eds.: Bethesda (MD), 2004; pp 129-154.

(59) McManus, O. B.; Garcia, M. L.; Weaver, D.; Bryant, M.; Titus, S.; Herrington, J. B. In *Assay Guidance Manual*, Sittampalam, G. S.; Coussens, N. P.; Brimacombe, K.; Grossman, A.; Arkin, M.; Auld, D.; Austin, C.; Baell, J.; Bejcek, B.; Chung, T. D. Y.; Dahlin, J. L.; Devanaryan, V.; Foley, T. L.; Glicksman, M.; Hall, M. D.; Hass, J. V.;

Inglese, J.; Iversen, P. W.; Lal-Nag, M.; Li, Z.; McGee, J.; McManus, O.; Riss, T.; Trask, O. J., Jr.; Weidner, J. R.; Xia, M.; Xu, X., Eds.: Bethesda (MD), 2004; pp 413-426.

(60) Bee, C.; Abdiche, Y. N.; Stone, D. M.; Collier, S.; Lindquist, K. C.; Pinkerton, A. C.; Pons, J.; Rajpal, A. *PLoS One* **2012**, *7*, e36261.

Chapter 3 A Universal Inhibition Surface Plasmon Resonance Immunosensor for Sensitive and Selective Detection of Small-Molecule Metabolite

3.1 Introduction

Small-molecule metabolites, the intermediates and products of metabolism, are now emerging as an important type of biomarker with the development of the field of metabolomics.[1,2] Metabolites sensing plays a key role in linking the metabolites profiles[3,4] to disease states. Thus, sensitive and selective detection of metabolites is critical for medical diagnostics. Compared to other biomarkers (proteins and nucleic acids), metabolites are small molecules with a molecular weight less than 1000 Da, which include amino acids, vitamins, nucleotides, hormones, and lipids.[5-8] Some difficulties exist in terms of designing metabolites sensing strategies: first, few molecular recognition elements (i.e. antibody or aptamer) with both good binding affinity and high specificity are available for small molecules; second, metabolites typically give very small direct detectable signal responses due to their sizes and low molecular weights. To this regards, sensitive and selective detection of small-molecule metabolites is challenging, especially when the physiological levels of targets fall to an extremely low concentration range, for example from picomolar (pM) to nanomolar (nM). Thus, facile, rapid, and quantitative multiplexed sensing platforms for small molecule metabolites will be important.

Surface plasmon resonance (SPR) is an optical sensing technique first developed in 1990s.[9] Due to its unique characteristics, including label-free, real-time, sensitive and quantitative to monitor bio-molecular interactions, SPR has found broad applications in

human health research[10-12], environmental monitoring[13,14], and homeland security[15]. This technique is very sensitive to the refractive-index change within a few hundreds nanometers of a metal-solution interface and has been widely applied to measure relatively large biomolecules like proteins and nucleic acids. There have been reports of the direct detection of small molecules using this technique but such demonstrations are sporadic probably due to the two difficulties mentioned above. People have incorporated a variety of nanomaterials in their assays to enhance the signal, thus to address the challenges associated with small molecules detection using SPR. Also, an indirect detection format, either inhibition or competition, may be utilized to tackle the challenges associated with direct detection of small molecules.

17β-estradiol (E2), the most potent form of mammalian estrogenic steroid hormones excreted by humans and domestic animals, is a category of endocrine disrupting compounds (EDCs).[16] EDCs are contaminants with increasing concerns due to their harmful effects on endocrine function of human and aquatic organisms.[17] E2 especially plays a big role in regulating the estrous female reproductive cycles.[18] The physiological levels of E2 in human blood range from 40 pM to 1.5 nM, depending on gender and age.[19] Therefore, a sensing strategy that enables sensitive and selective detection of E2 is key for reducing the deleterious effects associated with this type of EDCs. A few sensors have been developed to detect E2 in water samples, among which the transducing platforms are electrochemistry-based[20-22], colorimetry-based[23,24], and fluorescence-based techniques[25].

In this chapter, we have developed an indirect inhibition immunosensor based on SPR imaging for highly sensitive and selective detection of 17β-estradiol (E2) in the

physiological concentration range. Briefly, BSA-E2 conjugates are immobilized on the chip surface, which will compete with free E2 molecules in solution for the binding sites provided by anti-E2 monoclonal antibody (E2-Ab). Due to the inhibition mechanism of the strategy, the SPR signal response is inversely related to the concentration of E2, thus generating a calibration curve with a negative slope. The immobilization of BSA-E2 conjugate to gold chip surface was studied by SPR. The surface coverage of the BSA-E2 conjugate on E2-Ab binding were studied and optimized. It was found that the binding behavior of E2-Ab depends strongly on the surface coverage of BSA-E2 conjugate. Also, the best concentration of E2-Ab for the measurement of E2 was chosen. Under optimized conditions (21% surface coverage of BSA-E2 conjugate and 5 μg/mL of E2-Ab), the sensor shows good applicability to detect and quantitate E2 from 10 pM to 2 nM, covering the physiological levels of E2. The calibration curve has a sigmoidal shape with a negative slope, showing good sensitivity and reproducibility. Finally, the specificity of the immunosensor was studied using estrone (E1) as a potential interference. The immunosensor demonstrates high specificity to measure E2, showing negligible influence by E1.

3.2 Experimental

Chemicals and Reagents. BSA (bovine albumin serum), β-estradiol 6-(O-caboxymethyl)oxime : BSA (BSA-E2) conjugate, 17β-estradiol (E2), estrone (E1), and PBS (phosphate buffered saline) 10× concentrate were all purchased from Sigma-Aldrich and used as received. Estradiol monoclonal antibody [4S11(BGN/06/8811)] isolated from mouse was purchased from Thermo Fisher Scientific. 2-(2-{2-[2-(2-[2-(11-mercapto-

undecyloxy)-ethoxy]-ethoxy)-ethoxy]-ethoxy}-ethoxy)-ethoxy-acetic acid (HS-$(CH_2)_{11}$-EG_6-OCH_2-COO-NHS) was obtained from ProChimia Surfaces. (Tridecafluoro-1,1,2,2-tetrahydrooctyl)-1-dimethylchlorosilane was purchased from United Chemical Technologies. Anhydrous ethyl alcohol was obtained from Commercial Alcohols. Deionized (DI) water with a resistivity greater than 18 MΩ was filtered in a Barnstead Nanopure purification system.

Fabrication of SPRi Chip with Multiple Au Spots. An SF-10 glass sheet (100 mm × 100 mm × 1 mm) was purchased from Schott Glass. The sheet was cut into small square substrates (18 mm × 18 mm). The substrates were cleaned using hot piranha solution (1:4 30% H_2O_2:H_2SO_4) followed by thorough rinsing with DI water. Substrates were blown dry using Ar gas. [*Warning: Piranha solution should be handled with extreme care; it is a strong oxidant and reacts violently with many organic materials. It also presents an explosion danger. All work should be performed under a fume hood with appropriate personal safety equipment*.] The cleaned and dried substrates were mounted to a mask that expose nine 2 mm diameter round spots and placed into the chamber of a thermal evaporator (Torr International Inc., New Windsor, NY). Metal films of chromium (2 nm) and gold (42 nm) were sequentially coated on the glass substrate through the mask. After removal from the evaporator, the substrates were then exposed to a vapor of (tridecafluoro-1,1,2,2-tetrahydrooctyl)-1-dimethylchlorosilane under reduced pressure for 24 h to create a hydrophobic background on the glass surface. The SPRi chips were stored in a desiccator under vacuum at room temperature until use.

Immobilization of BSA-E2 Conjugate. The homemade SPRi chip was rinsed with pure ethanol and DI water and dried under an argon gas flow. A 2.5 μL droplet of 2

mM HS-$(CH_2)_{11}$-EG_6-OCH_2-COO-NHS solution was added to all gold spots of the chip. The modified chip with the solution droplets was stored in a humid petri dish overnight (~17 h) at room temperature to form a self-assembled monolayer (SAM). Then, the chip was rinsed with DI and dried under argon gas flow, then mounted to the SPRi instrument (Horizon SPRimager, GWC Technologies, Madison, MI) to measure the adsorption of BSA-E2 conjugate to the SH-NHS SAM. The apparatus has been described in detail previously.[26,27] BSA-E2 conjugate solutions at 7 different concentrations (1 μg/mL, 5 μg/mL, 10 μg/mL, 20 μg/mL, 50 μg/mL, 100 μg/mL, and 200 μg/mL) were prepared in PBS. The running buffer for SPRi measurement was PBS as well. The prepared 7 BSA-E2 conjugate solutions were sequentially exposed to the chip surface from the lowest concentration (1 μg/mL) to the highest concentration (200 μg/mL). A real-time SPRi sensorgram was thus recorded. Quantitative data were acquired by subtracting SPRi signal response at the steady state after one solution injection from the baseline. The data points were analyzed using the one-site ligand-binding model included in SigmaPlot (Systat Software, Inc., San Jose, CA), and corresponding least-squares fit of the Langmuir adsorption isotherm equation was obtained.

Estradiol Antibody (E2-Ab) Binding to BSA-E2 Conjugate under Different Surface Coverage. Similarly, a SH-NHS SAM was first formed on the chip surface. BSA and BSA-E2 conjugate were used as the control group and experimental group respectively. The chip surface was patterned by adding a droplet of 2.5 μL of 1 mg/mL BSA solution and a droplet of 2.5 μL of BSA-E2 conjugate solution at a certain concentration for 2 h. To optimize the BSA-E2 conjugate concentration, thus the surface coverage of BSA-E2 conjugate on the chip surface, we tested 3 different concentrations

of BSA-E2 conjugate solution: 1 μg/mL, 20 μg/mL, and 50 μg/mL. The surface coverage of BSA-E2 conjugate at a specific concentration can be calculated using the signal response at this concentration and the maximum signal response obtained from the Langmuir adsorption isotherm fit. Then, the unreacted NHS group was blocked by adding a droplet of 2.5 μL of 1 mg/mL BSA solution to all gold spots for 1 h. E2-Ab solutions at 5 different concentrations (5 μg/mL, 10 μg/mL, 25 μg/mL, 50 μg/mL, and 200 μg/mL) were continuously exposed to BSA (control) and BSA-E2 conjugate (experimental) surfaces. The real-time SPRi sensorgram was recorded and analyzed.

Sensing Performance. For E2 detection, we modified the SPRi chip surface the same way as we did for E2-Ab binding measurement, as described above. Under optimized concentration of E2-Ab and surface coverage of BSA-E2 conjugate, 7 mixed solutions of 5 μg/mL of E2-Ab solution and E2 standard solutions at a different concentrations (10 pM, 50 pM, 100 pM, 250 pM, 500 pM, 1 nM, and 2 nM) were pumped into the SPRi instrument continuously from the most concentrated E2 solution (2 nM) to the least concentrated E2 solution (10 pM). The quantitative data points were obtained by subtracting SPRi signal intensity after each mixed solution injection from the baseline. For sensor specificity study, estrone (E1) was chosen as a possible interference due to its similar structure to E2. Briefly, we mixed 5 μg/mL of E2-Ab solution with E1 solution at a certain concentration. Five E1 solutions at different concentrations (1 pM, 10 pM, 100 pM, 1 nM, 10 nM) were tested. By comparing the binding results for E1 to that for E2, we can evaluate the specificity of the immunosensor.

3.3 Results and Discussion

Detecting and quantitating 17β-estradiol (E2) in the physiological concentration range plays an important role in monitoring sexual development and various clinical conditions, as mentioned previously. The concentration of E2 in human blood is very low (<1.5 nM) compared to most metabolites, depending on gender and age.[19] Therefore, to monitor the level of E2, a sensor that is both sensitive and specific is highly required. Figure 3.1 illustrates the analytical principle of the indirect inhibition immunosensor: first, a competing reagent – BSA-E2 conjugate – is immobilized to the gold chip surface via NHS coupling; second, the specific binding of E2-Ab to BSA-E2 conjugate is explored by SPRi measurement, using BSA as the control; third, BSA-E2 conjugate on chip surface and E2 in solutions compete for binding sites provided by E2-Ab. We should note that the detectable signal response comes from the binding of E2-Ab to the BSA-E2 conjugate pre-immobilized on the chip surface. Based on the competition mechanism, a calibration curve with a negative slope can be generated. We optimized a few key factors before performing the immunosensor to detect and quantitate E2. These factors include the surface coverage of BSA-E2 conjugate on chip surface and the concentration of the E2-Ab used for the competition.

To design a biosensor, researchers need to consider the choice and immobilization of a molecular recognition element. Based on the initial design of the bio-interface on the chip surface (Figure 3.1), instead of immobilizing the molecular recognition element (E2-Ab), we immobilize the competing reagent (BSA-E2 conjugate) to the chip surface. As we know, the molecular weight of an antibody (150 kDa) is approximately two times

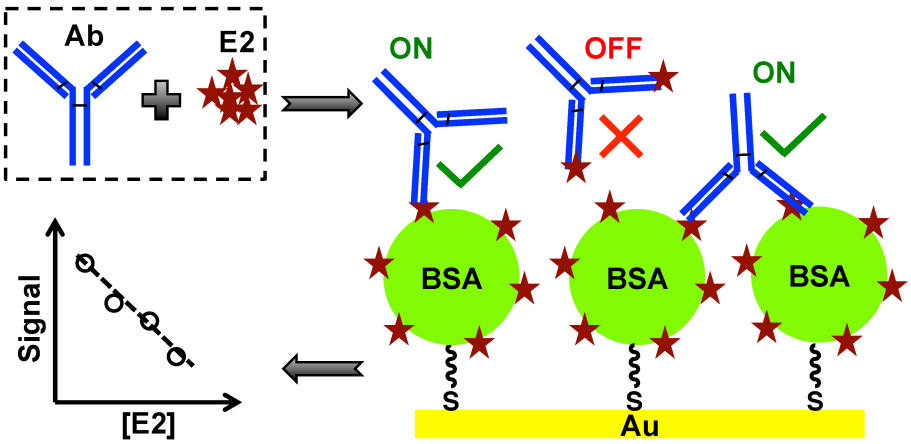

Figure 3.1 Schematic illustration of the analytical principle of the indirect inhibition immunosensor for 17β-estradiol (E2) analysis using surface plasmon resonance imaging. A SH-NHS monolayer containing ethylene glycol group was first formed on the gold chip surface, then BSA-E2 conjugates were immoblized via NHS coupling. BSA-E2 conjugates and free E2 molecules in solution compete for binidng sites provided by anti-E2 monocolonal antibody. A calibration curve with negative slope can be obtained due to the inhibition mechanism.

greater than a BSA molecule (~70 kDa). By immobilizing BSA-E2 conjugate instead of E2-Ab on the chip surface, we are detecting the binding of E2-Ab and thus can generate a higher SPRi signal response. A SH-NHS self-assembled monolayer (SAM) was formed on the chip surface due to strong Au-S interaction[28,29]. The reaction between the NHS ester group of the monolayer and primary amine ($-NH_2$) group in BSA-E2 conjugate results in the attachment of the BSA-E2 conjugate. Figure 3.2 shows the SPR measurement results for the BSA-E2 conjugate adsorption to SH-NHS SAM including some ethylene glycol groups. The continuous adsorption of BSA-E2 conjugate is observed, and the SPR signal increases as the increase of the BSA-E2 conjugate concentration from 1 μg/mL to 200 μg/mL (Figure 3.2A). A plot of SPR signal vs. BSA-E2 conjugate solution concentration is shown in Figure 3.2B. The data points fits well with the Langmuir adsorption equation ($R^2 = 0.9691$), and the dissociation constant (K_d) for the binding between BSA-E2 conjugate and SH-NHS monolayer is determined from the fit to be 8.8 ± 1.7 μg/mL or 126 ± 24 nM (assuming the molecular weight of BSA-E2 conjugate is 70 kDa). The K_d value determined here is comparable (same order of magnitude) to the dissociation constants reported previously for other proteins and thiol SAMs interactions.[30,31] For example, the K_d value for the interaction of streptavidin and EDC/NHS activated 11-mercaptoundecanoic acid SAM was reported to be 262 nM[30]. So these results give us confidence that BSA-E2 conjugate can be immobilized to the chip surface via interaction with SH-NHS monolayer. In addition, we can calculate the surface coverage of BSA-E2 conjugate at any concentration using the following equation: $\Theta = \Delta\%R/\Delta\%R_{max}$ (Θ is the surface coverage of BSA-E2 conjugate; $\Delta\%R$ is SPRi signal intensity generated by BSA-E2 conjugate adsorption at a specific concentration; $\Delta\%R_{max}$

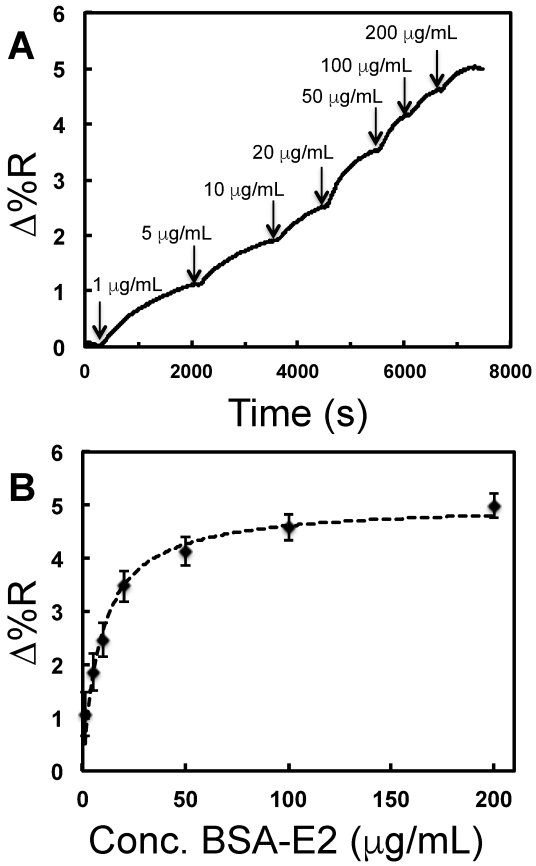

Figure 3.2 Results tracking the adsorption of BSA-E2 conjugate to SH-NHS monolayer on gold chip surface. (A) A representative sensorgram for continuous adsorption of 7 BSA-E2 conjugate solutions with different concentrations. The arrows indicate the injection of each concentration. (B) A plot of SPR signal vs. BSA-E2 conjugate solution concentration for adsorption to SH-NHS monolayer. The symbols are the data points and the dashed line is the least-squares fit of the Langmuir adsorption isotherm equation (R^2 = 0.9691). The error bars represent standard deviation of triplicate measurements.

is maximum SPRi signal intensity obtained from the Langmuir adsorption isotherm). In this case, $\Delta\%R_{max}$ equals to 5.02 ± 0.22 based on the fitting results. Thus 1 μg/mL, 5 μg/mL, 10 μg/mL, 20 μg/mL, 50 μg/mL, 100 μg/mL, and 200 μg/mL of BSA-E2 conjugate solutions give a surface coverage of 0.21, 0.37, 0.49, 0.69, 0.82, 0.91, and 0.99, respectively.

According to previous studies on heterogeneous antigen-antibody interactions[32], we suspect that the surface coverage/density of BSA-E2 conjugate may influence the binding of E2-Ab to BSA-E2 conjugate, thus affect the signal intensity for the following sensing performance. Since the surface coverage/density of the BSA-E2 conjugate on chip surface can be quantitatively controlled by changing the concentration of BSA-E2 conjugate solution (Figure 3.2B), it is feasible and important to study the effect of the surface coverage of BSA-E2 conjugate on E2-Ab binding. Three surface coverage of BSA-E2 conjugate were chosen: 0.21 (1 μg/mL), 0.49 (10 μg/mL), and 0.82 (50 μg/mL). Figure 3.3 demonstrates the binding results of 5 μg/mL of E2-Ab to BSA-E2 conjugate under these different surface coverage. As shown in Figure 3.3A, E2-Ab exhibits specific binding to BSA-E2 conjugate, while insignificant binding is observed for BSA control spots. More important, the SPR signal response decreases with the increase of surface density of BSA-E2 conjugate, as the surface coverage of 21 percent BSA-E2 conjugate gives the highest signal among the three. Figure 3.3B contains three plots of SPR signal vs. E2-Ab concentrations (5 μg/mL, 10 μg/mL, 25 μg/mL, 50 μg/mL, and 200 μg/mL). The data points fit well with Langmuir isotherm adsorption equation with reasonable correlations. The same trend is also observed directly in the difference image of the chip surface (Figure 3.3C), as the gold spots with a surface coverage of 21 percent

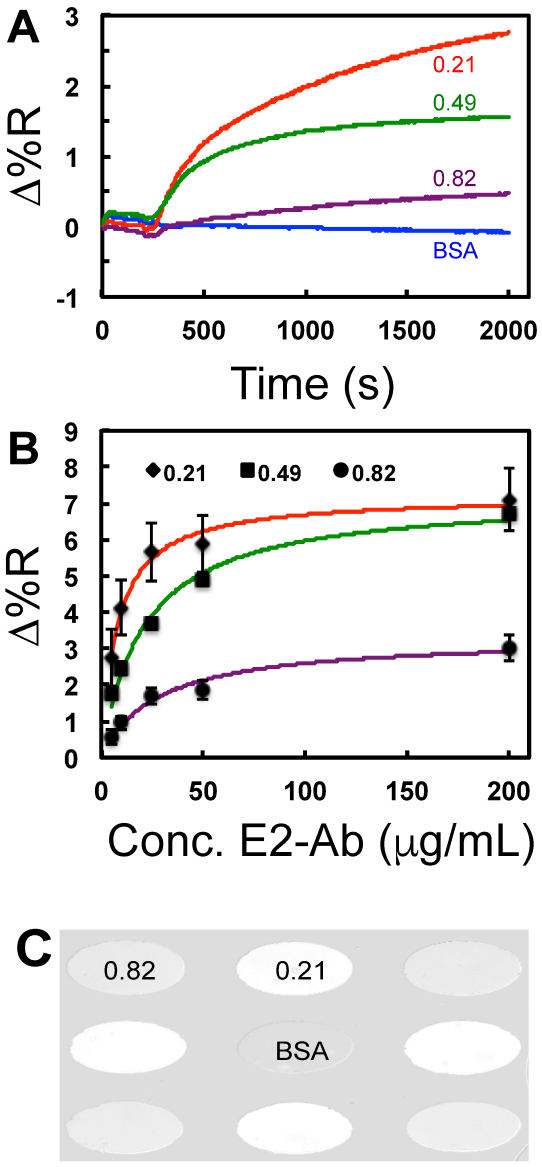

Figure 3.3 Binding of E2-Ab to BSA-E2 conjugate under different surface coverage (S.C.) on gold chip surface. (A) Representative sensorgrams for the binding of 5 μg/mL E2-Ab to BSA control (blue) and BSA-E2 conjugate at three S.C.: 0.21 (red), 0.49 (green), and 0.82 (purple). (B) Plots of SPR signal vs. E2-Ab concentrations (5 μg/mL, 10 μg/mL, 25 μg/mL, 50 μg/mL, and 200 μg/mL). The symbols are the data points and the solid lines are the least-squares fits of the Langmuir isotherm adsorption equation. The error bars represent standard deviation of triplicate measurements. (C) A

representative difference image of the chip after E2-Ab binding to BSA (control) and BSA-E2 conjugate with 0.21 S.C. (four spots in the middle) and 0.82 S.C. (four spots at the corners).

Table 3.1 Curve-Fitting Parameters for E2-Ab Binding Curves Shown in Figure 3.3B

[BSA-E2] (μg/mL)	Surface Coverage	K_d (μg/mL)	K_d (nM)	$\Delta\%R_{max}$	R
1	**0.21**	7.8 ± 1.0	**52 ± 7**	7.2 ± 0.2	0.9921
10	**0.49**	20.8 ± 3.5	**139 ± 23**	7.2 ± 0.4	0.9908
50	**0.82**	27.8 ± 7.0	**186 ± 46**	3.3 ± 0.3	0.9836

BSA-E2 conjugate are brightest compared to that with 82 percent surface coverage and BSA control spots. Table 3.1 summarizes the curve-fitting parameters for E2-Ab binding curves shown in Figure 3.3B. It is noteworthy from the results in Table 3.1 that K_d values (52 ± 7 nM, 139 ± 23 nM, and 186 ± 46 nM for 0.21, 0.49, and 0.82 respectively) determined from the fit decrease with decreasing surface coverage of BSA-E2 conjugate, meaning a higher binding affinity of E2-Ab to BSA-E2 conjugate is associated with a lower surface coverage. These K_d values are comparable to the dissociation constant values (0.3 – 5 nM) reported for other clones of estradiol antibodies[33,34]. It is not surprising that the K_d values reported here have a slightly higher number, because these values are measured in a heterogeneous solid-phase format instead of a homogeneous solution phase format. The effect of the surface coverage of the BSA-E2 conjugate on E2-Ab binding observed in Figure 3.3 and Table 3.1 can be attributed to the steric effect of BSA-E2 conjugate. Based on these studies, we determined the optimal surface coverage of BSA-E2 conjugate to be 21 percent, and the optimal concentration of E2-Ab is 5 μg/mL for the following sensing performance. At this concentration, the slope of the red binding curve in Figure 3.3B is biggest, which means the signal response will be most sensitive with any change of the effective E2-Ab concentration.

As noted above, E2 has been the target of many measurement studies. A variety of techniques have quantified FA in the concentration range of fM to μM, and most of them are electrochemical, colorimetric, or fluorescent-based.[20-25] The physiological concentration range of E2 is 40 pM – 1.5 nM in blood, depending on gender and age. The analytical performance of the inhibition immunosensor was tested to detect and quantitate E2 in the physiological concentration range. Solutions containing a fixed optimal

concentration of E2-Ab (5 μg/mL) and various concentrations of free E2 (2 nM, 1 nM, 500 pM, 250 pM, 100 pM, 50 pM, and 10 pM) were pre-mixed. After a certain time of incubation, the mixed solutions were continuously exposed to BSA-E2 conjugate on chip surface from the most concentrated E2 concentration to the least concentrated E2 concentration. The SPRi sensorgram for this experiment exhibit a continuous signal increase as the decrease of E2 concentration in the mixed solution (Figure 3.4A). Figure 3.4B is a plot of SPRi signal vs. free E2 concentration covering the physiological concentration range. The data points fit well with the dose-response ligand binding equation included in SigmaPlot ($R^2 = 0.9840$). The sigmoidal shape of the plot is similar to a dose-response curve in drug screening or enzyme inhibition assays.[35] The plot shows the expected negative slope and serves as a calibration curve for free E2 in solution. Figure 3.4B can be used to successfully quantitate E2 in the range of 10 pM to 2 nM. The specificity of the immunosensor was investigated using estrone (E1), which is also one of the natural estrogens, as a potential interference to E2. Mixed solutions of E2-Ab at a fixed concentration and E1 at various concentrations (1 pM, 10 pM, 100 pM, 1 nM, 10 nM) were exposed to BSA-E2 conjugate modified chip surface as well. Figure 3.5 contains the binding results (normalized SPR signal vs. E1 or E2 concentration) for both mixed solutions of E2-Ab with E2 and that of E2-Ab with E1. We can observe a big signal decrease from 1.0 to ~0.2 for E2, while the signal for E1 only decreases to ~0.7 even if the concentration of E1 is higher (10 nM) than the highest concentration of E2 used (2 nM). Despite the minor signal decrease observed for E1, we are still confident that the sensor is specific for E2 detection due to the fact that the tested E1 concentration is an order of magnitude higher than tested E2 concentration. It should also be noted that

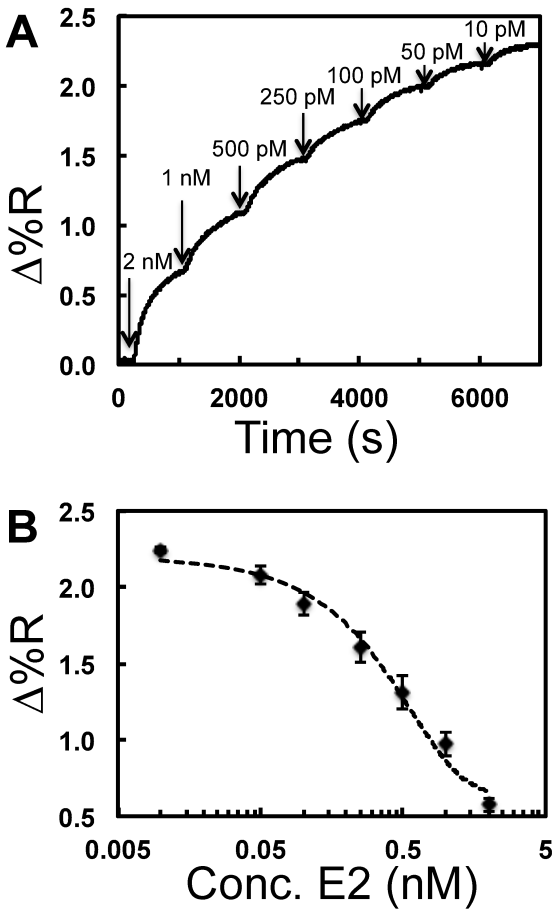

Figure 3.4 Detection of E2 in the physiological concentration range using the inhibition immunosensor. (A) A representative SPRi sensorgram for injecting 7 mixed solutions of E2-Ab at 5 μg/mL and E2 solutions (2 nM, 1 nM, 500 pM, 250 pM, 100 pM, 50 pM, 10 pM). The arrows indicate the injection of each concentration. (B) Calibration curve (SPRi signal vs. concentration of free E2) for the determination of E2. The symbols represent the mean of at least 3 repetitive measurements and the error bars are the standard deviation. The dashed line through the data is the least-squares fit of sigmoidal dose-response ligand binding equation (R^2=0.9840) using SigmaPlot program.

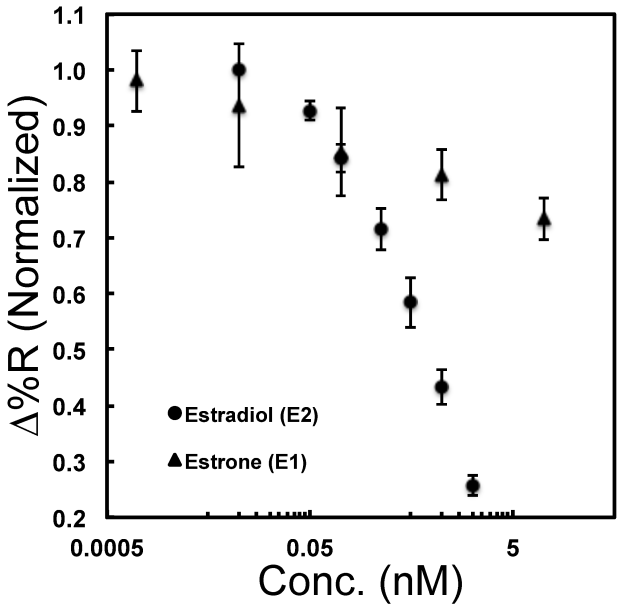

Figure 3.5 Specificity study of the inhibition immunosensor using estrone (E1) as a potential interference. Binding results for mixed solutions of E2-Ab with E2 (circle) and E1 (triangle) are shown, respectively. The symbols are the mean of at least 3 repetitive measurements and the error bars are the standard deviation.

the specificity of an immunosensor is usually determined by the specificity of the antibody used. We note that secondary antibody or secondary antibody conjugated nanomaterials (e.g. gold nanoparticles) can be utilized to enhance the signal further, but these studies are not carried out in this work. This is another reason to verify why we immobilize BSA-E2 conjugate but not E2-Ab on our chip surface.

3.4 CONCLUSION

We have developed an indirect inhibition immunosensor for sensitive and selective analysis of 17β-estradiol (E2) using surface plasmon resonance (SPR) imaging. This indirect inhibition detection format enables to overcome the challenges associated with direct detection of small molecules by SPR imaging. BSA-E2 conjugate is immobilized on chip surface, which allows us to generate a higher signal by detecting E2 antibody (E2-Ab) binding. Also, secondary antibody or secondary antibody conjugated nanomaterials can be used to further enhance the signal if needed. It is found that the binding affinity of E2-Ab increases with decreasing surface coverage/density of BSA-E2 conjugate, probably due to a decreasing steric effect. Under optimal conditions of BSA-E2 conjugate surface coverage/density and E2-Ab concentration, a sigmoidal calibration curve with a negative slope and a dynamic range from 10 pM to 2 nM was generated, showing good sensitivity and reproducibility to detect and quantitate E2 in the physiological concentration range. Moreover, the developed immunosensor is specific for E2 detection showing little interference from estrone. This work demonstrates the applicability of SPR imaging to detect small molecules and paves the way for future multiplexed detection of metabolites on a single SPR imaging chip.

3.5 References

(1) Hilvo, M.; de Santiago, I.; Gopalacharyulu, P.; Schmitt, W. D.; Budczies, J.; Kuhberg, M.; Dietel, M.; Aittokallio, T.; Markowetz, F.; Denkert, C.; Sehouli, J.; Frezza, C.; Darb-Esfahani, S.; Braicu, E. I. *Cancer Res.* **2016**, *76*, 796-804.

(2) Park, M. H.; Igarashi, K. *Biomol. Ther.* **2013**, *21*, 1-9.

(3) Johnson, C. H.; Ivanisevic, J.; Siuzdak, G. *Nat. Rev. Mol. Cell Biol.* **2016**, *17*, 451-459.

(4) Fernie, A. R.; Trethewey, R. N.; Krotzky, A. J.; Willmitzer, L. *Nat. Rev. Mol. Cell Biol.* **2004**. 5, 763-769.

(5) Wishart, D. S.; Mandal, R.; Stanislaus, A.; Ramirez-Gaona, M. *Metabolites* **2016**, *6*, 10.

(6) Wishart, D. S. *Nat. Rev. Drug Discovery* **2016**, *15*, 473-484.

(7) Bouatra, S.; Aziat, F.; Mandal, R.; Guo, A. C.; Wilson, M. R.; Knox, C.; Bjorndahl, T. C.; Krishnamurthy, R.; Saleem, F.; Liu, P.; Dame, Z. T.; Poelzer, J.; Huynh, J.; Yallou, F. S.; Psychogios, N.; Dong, E.; Bogumil, R.; Roehring, C.; Wishart, D. S. *PLoS One* **2013**, *8*, e73076.

(8) Psychogios, N.; Hau, D. D.; Peng, J.; Guo, A. C.; Mandal, R.; Bouatra, S.; Sinelnikov, I.; Krishnamurthy, R.; Eisner, R.; Gautam, B.; Young, N.; Xia, J.; Knox, C.; Dong, E.; Huang, P.; Hollander, Z.; Pedersen, T. L.; Smith, S. R.; Bamforth, F.; Greiner, R.; McManus, B.; Newman, J. W.; Goodfriend, T.; Wishart, D. S. *PLoS One* **2011**, *6*, e16957.

(9) Homola, J. *Chem. Rev.* **2008**, *108*, 462-493.

(10) McKeating, K. S.; Couture, M.; Dinel, M. P.; Garneau-Tsodikova, S.; Masson, J. F. *Analyst* **2016**, 141, 5120-5126.

(11) Zhao, S. S.; Bichelberger, M. A.; Colin, D. Y.; Robitaille, R.; Pelletier, J. N.; Masson, J. F. *Analyst* **2012**, *137*, 4742-4750.

(12) Bockova, M.; Chadtova Song, X.; Gedeonova, E.; Levova, K.; Kalousova, M.; Zima, T.; Homola, J. *Anal. Bioanal. Chem.* **2016**, 408, 7265-7269.

(13) Rebe Raz, S.; Haasnoot, W. *Trends Anal. Chem.* **2011**, *30*, 1526-1537.

(14) Rodriguez-Mozaz, S.; Marco, M. P.; Lopez de Alda, M. J.; Barcelo, D. *Anal. Bioanal. Chem.* **2004**, *378*, 588-598.

(15) Li, M.; Cushing, S. K.; Wu, N. *Analyst* **2015**, *140*, 386-406.

(16) Rosenfeldt, E. J.; Linden, K. G. *Environ. Sci. Technol.* **2004**, *38*, 5476-5483.

(17) Shanle, E. K.; Xu, W. *Chem. Res. Toxicol.* **2011**, *24*, 6-19.

(18) Ryan, K. J. *Cancer Res.* **1982**, *42*, 3342s-3344s.

(19) Stricker, R.; Eberhart, R.; Chevailler, M. C.; Quinn, F. A.; Bischof, P.; Stricker, R. *Clin. Chem. Lab. Med.* **2006**, *44*, 883-887.

(20) Han, Q.; Shen, X.; Zhu, W.; Zhu, C.; Zhou, X.; Jiang, H. *Biosens. Bioelectron.* **2016**, *79*, 180-186.

(21) Zhu, B.; Alsager, O. A.; Kumar, S.; Hodgkiss, J. M.; Travas-Sejdic, J. *Biosens. Bioelectron.* **2015**, *70*, 398-403.

(22) Kanso, H.; Inguimbert, N.; Barthelmebs, L.; Istamboulie, G.; Thomas, F.; Calas-Blanchard, C.; Noguer, T. *Chem. Commun.* **2014**, *50*, 1658-1661.

(23) Alsager, O. A.; Kumar, S.; Zhu, B.; Travas-Sejdic, J.; McNatty, K. P.; Hodgkiss, J. M. *Anal. Chem.* **2015**, *87*, 4201-4209.

(24) Liu, J.; Bai, W.; Niu, S.; Zhu, C.; Yang, S.; Chen, A. *Sci. Rep.* **2014**, *4*, 7571.

(25) Du, L.; Ji, W.; Zhang, Y.; Zhang, C.; Liu, G.; Wang, S. *Analyst* **2015**, *140*, 2001-2007.

(26) Nelson, B. P.; Frutos, A. G.; Brockman, J. M.; Corn, R. M. *Anal. Chem.* **1999**, *71*, 3928-3934.

(27) Kanda, V.; Kariuki, J. K.; Harrison, D. J.; McDermott, M. T. *Anal. Chem.* **2004**, *76*, 7257-7262.

(28) Bain, C. D.; Troughton, E. B.; Tao, Y. T.; Evall, J.; Whitesides, G. M.; Nuzzo, R. G. *J. Am. Chem. Soc.* **1989**, *111*, 321-335.

(29) Jadzinsky, P. D.; Calero, G.; Ackerson, C. J.; Bushnell, D. A.; Kornberg, R. D. *Science* **2007**, *318*, 430-433.

(30) Lee, J. W.; Sim, S. J.; Cho, S. M.; Lee, J. *Biosens. Bioelectron.* **2005**, *20*, 1422-1427.

(31) Ostuni, E.; Yan, L.; Whitesides, G. M. *Colloids Surf., B* **1999**, *15*, 3-30.

(32) Rhoden, J. J.; Dyas, G. L.; Wroblewski, V. J. *J. Biol. Chem.* **2016**, *291*, 11337-11347.

(33) Lamminmaki, U.; Westerlund-Karlsson, A.; Toivola, M.; Saviranta, P. *Protein Sci.* **2003**, *12*, 2549-2558.

(34) Monnet, C.; Bettsworth, F.; Stura, E. A.; Le Du, M. H.; Menez, R.; Derrien, L.; Zinn-Justin, S.; Gilquin, B.; Sibai, G.; Battail-Poirot, N.; Jolivet, M.; Menez, A.; Arnaud, M.; Ducancel, F.; Charbonnier, J. B. *J. Mol. Biol.* **2002**, *315*, 699-712.

(35) Auld, D. S.; Farmen, M. W.; Kahl, S. D.; Kriauciunas, A.; McKnight, K. L.; Montrose, C.; Weidner, J. R. In *Assay Guidance Manual*, Sittampalam, G. S.; Coussens, N. P.; Brimacombe, K.; Grossman, A.; Arkin, M.; Auld, D.; Austin, C.; Baell, J.; Bejcek,

B.; Chung, T. D. Y.; Dahlin, J. L.; Devanaryan, V.; Foley, T. L.; Glicksman, M.; Hall, M. D.; Hass, J. V.; Inglese, J.; Iversen, P. W.; Lal-Nag, M.; Li, Z.; McGee, J.; McManus, O.; Riss, T.; Trask, O. J., Jr.; Weidner, J. R.; Xia, M.; Xu, X., Eds.: Bethesda (MD), 2004; pp 129-154.

Chapter 4 Aptamer-Gold Nanoparticle Conjugate for Small-Molecule Metabolite Analysis Using Surface Plasmon Resonance Imaging

4.1 Introduction

Small-molecule metabolites (MW < 1000 Da), the intermediates and products of metabolism, are now serving as an important type of biomarker with the development of the field of metabolomics.[1,2] Metabolites sensing plays a crucial role in using the information for medical diagnostics. Dopamine (DA) is such a metabolite (or be more specific a neurotransmitter) that is a member of the catecholamine family in the brain, and is a precursor to epinephrine and norepinephrine.[3] In addition, DA is a major transmitter in the extrapyramidal system of the brain, important in regulating movement, and related to some neurodegenerative diseases, such as Parkinson's disease, Alzheimer's disease, and Huntington's disease.[4,5] Thus, sensitive and selective analysis of small-molecule metabolite is of great importance in human health monitoring. Sensing strategies that can provide fast, sensitive and selective analysis of metabolites are highly demanded.

Surface plasmon resonance (SPR) is an optical sensing platform first developed in the 1990s.[6] It has found broad applications in human health research[7-9], environmental monitoring[10,11], and homeland security[12], since it can provide label-free, real-time, sensitive and quantitative information of bio-molecular interactions. Most of the SPR-based assays and/or sensors are designed to analyze proteins[13-15] and nucleic acids[16], probably because these targets are relatively large and thus can result in a big refractive-index change. Due to the small size and low molecular weight, direct detection of

metabolite with SPR challenges this refractive-index change based technique. There have been reports of the direct detection of small molecules but such demonstrations are sporadic and these measurements generally suffer from poor sensitivity and low signal intensity.[17,18] Researchers have used nanomaterials[19,20] as labels to address the challenges of measuring small molecules with SPR. Different types of nanomaterials like metal nanoparticles[21-23], magnetic nanoparticles[24], quantum dots[25], and carbon-based nanomaterials[26,27] have been incorporated into the assays to enhance the signal, thus overcome the sensitivity issue associated with small molecule detection.

In this chapter, a general sensing strategy incorporating dopamine DNA aptamer (DAAPT)[28,29] and gold nanoparticle (AuNP) to detect and quantitate dopamine was developed using SPRi. The sensing strategy is shown in Figure 4.1. We first prepared the 10 nm DAAPT-AuNP conjugate, which is quite stable in PBS buffer solution. Since the DAAPT can bind to dopamine with a high affinity, the whole conjugate is "OFF" in the presence of DA, and is "ON" in the absence of DA. On the chip surface, a complementary single-stranded DNA (cDNA) probe is immobilized that can bind to DAAPT as well. The polydopamine surface chemistry enables the attachment of the amine-terminated cDNA probe via Michael addition reaction. When the DAAPT-AuNP probe is "OFF" (DA present), it cannot bind to the cDNA probe on chip surface, thus no signal will be observed. On the contrary, the DAAPT-AuNP probe that is "ON" (DA absent) will bind to the cDNA probe, generating a big signal intensity. Based on this strategy, a negative correlation is created between the SPRi signal response and the concentration of DA. The as-prepared 10 nm DAAPT-AuNP conjugate probe shows strong binding affinity (K_d = 3.1 ± 1.4 nM) to the cDNA probe measured by SPRi. We

performed the inhibition assay to detect and quantitate DA in two different concentration ranges: 100 μM – 2 mM and 200 fM – 20 nM. Both calibration curves have a negative slope, show good sensitivity and reproducibility. Moreover, our assay was approved to be specific for DA analysis, with little interference observed from DA analogs and other metabolites.

4.2 Experimental

Chemicals and Reagents. 10 nm (5.7×10^{12} particles/mL, 9.47 nM), 20 nm (7.0×10^{11} particles/mL, 1.16 nM), 30 nm (2.0×10^{11} particles/mL, 0.33 nM), and 40 nm (9.0×10^{10} particles/mL, 0.15 nM) of citrate-capped gold nanoparticle stock solutions were purchased from Ted Pella, Inc. Deionized (DI) water (H_2O) with a resistivity greater than 18 MΩ was filtered in a Barnstead Nanopure purification system. 10 × PBS (phosphate buffered saline) buffer, dopamine (DA) hydrochloride, folic acid (FA), 17β-estradiol (E2), L-3,4-dihydroxyphenylalanine (DOPA), 3,4-dihydroxyphenylacetic acid (DOPAC), 1,2-dihydroxybenzene (Catechol), epinephrine (EP), homovanillic acid (HVA), L-ascorbic acid (AA) were all purchased from Sigma-Aldrich and used as received. Tris-HCl buffer (10 mM, pH 8.5) was obtained from bioWORLD of GeneLinx International, Inc. 20× TBS (tris buffered saline, 1× = 25 mM Tris, 0.15 M NaCl) was purchased from ThermoFisher Scientific. SF-10 glass sheet (100 mm × 100 mm × 1 mm) was purchased from Schott Glass. (Tridecafluoro-1,1,2,2-tetrahydrooctyl)-1-dimethylchlorosilane was purchased from United Chemical Technologies. All DNA oligos at 250 nmole with HPLC purification were ordered from Integrated DNA Technologies, Inc. The sequence information of all single-straded DNA oligos are as follows: a thiol-terminated dopamine

DNA aptamer (DAAPT) (5'-S-S(CH_2)$_6$-GTC TCT GTG TGC GCC AGA GAC ACT GGG GCA GAT ATG GGC CAG CAC AGA ATG AGG CCC-3'), an amine-terminated complementary DNA (cDNA) probe (P20) (5'-NH_2(CH_2)$_{12}$-GGG CCT CAT TCT GTG CTG GC-3'), and an amine-terminated negative control DNA probe (A20) (5'-NH_2(CH_2)$_{12}$-AAA AAA AAA AAA AAA AAA AA-3').

Fabrication of SPRi Chip with Multiple Au Spots. The purchased SF-10 glass sheet (100 mm × 100 mm × 1 mm) was cut into small square substrate (18 mm × 18 mm × 1 mm). The substrates were cleaned using hot piranha solution (1:4 30% H_2O_2:H_2SO_4) followed by thorough rinsing with DI water. Substrates were blown dry using Ar gas. [*Warning: Piranha solution should be handled with extreme care; it is a strong oxidant and reacts violently with many organic materials. It also presents an explosion danger. All work should be performed under a fume hood with appropriate personal safety equipment*.] The cleaned and dried substrates were mounted to a mask that expose nine 2 mm diameter round spots and placed into the chamber of a thermal evaporator (Torr International Inc., New Windsor, NY). Metal films of chromium (2 nm) and gold (42 nm) were sequentially coated on the glass substrate through the mask. After removal from the evaporator, the substrates were then exposed to a vapor of (tridecafluoro-1,1,2,2-tetrahydrooctyl)-1-dimethylchlorosilane under reduced pressure for 24 h to create a hydrophobic background on the glass surface. The SPRi chips were stored in a desiccator under vacuum at room temperature until use.

Dopamine DNA Aptamer-Gold Nanoparticle (DAAPT-AuNP) Conjugate Preparation. 10 μL of 100 μM of the thiol-terminated DAAPT solution (in PBS) was added to 1mL of 10 nm, 20 nm, 30 nm, 40 nm citrate-capped gold nanoparticle stock

solutions, respectively. The mixed solutions were incubated at room temperature for 24 h. Next, 500 μL of PBS buffer (10 mM phosphate and 154 mM sodium chloride, pH 7.4) was added to each mixed solution, which was incubated at room temperature for another 24 h. The 10 nm, 20 nm, 30 nm, and 40 nm mixed solutions were centrifuged (Eppendorf a5417R microcentrifuge) under 14000 rpm for 45 min, 13000 rpm for 30 min, 10000 rpm for 30 min, and 10000 rpm for 30 min, respectively. The supernatant of each solution was carefully removed to avoid any loss of the particles. The AuNP pellet was re-dispersed in 1 mL DI H_2O, or PBS buffer, or TBS buffer, and stored at 4 °C until use.

UV-Vis Spectroscopy. Extinction spectra of 10 nm, 20 nm, 30 nm, and 40 nm citrate-capped AuNP stock solutions and corresponding DAAPT-AuNP conjugate solutions in different media (DI H_2O, PBS, TBS) were obtained by UV-Vis spectroscopy. 500 μL of each AuNP solution was added to a quartz micro-cuvette for UV-Vis measurement. All solutions were measured in transmission mode in a double-beam Perkin-Elmer Lambda 35 instrument. For each measurement, the corresponding medium used for re-dispersing gold nanoparticle pellet was used as a reference.

SPRi Measurement of Adsorption of Polydopamine (PDA). We followed the protocol reported in this literature[30] to measure the surface PDA multilayer formation on gold spots surface. Briefly, 10.5 mM dopamine solutions in a pH 8.5 Tris buffer were exposed to the bare gold SPRi chip surface. Real-time sensorgram was recorded, and continuous PDA film growth was observed.

SPRi Measurement of 10 nm DAAPT-AuNP Conjugate Binding to cDNA Probe. Prior to the modification, the homemade SPRi chip was rinsed with pure ethanol and DI water and dried under an argon gas flow. Polydopamine (PDA) surface chemistry

described elsewhere was used to immobilize cDNA probe (P20) to the gold chip surface.[30] Briefly, a 2.5 μL droplet of 10.5 mM DA in Tris buffer (pH 8.5) was added to each gold spot of the chip. The chip with the solution droplets was stored in a humid petri dish for 10 min at room temperature. Then, the chip was rinsed with DI water and dried under argon gas flow. Each spot of the chip was next exposed to a 2.5 μL droplet of 250 μM of amine-terminated cDNA (P20) probe or negative control DNA (A20) for 12 h in the petri dish. The surface was then blocked by 1 mg/mL ethanolamine solution for 1 h. After rinsing and drying, the modified chip was mounted to the SPRi instrument (Horizon SPRimager, GWC Technologies, Madison, MI) to measure the binding of 10 nm DAAPT-AuNP conjugate to the cDNA probe. The apparatus has been described in detail elsewhere.[31,32] 10 nm DAAPT-AuNP conjugate in PBS buffer solutions at 6 concentrations (0.095 nM, 0.24 nM, 0.47 nM, 0.95 nM, 2.4 nM, 4.7 nM) were prepared from the stock DAAPT-AuNP solution (9.5 nM). Each solution was exposed to the modified chip surface, and the real-time SPRi sensorgram was recorded and analyzed.

Inhibition Assays. All assays were carried out on chips containing cDNA (P20) and negative control (A20) spots. As described below, two concentration ranges of DA were studied. For the higher (μM to mM) range, 500 μL of 9.5 nM 10 nm DAAPT-AuNP conjugate solution (in PBS buffer) was mixed with 500 μL of DA standard solution (in PBS buffer) at a specific concentration (100 μM, 200 μM, 300 μM, 500 μM, 1 mM, 2 mM) for 1 h. Each mixed solution was flowed into the instrument and exposed to gold chip surface modified with P20 and A20 DNA probes, and then a real-time SPRi sensorgram was obtained for each mixed solution. For the lower (fM to nM) range, we decreased the concentration of the 10 nm DAAPT-AuNP conjugate solution to 1.9 nM.

The NP solution was mixed with DA standard solutions (200 fM, 300 fM, 500 fM, 2 pM, 20 pM, 20 nM, 20 μM) for 1 h. Each solution was flowed into the instrument and the SPRi sensorgram was obtained.

Specificity Studies. To test the specificity of the assay, we chose a variety of DA analogs (DOPA, DOPAC, Catechol, EP, HVA, AA) and other two metabolites (FA, E2). 500 μL of 1.9 nM 10 nm DAAPT-AuNP conjugate solution (in PBS buffer) was mixed with 500 μL of 20 nM of the possible interferences standard solutions described above for 1 h. Each mixed solution was measured using SPRi, and the result was compared with that for DA.

4.3 Results and Discussion

Sensitive and selective detection of DA as well as other critical neurotransmitters plays a significant role in monitoring some neurodegenerative diseases, such as Parkinson's, Alzheimer's, and Huntington's diseases, as mentioned above. Herein, we have developed an aptamer-gold nanoparticle conjugate-enhanced inhibition assay using surface plasmon resonance imaging that enables sensitive and selective detection of DA down to the higher fM concentration range. First, we attach the bio-recognition element – a DNA aptamer for DA (DAAPT) – to gold nanoparticle (AuNP) surface, and obtain this critical DAAPT-AuNP conjugate. The sensing strategy of the DAAPT-AuNP conjugate-enhanced inhibition assay is shown in Figure 4.1. In the absence of DA, no binding happened between DAAPT on AuNP surface and DA, the conjugate probe is in its "ON" state. With a partially complementary single-stranded DNA (cDNA) probe on

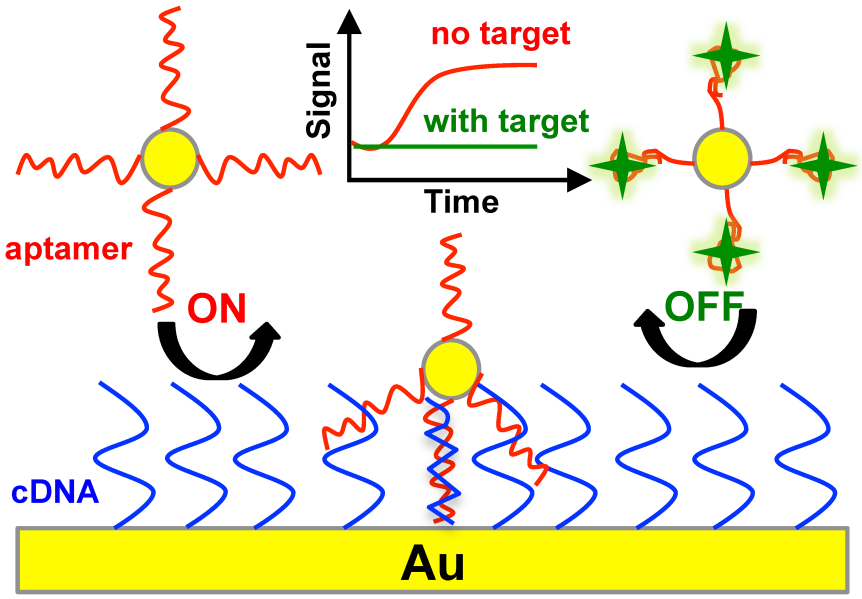

Figure 4.1 Schematic illustration of the DNA aptamer-gold nanoparticle conjugate enhanced sensing strategy for dopamine (DA) analysis using SPR imaging. Amine-terminated single-stranded complementary DNA (cDNA) to DNA aptamer is immobilized on gold chip surface via polydopamine surface chemistry. In the absence and presence of DA, the conjugate is in its 'ON' and 'OFF' states respectively. 'ON' state means the conjugate can bind to the immobilized cDNA, thus generate a big SPR signal. On the contrary, 'OFF' state means no binding will occur between the conjugate and the cDNA due to the blocking of DNA aptamer by the binding of DA.

the SPRi chip surface, we can detect the binding of the conjugate to the cDNA probe. As a result, a big signal response will be generated. On the contrary, in the presence of a higher concentration of DA, all the DAAPTs on the AuNP conjugate surface will bind to their target, so the conjugate probe is in its "OFF" state. This time, the conjugate will not bind to cDNA on chip surface due to the blocking of the DNA aptamer by the binding of DA, thus no signal response will be observed. During the whole process, the target DA molecule serves as a "key" to turn "ON" and "OFF" the DAAPT-AuNP conjugate. In theory, if we fix the initial concentration of the conjugate, the effective concentration of the probe that can bind to cDNA surface will decrease with increasing DA concentration. Therefore, the signal response is inversely related to the concentration of DA, and we will see a negative slope for the calibration curve.

We prepared 10 nm, 20 nm, 30 nm, and 40 nm DAAPT-AuNP conjugate probes via the strong Au-S interaction[33,34] between the thiol-terminated DAAPT and AuNP. Figure 4.2A shows the extinction spectra of 10 nm citrate-capped AuNP in H_2O and 10 nm DAAPT-AuNP conjugate in three different media (H_2O, PBS, TBS). All the spectra have a good shape with the localized surface plasmon resonance (LSPR) peaks located around 520 nm. Taking a closer look at the amplified portion around the maximum extinction of the spectra (Figure 4.2B), we can observe clear red shifts of the LSPR peaks from 517 nm (citrate-capped, H_2O) to 525 nm (DAAPT-AuNP, H_2O), to 524 nm (DAAPT-AuNP, PBS/TBS). The observed red shifts of the LSPR peaks confirm the successful conjugation of DAAPT to AuNP surface. Moreover, the good shape of the spectra in PBS/TBS means the prepared 10 nm DAAPT-AuNP conjugate is quite stable in buffer solution with high salts concentration. The stability of 10 nm DAAPT-AuNP

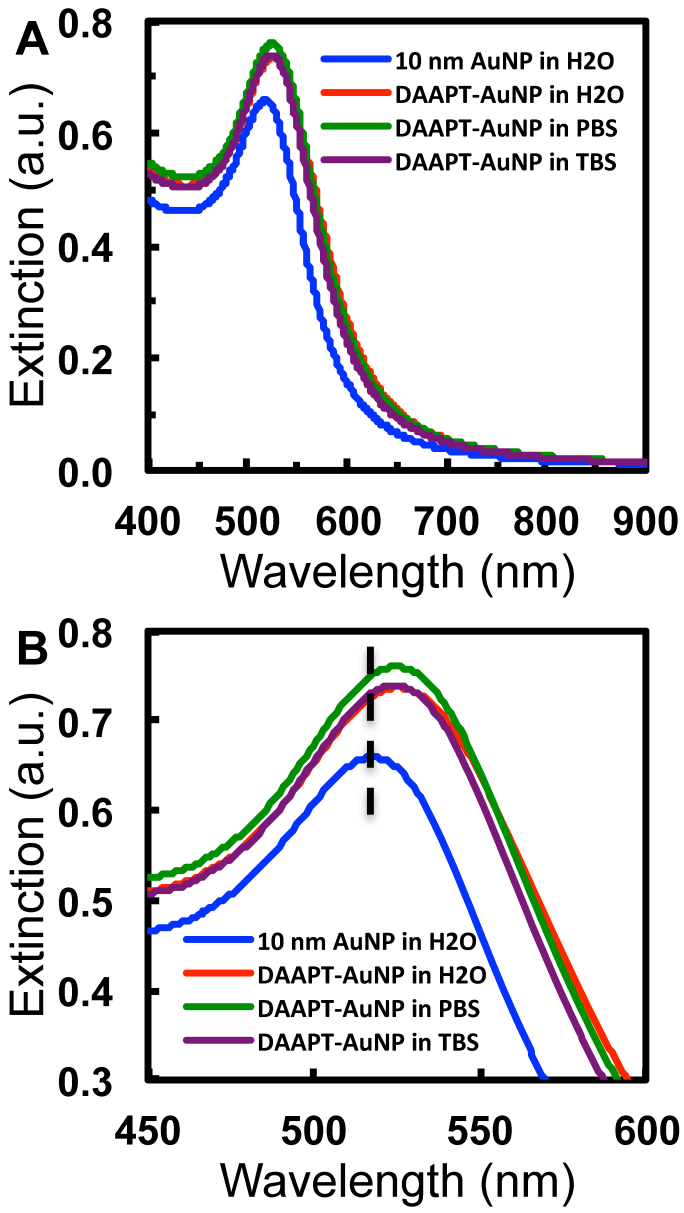

Figure 4.2 UV-vis characterization of the as-prepared 10 nm dopamine aptamer-gold nanoparticle (DAAPT-AuNP) conjugate in H_2O and buffers. (A) Extinction spectra for as-purchased 10 nm citrate-AuNP in H_2O (blue) and as-prepared 10 nm DAAPT-AuNP conjugate in H_2O (red), PBS (green), and TBS (purple). (B) Amplified portion around the maximum extinction for clarity. The dashed line marks the maximum extinction of 10 nm citrate-AuNP.

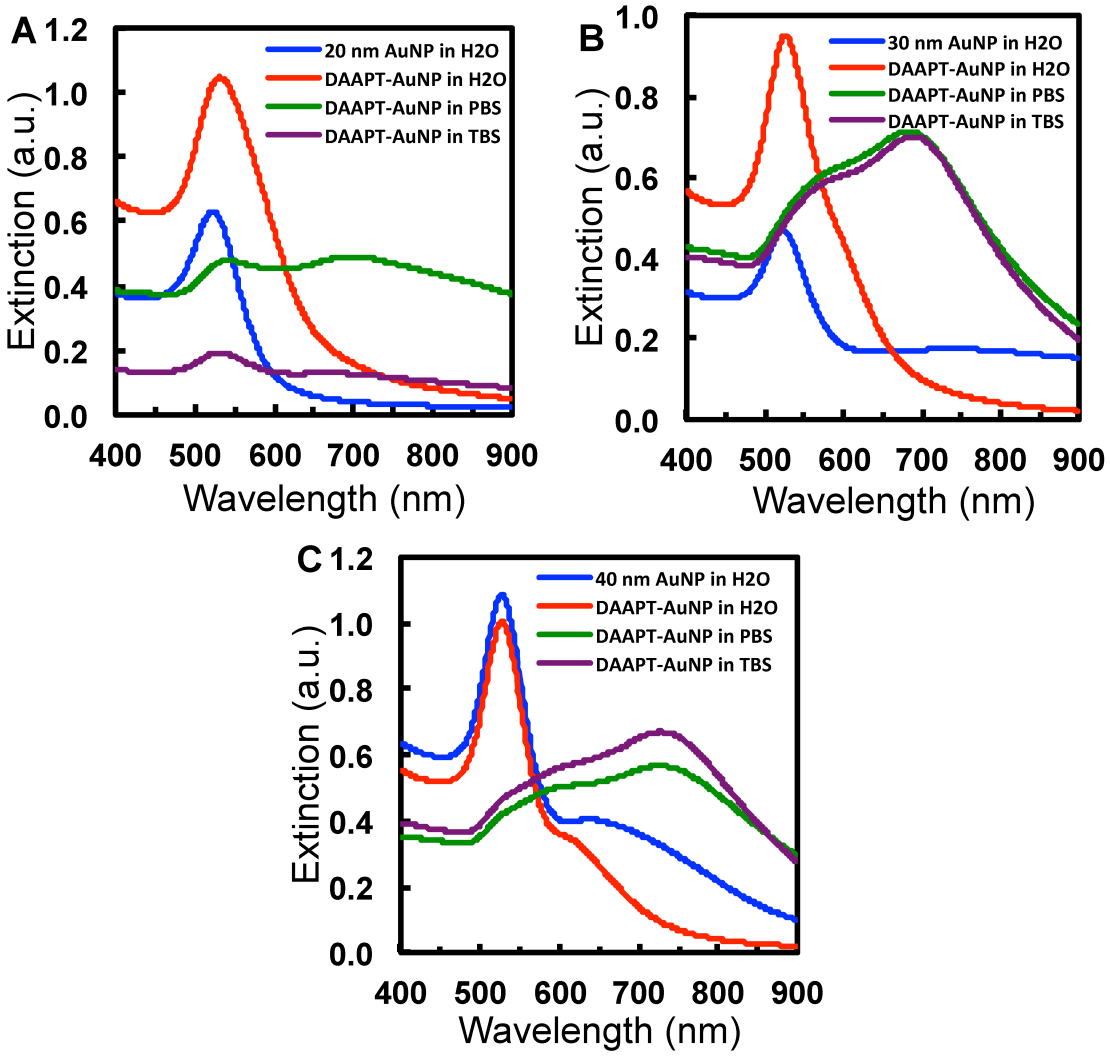

Figure 4.3 Extinction spectra for 20 nm (A), 30 nm (B), and 40 nm (C) citrate-AuNPs in H_2O (blue) and DAAPT-AuNP conjugates in H_2O (red), PBS (green), and TBS (purple).

conjugate in buffer solution is key for the success of the inhibition assay, because the conjugate will mix with DA standard solution or unknown sample solution with a high salt environment. Extinction spectra for 20 nm, 30 nm, and 40 nm DAAPT-AuNP conjugates are shown in Figure 4.3. Compared to 10 nm DAAPT-AuNP conjugate, 20 nm and 30 nm conjugates do show red shifts of the LSPR peaks, but they are not stable in buffer solution. For 40 nm conjugate, no red shift of the LSPR peaks is observed. Based on these studies, we chose 10 nm DAAPT-AuNP conjugate and used it in the inhibition assay. It has been reported that spherical nucleic acid gold nanoparticle conjugate can be formed by densely functionalizing the gold cores with a surface shell of DNA coordinated via sulfur groups to the gold, and the size of the gold core in the original work is 13 nm.[35,36]

To immobilize the cDNA probe to the SPRi chip surface, we used polydopamine (PDA) surface chemistry that allows the Michael addition of amine-terminated cDNA molecule to PDA film on chip surface.[37,38] The protocol reported elsewhere[30] was followed, which have approved the successful attachment of amine-terminated DNA molecule to the gold spot surface. The SPRi sensorgram for the growth of PDA film on gold spots surface is shown in Figure 4.4. The binding of 10 nm DAAPT-AuNP conjugate to cDNA probe on chip surface was investigated by SPRi measurement. Figure 4.5A contains the SPRi sensorgrams for 10 nm DAAPT-AuNP conjugate binding under different concentrations: 0.095 nM, 0.24 nM, 0.47 nM, 0.95 nM, 2.4 nM, and 4.7 nM. The SPRi signal intensity increases with increasing 10 nm DAAPT-AuNP conjugate concentrations. The least concentrated (0.095 nM) and most concentrated (4.7 nM) 10 nm DAAPT-AuNP conjugate solutions give 0.4 ± 0.1 and 13.6 ± 0.4 of change in percent

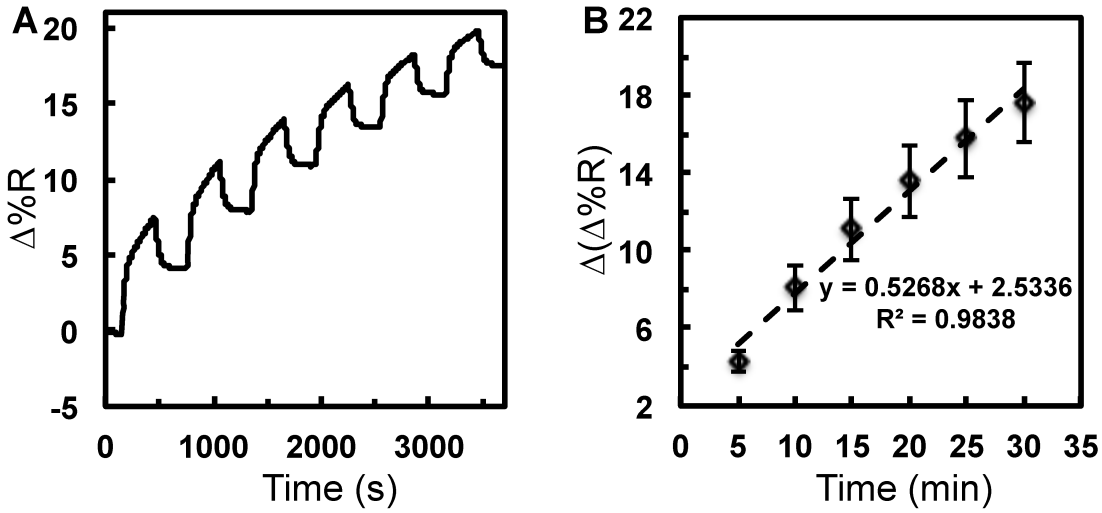

Figure 4.4 (A) SPRi sensorgrams for the adsorption of 10.5 mM PDA solution to bare gold spots surface; (B) quantitative analysis of the signal response as a function of time after PDA solution exposure. Error bars represent standard deviation for triplicate measurements.

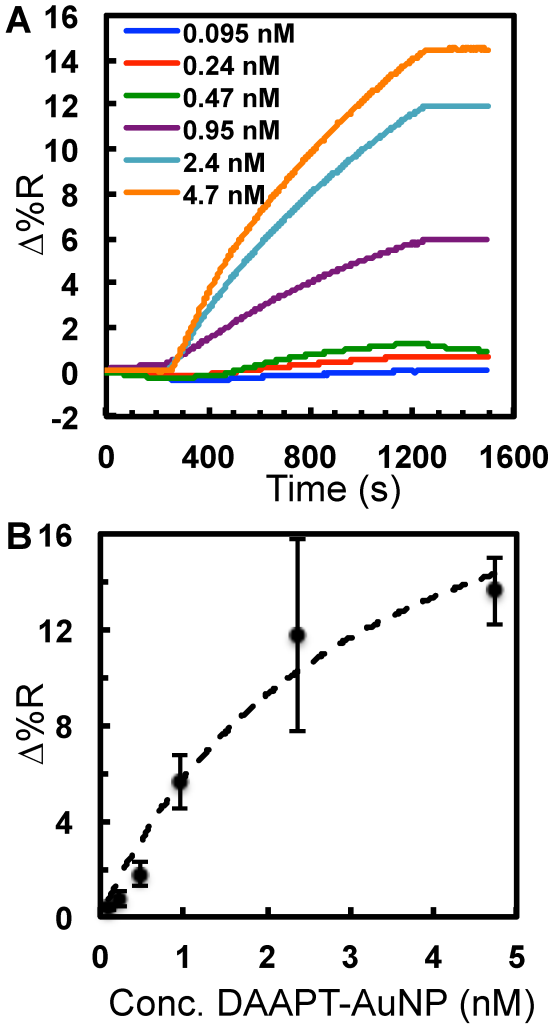

Figure 4.5 Binding of 10 nm DAAPT-AuNP conjugate to cDNA probe on gold chip surface. (A) Typical SPRi sensorgrams for the binding of 10 nm DAAPT-AuNP at six concentrations: 0.095 nM (blue), 0.24 nM (red), 0.47 nM (green), 0.95 nM (purple), 2.5 nM (cyan), and 4.7 nM (orange). (B) A plot of SPR signal vs. DAAPT-AuNP solution concentration for adsorption to cDNA. The symbols are the data points and the dashed line is the least-squares fit of Langmuir adsorption isotherm equation (R^2 = 0.9669). The error bars represent standard deviation for triplicate measurements.

reflectivity (Δ%R), respectively. By comparing the two signals, we conclude that the signal response is coming from specific binding of 10 nm DAAPT-AuNP conjugate to the cDNA probe. Isotherm was constructed for 10 nm DAAPT-AuNP conjugate and cDNA binding from sensorgrams shown in Figure 4.5A. The 10 nm conjugate binding data points were fitted with a Langmuir isotherm (Figure 4.5B) equation using the one-site ligand-binding model included in SigmaPlot (Systat Software, Inc., San Jose, CA). The binding data agree well (R^2 = 0.9669) with the Langmuir isotherm, and the dissociation constant (K_d) and the maximum signal intensity ($\Delta\%R_{max}$) for the binding were determined to be 3.1 ± 1.4 nM and 23.8 ± 5.6, respectively. It was reported in the literature that the binding constant between spherical nucleic acid functionalized gold nanoparticle conjugate and its complementary oligonucleotide sequence in a homogeneous solution can be down to the picomolar range, or even lower, depending on the density of the spherical nucleic acid on nanoparticle surface and the length of the complementary nucleic acid.[39,40] The binding constant value reported here is a few orders of magnitude higher than the literature values, probably because our assay is heterogeneous and the complementary DNA probe is immobilized on a solid surface. This may introduce more steric effect and hindrance to the binding, which results in a lower binding affinity.

To detect and quantitate DA, the 10 nm DAAPT-AuNP conjugate solution at a fixed concentration was mixed with DA standard solution at a specific concentration. By pre-mixing the two solutions, DA molecules will bind to DAAPT-AuNP conjugates, thus decreasing the effective concentration of DAAPT-AuNP conjugate that can bind to cDNA probe on chip surface. Here, we can play with two crucial factors: the

concentration of 10 nm DAAPT-AuNP conjugate as well as the concentration of DA standard solution. As stated previously, the signal intensity should decrease with increasing DA concentration in the mixed solution. Also, the dynamic range of the calibration curve can be easily adjusted by simply changing the concentration of 10 nm DAAPT-AuNP conjugate solution. We started with the most concentrated (9.5 nM) 10 nm DAAPT-AuNP conjugate solution, and mixed it with DA standard solutions ranging from 100 μM to 2 mM in a 1:1 volume ratio. Some representative SPRi sensorgrams for the exposure of these mixed solutions to cDNA on chip surface are shown in Figure 4.6A. As expected, we see a decrease of signal response with increasing DA concentration in the mixed solutions. The signal intensities for the least concentrated (100 μM) and the most concentrated (2 mM) DA solutions are 13.91 ± 2.69 and 1.15 ± 0.14, respectively. The signal intensity for the most concentrated is approximately 8% of that for the least concentrated. The calibration curve (Figure 4.6B), a plot of signal response vs. dopamine concentration, demonstrates this trend with a negative slope. Also, the calibration curve exhibits good sensitivity and reproducibility, which enables detecting of DA ranging from 100 μM to 2 mM. To further decrease the dynamic range, we lowered the concentration of 10 nm DAAPT-AuNP conjugate to 1.9 nM. Figure 4.7A shows some representative SPRi sensorgrams for the exposure of mixed solutions of 1.9 nM 10 nm DAAPT-AuNP conjugate solution and DA standard solutions ranging from 0.2 pM to 2 μM. Similarly, the signal decreases from 5.64 ± 0.20 (blank) to 1.70 ± 0.33 (2 μM). The calibration curve (Figure 4.7B) has a negative slope, good sensitivity, and reproducibility, showing a two-orders-of-magnitude dynamic range from 0.2 pM to 20 pM. Last but not least, the specificity of the proposed assay for DA detection was studied by choosing a

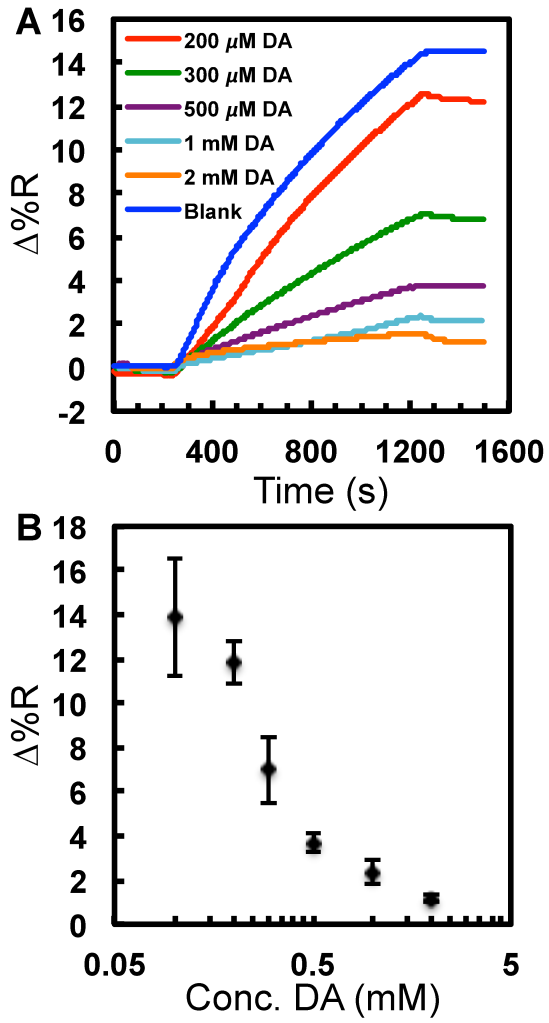

Figure 4.6 Detection of DA using the inhibition assay from higher micromolar (μM) range to lower milimolar (mM) range. (A) Representative SPRi sensorgrams for mixed solutions (1:1 volume ratio) of 10 nm DAAPT-AuNP solution at fixed concentration (9.5 nM) and DA standard solutions at different concentrations: blank (no DA, blue), 200 μM (red), 300 μM (green), 500 μM (purple), 1 mM (cyan), and 2 mM (orange). (B) Calibration curve (SPR signal vs. DA concentration) for the determination of DA in the corresponding concentration range. The error bars represent standard deviation for triplicate measurements.

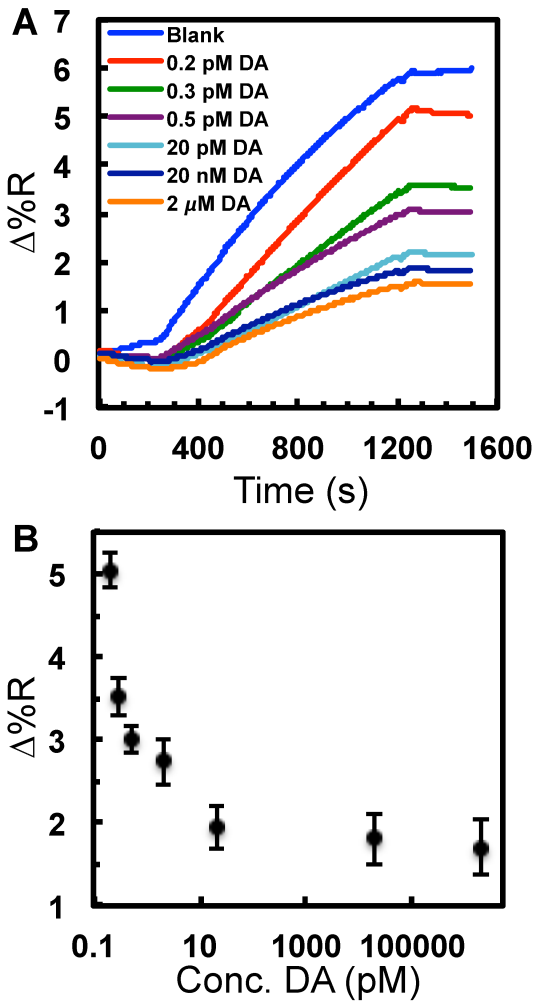

Figure 4.7 Detection of DA using the inhibition assay from higher femtomolar (fM) range to lower picomolar (pM) range. (A) Representative SPRi sensorgrams for mixed solutions (1:1 volume ratio) of 10 nm DAAPT-AuNP solution at fixed concentration (1.9 nM) and DA standard solutions at different concentrations: blank (no DA, blue), 200 fM (red), 300 fM (green), 500 fM (purple), 20 pM (cyan), 20 nM (dark blue), and 2 μM (orange). (B) Calibration curve (SPR signal vs. DA concentration) for the determination of DA in the corresponding concentration range. The error bars represent standard deviation for triplicate measurements.

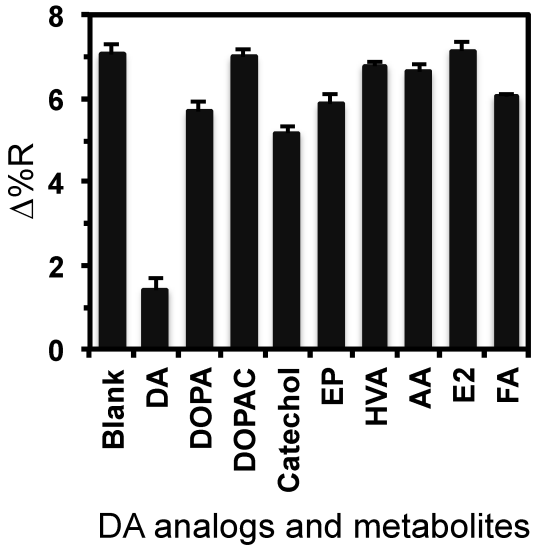

Figure 4.8 Specificity study of the inhibition assay using DA analogs (DOPA, DOPAC, catechol, epinephrine, homovanillic acid, ascorbic acid) and other metabolites (estradiol and folic acid) as potential interferences. The error bars represent standard deviation for at least triplicate measurements of each small molecule. The concentration of the interference is 20 nM in the mixed solution.

series of DA analogs and other metabolites, including DOPA, DOPAC, catechol, epinephrine (EP), homovanillic acid (HVA), ascorbic acid (AA), folic acid (FA), and 17β-estradiol (E2). Some of the analogs get involved in the metabolic pathway for dopamine metabolism as well, thus are good candidates for assay specificity studies.[3,41,42] For each possible interference, DA standard solution in the mixed solution containing 1.9 nM DAAPT-AuNP conjugate was replaced to one of these DA analogs or metabolites at a certain concentration, and exposed to cDNA on SPRi chip surface. The results are summarized in Figure 4.8. A big signal decrease was observed for mixed solution containing DA. Minor signal decrease is observed for DOPA, Catechol, EP, and FA. However, the magnitudes of signal decrease for DOPA and EP are almost negligible when compared to that for DA. This gives us confidence that the proposed assay is specific for DA analysis, with little interference from its analogs and other metabolites.

4.4 Conclusion

We have successfully developed a general sensing strategy incorporating dopamine DNA aptamer (DAAPT) and gold nanoparticle (AuNP) for sensitive and selective detection and quantitation of DA using surface plasmon resonance imaging. By pre-mixing the 10 nm DAAPT-AuNP conjugate with DA, the conjugate probe can be turned "ON" and "OFF" by controlling the concentration of DA standard solutions. A negative correlation between SPRi signal intensity and DA concentration is established based on this detection format. The as-prepared 10 nm DAAPT-AuNP conjugate probe shows high binding affinity to the partially complementary DNA probe on chip surface,

with a dissociation constant (K_d) equal to 3.1 ± 1.4 nM. Two calibration curves were generated with dynamic ranges from 100 μM to 2 mM, and from 200 fM to 20 pM, respectively, which suggests that the dynamic range can be adjusted by changing the concentration of 10 nm DAAPT-AuNP conjugate probe. In addition, the proposed assay exhibits good sensitivity, reproducibility, and high specificity for DA detection. More importantly, this general sensing strategy can be utilized to detect other analytes as well, as long as the target has a corresponding aptamer.

4.5 References

(1) Hilvo, M.; de Santiago, I.; Gopalacharyulu, P.; Schmitt, W. D.; Budczies, J.; Kuhberg, M.; Dietel, M.; Aittokallio, T.; Markowetz, F.; Denkert, C.; Sehouli, J.; Frezza, C.; Darb-Esfahani, S.; Braicu, E. I. *Cancer Res.* **2016**, *76*, 796-804.

(2) Park, M. H.; Igarashi, K. *Biomol. Ther.* **2013**, *21*, 1-9.

(3) Wang, P. C.; Kuchel, O.; Buu, N. T.; Genest, J. *J. Neurochem.* **1983**, *40*, 1435-1440.

(4) Cohen, J. Y. *Science* **2015**, *350*, 47-48.

(5) Meek, S.; Thomson, A. J.; Sutherland, L.; Sharp, M. G.; Thomson, J.; Bishop, V.; Meddle, S. L.; Gloaguen, Y.; Weidt, S.; Singh-Dolt, K.; Buehr, M.; Brown, H. K.; Gill, A. C.; Burdon, T. *Sci. Rep.* **2016**, *6*, 25592.

(6) Homola, J. *Chem. Rev.* **2008**, *108*, 462-493.

(7) McKeating, K. S.; Aube, A.; Masson, J. F. *Analyst* **2016**, *141*, 429-449.

(8) Zhao, S. S.; Bukar, N.; Toulouse, J. L.; Pelechacz, D.; Robitaille, R.; Pelletier, J. N.; Masson, J. F. *Biosens. Bioelectron.* **2015**, *64*, 664-670.

(9) Bockova, M.; Chadtova Song, X.; Gedeonova, E.; Levova, K.; Kalousova, M.; Zima, T.; Homola, J. *Anal. Bioanal. Chem.* **2016**, *408*, 7265-7269.

(10) Rebe Raz, S.; Haasnoot, W. *Trends Anal. Chem.* **2011**, *30*, 1526-1537.

(11) Rodriguez-Mozaz, S.; Marco, M. P.; Lopez de Alda, M. J.; Barcelo, D. *Anal. Bioanal. Chem.* **2004**, *378*, 588-598.

(12) Li, M.; Cushing, S. K.; Wu, N. *Analyst* **2015**, *140*, 386-406.

(13) Maisonneuve, M.; Valsecchi, C.; Wang, C.; Brolo, A. G.; Meunier, M. *Biosens. Bioelectron.* **2015**, *63*, 80-85.

(14) Martinez-Perdiguero, J.; Retolaza, A.; Bujanda, L.; Merino, S. *Talanta* **2014**, *119*, 492-497.

(15) Jang, H. R.; Wark, A. W.; Baek, S. H.; Chung, B. H.; Lee, H. J. *Anal. Chem.* **2014**, *86*, 814-819.

(16) Mousavi, M. Z.; Chen, H. Y.; Lee, K. L.; Lin, H.; Chen, H. H.; Lin, Y. F.; Wong, C. S.; Li, H. F.; Wei, P. K.; Cheng, J. Y. *Analyst* **2015**, *140*, 4097-4104.

(17) Li, S.; Yang, M.; Zhou, W.; Johnston, T. G.; Wang, R.; Zhu, J. *Appl. Surf. Sci.* **2015**, *355*, 570-576.

(18) Liang, W.; Wang, S.; Festa, F.; Wiktor, P.; Wang, W.; Magee, M.; LaBaer, J.; Tao, N. *Anal. Chem.* **2014**, *86*, 9860-9865.

(19) Zeng, S.; Baillargeat, D.; Ho, H. P.; Yong, K. T. *Chem. Soc. Rev.* **2014**, *43*, 3426-3452.

(20) Bolduc, O. R.; Masson, J. F. *Anal. Chem.* **2011**, *83*, 8057-8062.

(21) Wu, B.; Jiang, R.; Wang, Q.; Huang, J.; Yang, X.; Wang, K.; Li, W.; Chen, N.; Li, Q. *Chem. Commun.* **2016**, *52*, 3568-3571.

(22) He, L.; Musick, M. D.; Nicewarner, S. R.; Salinas, F. G.; Benkovic, S. J.; Natan, M. J.; Keating, C. D. *J. Am. Chem. Soc.* **2000**, *122*, 9071-9077.

(23) Jain, P. K.; Huang, X.; El-Sayed, I. H.; El-Sayad, M. A. *Plasmonics* **2007**, *2*, 107-118.

(24) Wang, J. L.; Munir, A.; Zhu, Z. Z.; Zhou, H. S. *Anal. Chem.* **2010**, *82*, 6782-6789.

(25) Malic, L.; Sandros, M. G.; Tabrizian, M. *Anal. Chem.* **2011**, *83*, 5222-5229.

(26) Singh, M.; Holzinger, M.; Tabrizian, M.; Winters, S.; Berner, N. C.; Cosnier, S.; Duesberg, G. S. *J. Am. Chem. Soc.* **2015**, *137*, 2800-2803.

(27) Zagorodko, O.; Spadavecchia, J.; Serrano, A. Y.; Larroulet, I.; Pesquera, A.; Zurutuza, A.; Boukherroub, R.; Szunerits, S. *Anal. Chem.* **2014**, *86*, 11211-11216.

(28) Walsh, R.; DeRosa, M. C. *Biochem. Biophys. Res. Commun.* **2009**, *388*, 732-735.

(29) Mannironi, C.; Di Nardo, A.; Fruscoloni, P.; Tocchini-Valentini, G. P. *Biochemistry* **1997**, *36*, 9726-9734.

(30) Wood, J. B.; Szyndler, M. W.; Halpern, A. R.; Cho, K.; Corn, R. M. *Langmuir* **2013**, *29*, 10868-10873.

(31) Kanda, V.; Kariuki, J. K.; Harrison, D. J.; McDermott, M. T. *Anal. Chem.* **2004**, *76*, 7257-7262.

(32) Nelson, B. P.; Frutos, A. G.; Brockman, J. M.; Corn, R. M. *Anal. Chem.* **1999**, *71*, 3928-3934.

(33) Bain, C. D.; Troughton, E. B.; Tao, Y. T.; Evall, J.; Whitesides, G. M.; Nuzzo, R. G. *J. Am. Chem. Soc.* **1989**, *111*, 321-335.

(34) Jadzinsky, P. D.; Calero, G.; Ackerson, C. J.; Bushnell, D. A.; Kornberg, R. D. *Science* **2007**, *318*, 430-433.

(35) Cutler, J. I.; Auyeung, E.; Mirkin, C. A. *J. Am. Chem. Soc.* **2012**, *134*, 1376-1391.

(36) Rosi, N. L.; Giljohann, D. A.; Thaxton, C. S.; Lytton-Jean, A. K. R.; Han, M. S.; Mirkin, C. A. *Science* **2006**, *312*, 1027-1030.

(37) Liu, Y.; Ai, K.; Lu, L. *Chem. Rev.* **2014**, *114*, 5057-5115.

(38) Loget, G.; Wood, J. B.; Cho, K.; Halpern, A. R.; Corn, R. M. *Anal. Chem.* **2013**, *85*, 9991-9995.

(39) Lytton-Jean, A. K. R.; Mirkin, C. A. *J. Am. Chem. Soc.* **2005**, *127*, 12754-12755.

(40) Randeria, P. S.; Jones, M. R.; Kohlstedt, K. L.; Banga, R. J.; Olvera de la Cruz, M.; Schatz, G. C.; Mirkin, C. A. *J. Am. Chem. Soc.* **2015**, *137*, 3486-3489.

(41) Youdim, M. B.; Edmondson, D.; Tipton, K. F. *Nat. Rev. Neurosci.* **2006**, *7*, 295-309.

(42) Weinshenker, D. *Nat. Med.* **2010**, *16*, 969-970.

Chapter 5 Small-Molecule (Micro)Arrays for the Multiplexed Detection of Metabolites by Surface Plasmon Resonance Imaging

5.1 Introduction

The development of sensor based approaches for the detection and quantitative measurement of small molecules (MW < 1000 Da) is an active field of research, which is impacting areas such as human health[1,2], environmental monitoring[3], and pharmaceutical research[4,5] . For example, the measurement of small-molecule metabolites is of great importance due to the promise of linking the metabolite profiles to disease states.[6] By now, the identification and quantification of metabolites are being mainly driven by the development of nuclear magnetic resonance[7-9] (NMR) and mass spectrometry[10] (MS) methodologies. These powerful tools are promising and will continue to generate metabolite profiles that can benefit biomarker discovery and medical diagnostic. It is expected that the determination of the quantities of metabolites in a panel through a single measurement will greatly aid the diagnosis and treatment of an expanded number of diseases. To this regard, rapid, facile, and quantitative multiplexed sensing platforms that enable us to detect and quantitate multiple metabolites simultaneously will be significant and highly demanded.

Surface plasmon resonance imaging (SPRi) is such a sensing platform with great multiplex capability, which combines the unique characteristics of regular surface plasmon resonance (SPR) technique and the imaging power of a CCD camera.[11,12] Generally, SPR is a label-free optical technique, very sensitive to the refractive index change introduced by the adsorption and/or desorption of molecules within a few

hundreds nanometers (nm) to the metal-medium interface.[13] This unique mechanism allows researchers to detect and quantitate biomolecular interaction in real-time and in situ, thus provides SPR with broad applications in sensing proteins[14-16] and nucleic acids[17]. However, the detection of a single small molecule using this technique is not commonly demonstrated, not even the multiplexed detection of multiple small molecules simultaneously, probably due to the sensitivity challenge associated with the low refractive index change from small molecule adsorption. People have been employing nanomaterials[18] to enhance the signal intensity or using other detection format such as competition[19] instead of direct detection to measure a single small molecule target.

Small-molecule microarray (SMM) is a concept developed by Schreiber et al in 1990s, where a broad range of random small molecules are covalently patterned on a solid (typically glass) surface in a microarray format.[20-22] Such a platform allows the probe of interactions between SMMs and proteins of interest, thus the detection of protein-ligand interactions in a parallel and high-throughput fashion. The microarray platform enables the discovery of novel interactions with potential applications to ligand discovery, immunoglobulin profiling, and comparative analysis of cellular states.[23,24]

In this chapter, by combining the multiplex capability of SPRi with the high-throughput advantage of SMMs, we successfully developed small-molecule arrays (SMAs) on our homemade chip surface to conveniently detect and quantitate multiple metabolites simultaneously through a single SPRi measurement. It should be pointed out here we name it small-molecule arrays, not microarrays, because the size of the gold spots on our homemade SPRi chip is in the millimeter length scale. To the best of our

knowledge, this is the first report using SPR/SPRi technique to do multiplexed small-molecule metabolites detection.

5.2 Experimental

Chemicals and reagents. Folic acid (FA), dopamine (DA), cysteine (Cys), N-hydroxy-succinimide (NHS), N-(3-dimethylaminopropyl)-N'-ethylcarbodiimide hydrochloride (EDC), hydrogen peroxide solution (30% (w/w) in water), ethanolamine solution, and phosphate buffered saline (PBS) 10× concentrate were all purchased from Sigma-Aldrich and used as received. Anti-FA antibody (mouse monoclonal [B762F]), anti-DA antibody (mouse monoclonal [2B11]), and anti-cysteine antibody (mouse monoclonal [3A4]) were purchased from Abcam and received in storage buffer (0.05% sodium azide and PBS). Goat anti-mouse IgG (H+L) was obtained from MP Biomedicals in solid form. 2-(2-{2-[2-(2-[2-(11-mercapto-undecyloxy)-ethoxy]-ethoxy)-ethoxy]-ethoxy}-ethoxy)-ethoxy-acetic acid (HS-$(CH_2)_{11}$-EG_6-OCH_2-COOH) and 2-(2-{2-[2-(2-[2-(11-mercapto-undecyloxy)-ethoxy]-ethoxy)-ethoxy]-ethoxy}-ethoxy)-ethoxy-ethanol (HS-$(CH_2)_{11}$-EG_6-OH) were purchased from ProChimia Surfaces. (Tridecafluoro-1,1,2,2-tetrahydrooctyl)-1-dimethylchlorosilane was purchased from United Chemical Technologies. Anhydrous ethyl alcohol was obtained from Commercial Alcohols. Deionized (DI) water with a resistivity greater than 18 MΩ•cm was filtered in a Barnstead Nanopure purification system.

Fabrication of SPRi chip with 9 gold spots. An SF-10 glass sheet (100 mm × 100 mm × 1 mm) was purchased from Schott Glass. The sheet was cut into small square substrates (18 mm × 18 mm). The substrates were cleaned using hot piranha solution (1:4

30% H_2O_2:H_2SO_4) followed by thorough rinsing with DI water. Substrates were blown dry using Ar gas. [*Warning: Piranha solution should be handled with extreme care; it is a strong oxidant and reacts violently with many organic materials. It also presents an explosion danger. All work should be performed under a fume hood with appropriate personal safety equipment*.] The cleaned and dried substrates were mounted to a mask that expose nine 2 mm diameter round spots and placed into the chamber of a thermal evaporator (Torr International Inc., New Windsor, NY). Metal films of chromium (2 nm) and gold (42 nm) were sequentially coated on the glass substrate through the mask. After removal from the evaporator, the substrates were then exposed to a vapor of (tridecafluoro-1,1,2,2-tetrahydrooctyl)-1-dimethylchlorosilane under reduced pressure for 24 h to create a hydrophobic background on the glass surface. The SPRi chips were stored in a desiccator under vacuum at room temperature until use.

Design and fabrication of small-molecule arrays (SMAs). The homemade SPRi chip was rinsed with pure ethanol and deionized water and dried under an argon gas flow. A 2.5 μL droplet of 1 mM mixed solutions of HS-$(CH_2)_{11}$-EG_6-OCH_2-COOH and HS-$(CH_2)_{11}$-EG_6-OH with different COOH/OH ratios (0, 0.2, 0.5, 0.8, 1.0) was added to all gold spots of the chip. The modified chip with the solution droplets was stored in a humid petri dish overnight (~17 h) at room temperature to form a self-assembled monolayer (SAM). Then, the chip was rinsed with DI water and dried under argon gas flow. A 2.5 μL droplet of mixed 5 mM EDC and 1 mM NHS solution was added to each gold spot of the chip. The chip was incubated in a humid petri dish for 30 min at room temperature. After chip cleaning and drying, 1 mM of metabolite (FA, DA, Cys) solution was used to modify all spots for another 2 h. Next, ethanolamine was employed to block the surface.

For a single metabolite chip surface, each ratio of COOH/OH (0.2, 0.5, 0.8, 1.0) includes two gold spots, while only one gold spot contains the COOH/OH ratio of 0 (negative control, all OH groups on the surface). For the SMAs surface, the chip has three gold spots for each metabolite, respectively.

Binding of primary antibodies and/or secondary antibody. The binding of primary antibodies and/or secondary antibody to their metabolite antigens was measured by SPRi. Briefly, a single metabolite chip surface was prepared according to the procedure described above; the modified chip was mounted to the SPRi instrument (Horizon SPRimager, GWC Technologies, Madison, MI) and antibody solutions were exposed to the metabolite surface continuously. A real-time SPRi sensorgram was obtained and quantitative data were acquired by subtracting SPRi signal intensity at steady state after one solution injection from baseline. For folic acid surface, the concentration of folic acid primary antibody is 5.0 μg/mL (33 nM); for dopamine surface, the concentrations of dopamine primary antibody and secondary antibody (goat-anti-mouse IgG) are 10.0 μg/mL (67 nM) and 22.4 μg/mL (150 nM) respectively; for cysteine surface, the concentrations of cysteine primary antibody and secondary antibody are 5 μg/mL (33 nM) and 22.4 μg/mL (150 nM) respectively.

Cross-reactivity evaluation of primary antibodies. To evaluate the cross-reactivity of each primary antibody, the SMAs surface was used. The binding of 10 μg/mL (200 nM) primary antibody to the SMAs surface was measured by SPRi. The real-time SPRi sensorgrams were recorded and analyzed.

Sensing performance based on inhibition format. 20.0 μg/mL (133 nM) dopamine antibody and 22.4 μg/mL (150 nM) goat-anti-mouse IgG were continuously

exposed to dopamine surface with 0, 0.8, and 1.0 ratios of COOH/OH. For inhibition study, a mixed solution of 20.0 μg/mL (133 nM) and 100 μM dopamine was first incubated at room temperature for 1 h. Then, the mixed solution and 22.4 μg/mL (150 nM) were exposed to the same dopamine chip surface for SPRi measurement.

Sensing performance based on displacement format. We used the SMAs surface to do the multiplexed detection of dopamine, folic acid, and cysteine. Briefly, a mixed solution of 30.0 μg/mL (200 nM) dopamine antibody, 30.0 μg/mL folic acid antibody, and 30.0 μg/mL cysteine antibody, then a mixed solution of metabolites with different concentrations were exposed to the SMAs surface continuously. The real-time SPRi sensorgrams were recorded and analyzed. The concentrations of metabolites are as follows: 2, 10, 20, 50, 200 μM dopamine; 5 nM, 10 nM, 50 nM, 100 nM, 10 μM folic acid; 2, 10, 50, 100, 200 μM cysteine.

5.3 Results and Discussion

The fabrication process of the SMAs on the SPRi chip surface with 9 gold spots is illustrated in Figure 5.1. Metabolites of interest are patterned on SPRi chip surface via self-assembled monolayers (SAMs) and EDC/NHS chemistry. First, a mixed thiolate SAMs terminated with carboxyl (-COOH) group and hydroxyl (-OH) group are formed on chip surface via strong gold-thiol interaction[25]; then the COOH group is activated by EDC/NHS chemistry, and metabolites containing primary amino ($-NH_2$) group are covalently attached through the reaction between NH_2 group and NHS group.[26] By this simple method, we can easily attach any primary amine-containing metabolites, deliberately design the pattern of the SMAs, and control the number of metabolites

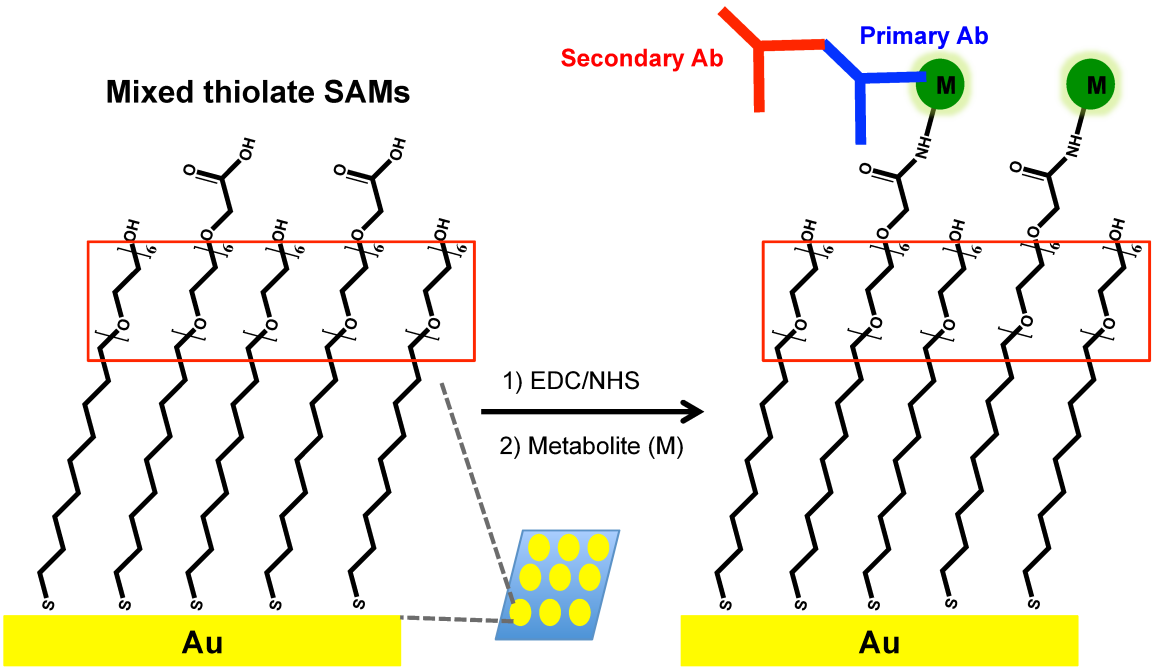

Figure 5.1 Schematic illustration of the fabrication of the small-molecule arrays (SMAs) on the SRPi chip surface with 9 gold spots. Mixed thiolate self-assembled monolayers (SAMs) terminated with carboxyl (-COOH) group and hydroxyl (-OH) group are formed on chip surface via gold-thiol interaction. Metabolites containing primary amino ($-NH_2$) group are immobilized to chip surface via EDC/NHS chemistry. The pattern of the SMA and the number of metabolites can be controlled accordingly. The binding of the primary antibody (Ab) and secondary Ab can be measured by SPRi. Poly(ethylene glycol groups) introduced by the formation of thiolate SAMs are highlighted in the red rectangles.

accordingly. The specific interactions of metabolites and their primary antibodies allow the binding of antibodies to the chip surface, therefore the detection of the binding through SPRi measurement. In contrast to the conventional way, analytes instead of the molecular recognition elements are patterned on chip surface, which makes it fairly easy to detect the relatively bigger antibodies (MW 150 kDa) binding and thus overcome the sensitivity issue associated with small molecules (MW< 1000 Da) binding. Secondary antibody (demonstrated in this work) or secondary antibody conjugated metal (i.e. Au or Ag) nanoparticles (not demonstrated in this work) can serve as a further signal amplifier to enhance the signal intensity. Both inhibition and displacement detection formats are included in this work. The former detection format is just shown as a proof of concept to detect dopamine, whereas the latter format is mainly used to do the multiplexed detection of three metabolites simultaneously.

Dopamine (DA), folic acid (FA), and cysteine (Cys) are selected as model metabolite targets, and their corresponding mouse monoclonal antibodies (Ab): DA-Ab, FA-Ab, Cys-Ab, are used as the molecular recognition elements and primary antibodies. To further enhance the signal, goat-anti-mouse antibody (G-a-M Ab) is employed as the secondary antibody. We first studied the binding of primary antibodies to their metabolite targets and optimized the density of metabolites on chip surface through SPRi measurements. It is expected that the density of small-molecule metabolite on a solid surface could affect the binding affinity of its antibody in such a heterogeneous assay, based on our previous study. Also, a mixed SAMs method[27] is commonly used to tune the useful functional group ratio on a surface to attach the bioreceptor as well as avoid nonspecific adsorption. Thus, we chose five different COOH/OH ratios (0, 0.2, 0.5, 0.8,

1.0) in the mixed thiolate SAMs on chip surface. Here, OH group serves as a surface diluent, and the density of metabolite is determined by the percentage of COOH group (useful functional group) on the surface. Ideally, a higher percentage of COOH group will generate a higher density of metabolite. It is noted that poly(ethylene glycol) groups (red rectangles in Figure 5.1) are introduced to the surface as well by the formation of thiolate SAMs to reduce the nonspecific adsorption. Figure 5.2 shows the SPRi measurement results of continuous binding of DA-Ab and G-a-M Ab to DA chip surface with different DA densities. Two big signal increase regimes are clearly observed in the SPRi sensorgrams (Figure 5.2A) after injections of 10.0 μg/mL (67 nM) DA-Ab and 22.4 μg/mL (150 nM) G-a-M Ab, respectively. The big signal increase regimes are attributed to the binding of the primary antibody and the secondary antibody, which is as expected. While for the negative control spot (COOH/OH = 0), no signal increase is observed. More importantly, a surface ratio of 0.8 COOH/OH gives the highest signal increase (Figure 5.2B), no matter which regime is used to determine the signal output. The binding results for 5.0 μg/mL (33 nM) FA-Ab and Cys-Ab are included in Figure 5.3 and Figure 5.4, respectively. Interestingly, the highest signal increase observed for FA-Ab binding occurs under a surface ratio of 0.2 COOH/OH, while that observed for Cys-Ab binding happens under a surface ratio of 0.5 COOH/OH. All these results confirm: 1) the surface density of metabolites does have a significant effect on Abs binding, which is consistent with our previous study; 2) the optimal surface densities for different metabolite targets vary, probably depending on the sizes of the metabolite molecules and the orientation of these molecules on the chip surface. Since for a relatively larger

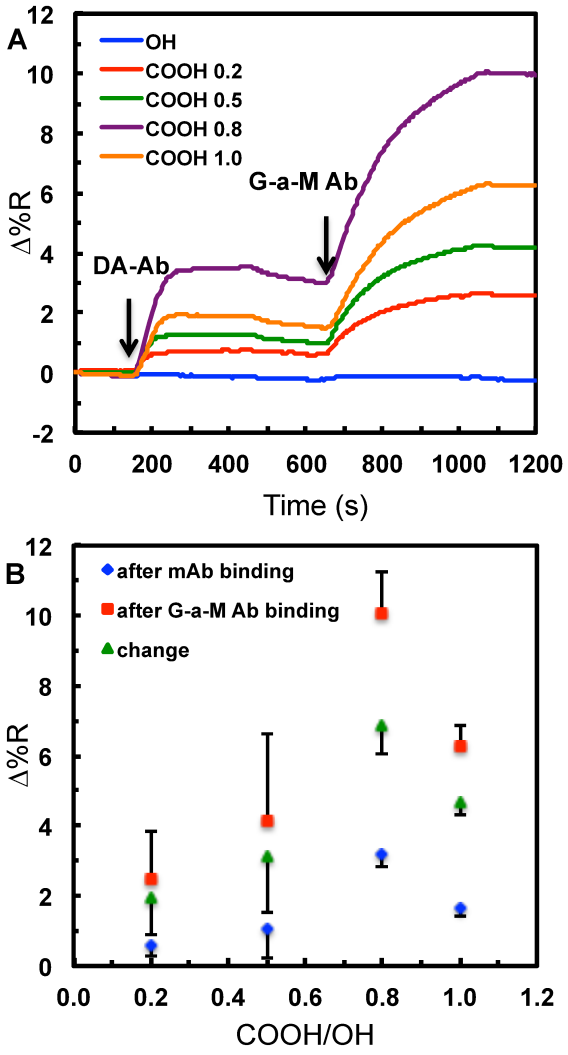

Figure 5.2 SPRi measurement of the continuous binding of dopamine primary antibody (DA-Ab) and goat-anti-mouse secondary antibody (G-a-M Ab) to dopamine chip surface with different COOH/OH ratios (i.e. different DA surface densities). (A) SPRi sensorgrams for the binding of 10.0 μg/mL (67 nM) DA-Ab, and then 22.4 μg/mL (150 nM) G-a-M Ab to a single chip surface patterned with 0, 0.2, 0.5, 0.8, and 1.0 ratios of COOH/OH. The arrows indicate the injection of the primary antibody and the secondary antibody. (B) Plots of SPRi signal vs. COOH/OH ratio. The data points are the mean of triplicate measurements, and the error bars are the standard deviation.

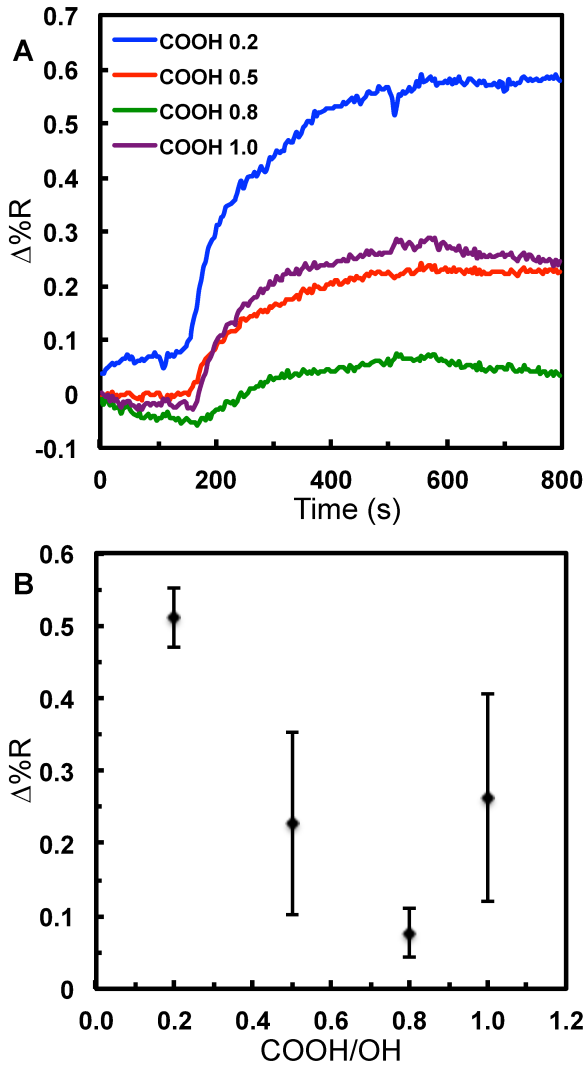

Figure 5.3 SPRi measurement of the binding of folic acid primary antibody (FA-Ab) to folic acid chip surface with different COOH/OH ratios (i.e. different FA surface densities). (A) Corrected SPRi sensorgrams for the binding of 5.0 μg/mL (33 nM) FA-Ab to a single chip surface patterned with 0.2, 0.5, 0.8, and 1.0 ratios of COOH/OH. (B) Plot of SPRi signal vs. COOH/OH ratio. The data points are the mean of triplicate measurements, and the error bars are the standard deviation.

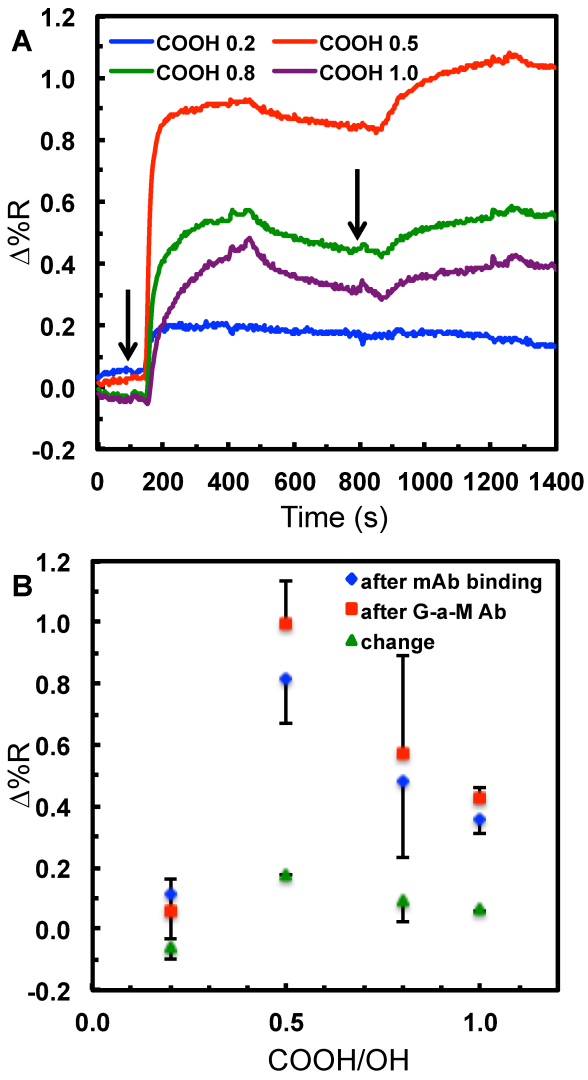

Figure 5.4 SPRi measurement of the continuous binding of cysteine primary antibody (Cys-Ab) and goat-anti-mouse secondary antibody (G-a-M Ab) to cysteine chip surface with different COOH/OH ratios (i.e. different Cys surface densities). (A) Corrected SPRi sensorgrams for the binding of 5.0 μg/mL (33 nM) DA-Ab, and then 22.4 μg/mL (150 nM) G-a-M Ab to a single chip surface patterned with 0.2, 0.5, 0.8, and 1.0 ratios of COOH/OH. The arrows indicate the injection of the primary antibody and the secondary antibody. (B) Plots of SPRi signal vs. COOH/OH ratio. The data points are the mean of triplicate measurements, and the error bars are the standard deviation.

metabolite molecule (e.g. FA), a lower surface density (i.e. 0.2 COOH/OH) will lead to less steric hindrance effect on protein molecule's binding, and vice versa.

Under optimized surface densities of metabolites on chip surface, we investigated a second key factor, which is the cross-reactivity of each primary Ab, since the ultimate goal is to pattern all the metabolites on the same chip surface (i.e. SMA) and let their corresponding primary Abs bind to the SMAs. The results are included in Figure 5.5, which give us confidence that all primary antibodies show reasonably specific binding to their metabolite antigens, with little or negligible cross-reactivity observed.

There are two ways to do the multiplexed detection of metabolites using the small-molecule arrays: inhibition and displacement. Inhibition means we need to mix primary Abs with metabolites first, and let them react for a certain time. Then the mixed solution will be exposed to the small-molecule arrays surface. So the higher the concentration of metabolites in the mixed solution, the less Abs will bind to the arrays surface, which results in a signal decrease due to the decreased number of Abs bound. For the displacement detection format, we will first expose Abs to the small-molecule arrays surface, then inject mixed metabolites solution to displace bound Abs from the chip surface, thus generate a decreased signal that corresponds to the desorption of Abs from the surface. The inhibition format is only used to detect DA as a proof of concept, while the displacement format is used to do the multiplexed detection of DA, FA, and Cys. The reason to choose displacement instead of inhibition is because, in our opinion, inhibition involves an extra incubation step (Abs + metabolites) that will increase the total assay time by at least 1 h, while in some cases even more incubation time may be needed. The results for DA detection using the inhibition format are demonstrated in

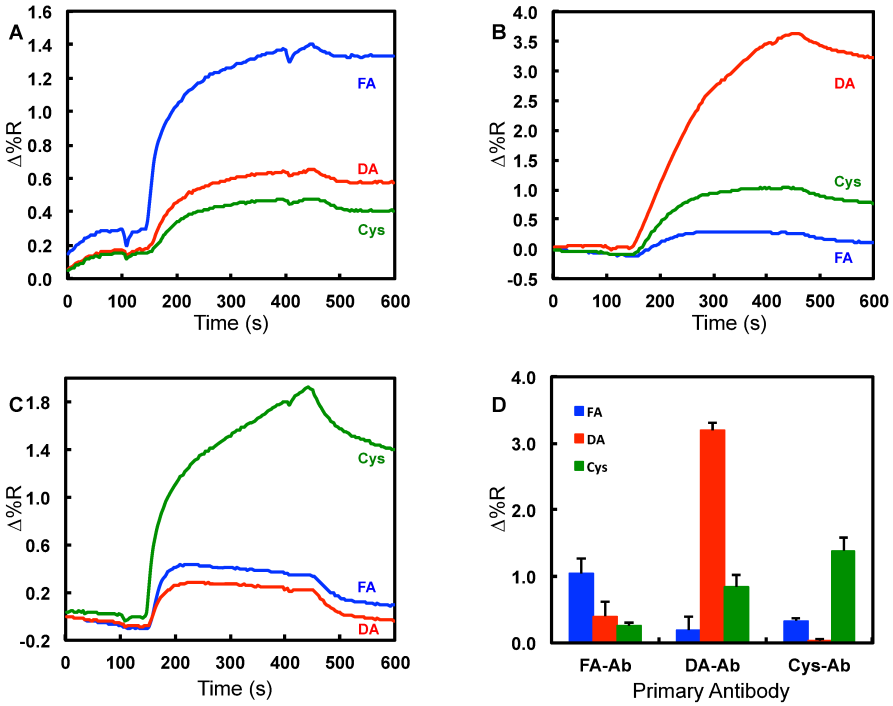

Figure 5.5 Characterization of the primary antibodies' (Abs) cross-reactivity using the small-molecule arrays (SMAs) patterned with dopamine (DA), folic acid (FA), and cysteine (Cys) with optimal surface densities. SPRi sensorgrams for the binding of 10 μg/mL (67 nM) (A) FA-Ab, (B) DA-Ab, (C) Cys-Ab. (D) Cross-reactivity of the Abs to different metabolites surfaces on the same chip. The bar height represents the mean SPRi signal of triplicate measurements, and the error bars are the standard deviation.

Figure 5.6. Continuous binding of 20.0 μg/mL (133 nM) DA-Ab and 22.4 μg/mL (150 nM) G-a-M Ab is observed under two surface ratios (0.8 and 1.0) of COOH/OH (Figure 5.6A). Mixing 100 μM DA with the same concentration of DA-Ab can almost inhibit all the DA-Abs (Figure 5.6B) and decrease the signal intensity from roughly 5.0 to 0.2 for surface ratio of 0.8 COOH/OH after primary Ab binding (Figure 5.6C). This inhibition effect is also directly indicated by the 3D difference image inserted in Figure 5.6A and Figure 5.6B. All the results in Figure 5.6 suggest that inhibition format is applicable for metabolites detection. Figure 5.7 contains the results for the multiplexed detection of DA, FA, and Cys using the SMAs and the displacement format. Mixed solutions of primary antibodies (DA-Ab, FA-Ab, Cys-Ab) and mixed solutions of metabolites (DA, FA, Cys) are continuously injected and exposed to the SMAs surface. We first see the signal increase due to primary Abs binding, and then the signal decrease due to the displacement of Abs, shown in Figure 5.7A. Thus, the magnitudes of signal decrease are related to the concentrations of metabolites in the mixed solution, and can be employed as the signal output in the calibration curves (Figure 5.7B, Figure 5.7C, Figure 5.7D). The dynamic ranges for DA, FA, and Cys are 2 – 200 μM, 5 nM – 10 μM, and 2 – 200 μM, respectively. All these dynamic ranges cover the physiological levels for the three metabolites reported in the Human Metabolome Database[28]. Considering the reduced assay time and good sensing performance, we believe the displacement format is a rapid, facile, and quantitative way to do the multiplexed sensing.

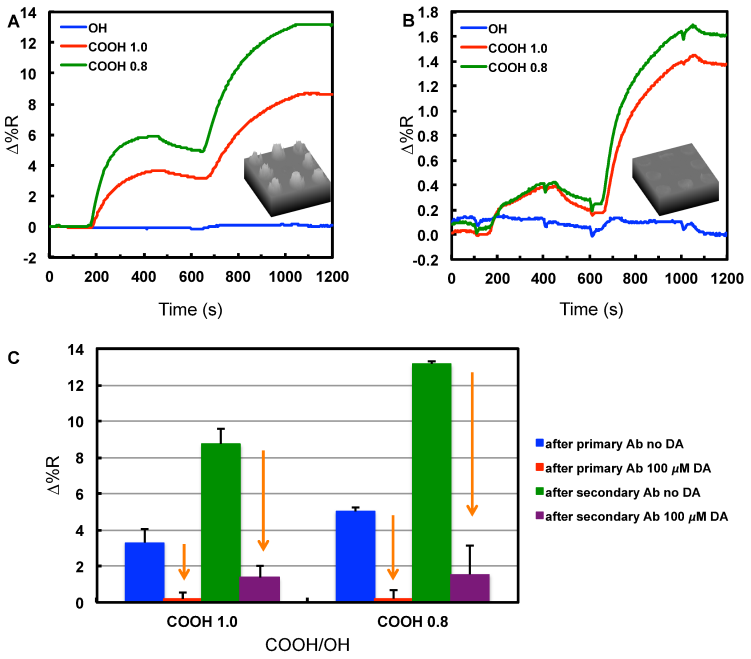

Figure 5.6 The inhibition of dopamine (DA) on antibody binding. SRPi sensorgrams for the continuous binding of (A) 20.0 μg/mL (133 nM) DA-Ab and 22.4 μg/mL (150 nM) G-a-M Ab; (B) mixed 20.0 μg/mL DA-Ab with 100 μM DA and 22.4 μg/mL G-a-M Ab. Insets are 3D difference images showing the chip surface after SPRi measurements of (A) and (B) respectively. The spot in the center of the chip is the negative control with 0 COOH/OH ratio, while the four spots at the corners and that in the middles have 1.0 and 0.8 COOH/OH ratios, respectively. (C) The inhibition effect after primary Ab binding and secondary Ab binding. The bars height represents the mean signal intensity of triplicate measurements, and the error bars are standard deviations.

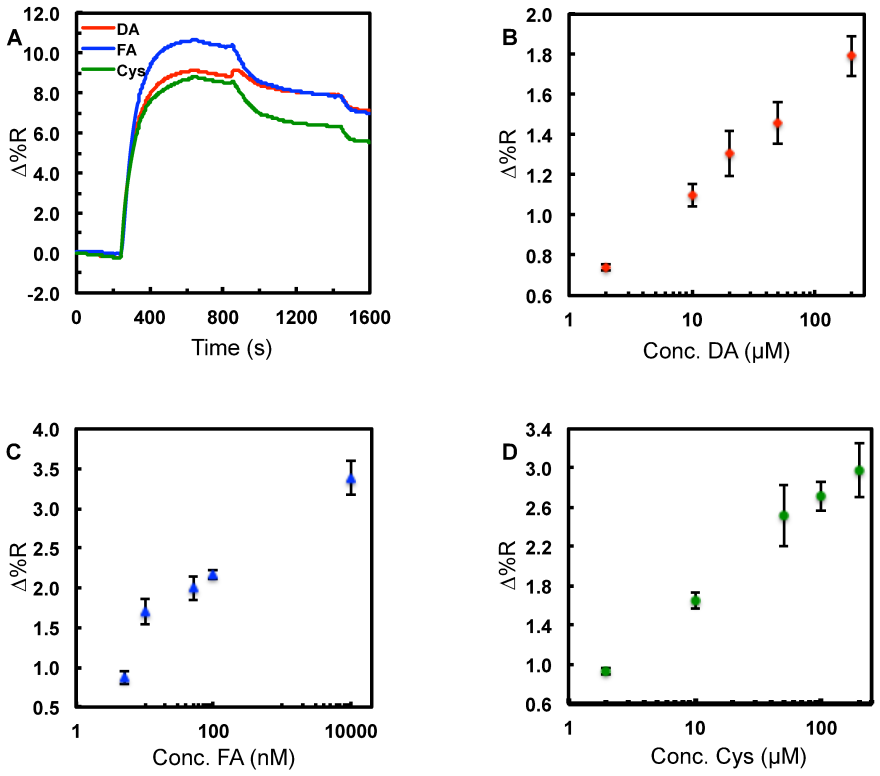

Figure 5.7 Multiplexed detection of dopamine (DA), folic acid (FA), and cysteine (Cys) using the SMAs. (A) Representative SPRi sensorgrams for the binding of a mixed solution of Abs (30.0 μg/mL of DA-Ab, 30.0 μg/mL of FA-Ab, and 30.0 μg/mL of Cys-Ab), then a mixed solution of metabolites (10 μM FA, 200 μM DA, and 200 μM Cys) to DA surface (red), FA surface (blue), and Cys surface (green) on a single SPRi chip. Calibration curves (plots of SPRi signal vs. metabolite concentration) for the determination of (B) DA, (C) FA, and (D) Cys. In all plots, the symbols represent the mean of triplicate measurements, and the error bars are the standard deviation.

5.4 Conclusion

In summary, small-molecule arrays were developed for the multiplexed detection of metabolites by surface plasmon resonance imaging. Primary antibodies and secondary antibody are good reagents to enhance the signal intensity, thus overcome the sensitivity issue associated with direct small molecule detection using this technique. Both inhibition and displacement detection formats demonstrate success on metabolites detection, but displacement format can reduce the total assay time due to the elimination of an extra incubation step. Last, but not least, surface density of metabolites on chip surface is a significant factor to bear in mind in terms of surface chemistry choices, assay design, optimization, and performance. This work demonstrates the applicability of array concept as well as SPRi platform with great potential to do multiplexed metabolite sensing and protein profiling.

5.5 References

(1) Donia, M. S.; Fischbach, M. A. *Science* **2015**, *349*, 1254766.

(2) Li, X. J.; Hu, B. Y.; Jones, S. A.; Zhang, Y. S.; Lavaute, T.; Du, Z. W.; Zhang, S. C. *Stem Cells* **2008**, *26*, 886-893.

(3) Akki, S. U.; Werth, C. J.; Silverman, S. K. *Environ. Sci. Technol.* **2015**, *49*, 9905-9913.

(4) Guan, Y.; Shan, X.; Zhang, F.; Wang, S.; Chen, H. Y.; Tao, N. *Sci. Adv.* **2015**, *1*, e1500633.

(5) McKeating, K. S.; Aube, A.; Masson, J. F. *Analyst* **2016**, *141*, 429-449.

(6) Johnson, C. H.; Ivanisevic, J.; Siuzdak, G. *Nat. Rev. Mol. Cell Biol.* **2016**, *17*, 451-459.

(7) Larive, C. K.; Barding, G. A.; Dinges, M. M. *Anal. Chem.* **2015**, *87*, 133-146.

(8) Clendinen, C. S.; Pasquel, C.; Ajredini, R.; Edison, A. S. *Anal. Chem.* **2015**, *87*, 5698-5706.

(9) Guennec, A. L.; Giraudeau, P.; Caldarelli, S. *Anal. Chem.* **2014**, *86*, 5946-5954.

(10) Huan, T.; Troyer, D. A.; Li, L. *Sci. Rep.* **2016**, *6*, 32272.

(11) Nelson, B. P.; Frutos, A. G.; Brockman, J. M.; Corn, R. M. *Anal. Chem.* **1999**, *71*, 3928-3934.

(12) Spoto, G.; Minunni, M. *J. Phys. Chem. Lett.* **2012**, *3*, 2682-2691.

(13) Homola, J. *Chem. Rev.* **2008**, *108*, 462-493.

(14) Chen, Y.; Nakamoto, K.; Niwa, O.; Corn, R. M. *Langmuir* **2012**, *28*, 8281-8285.

(15) Maisonneuve, M.; Valsecchi, C.; Wang, C.; Brolo, A. G.; Meunier, M. *Biosens. Bioelectron.* **2015**, *63*, 80-85.

(16) Wu, B.; Jiang, R.; Wang, Q.; Huang, J.; Yang, X.; Wang, K.; Li, W.; Chen, N.; Li, Q. *Chem. Commun.* **2016**, *52*, 3568-3571.

(17) Li, X. M.; Wang, Y.; Wang, L. L.; Wei, Q. L. *Chem. Commun.* **2014**, *50*, 5049-5052.

(18) Wang, J.; Zhou, H. S. *Anal. Chem.* **2008**, *80*, 7174-7178.

(19) Zhao, S. S.; Bichelberger, M. A.; Colin, D. Y.; Robitaille, R.; Pelletier, J. N.; Masson, J. F. *Analyst* **2012**, *137*, 4742-4750.

(20) Hergenrother, P. J.; Depew, K. M.; Schreiber, S. L. *J. Am. Chem. Soc.* **2000**, *122*, 7849-7850.

(21) MacBeath, G.; Koehler, A. N.; Schreiber, S. L. *J. Am. Chem. Soc.* **1999**, *121*, 7967-7968.

(22) Kuruvilla, F. G.; Shamji, A. F.; Sternson, S. M.; Hergenrother, P. J.; Schreiber, S. L. *Nature* **2002**, *416*, 653-657.

(23) Winssinger, N.; Ficarro, S.; Schultz, P. G.; Harris, J. L. *Proc. Natl. Acad. Sci. U. S. A.* **2002**, *99*, 11139-11144.

(24) Bradner, J. E.; McPherson, O. M.; Koehler, A. N. *Nat. Protoc.* **2006**, *1*, 2344-2352.

(25) Bain, C. D.; Troughton, E. B.; Tao, Y. T.; Evall, J.; Whitesides, G. M.; Nuzzo, R. G. *J. Am. Chem. Soc.* **1989**, *111*, 321-335.

(26) Lim, C. Y.; Owens, N. A.; Wampler, R. D.; Ying, Y.; Granger, J. H.; Porter, M. D.; Takahashi, M.; Shimazu, K. *Langmuir* **2014**, *30*, 12868-12878.

(27) Frederix, F.; Bonroy, K.; Laureyn, W.; Reekmans, G.; Campitelli, A.; Dehaen, W.; Maes, G. *Langmuir* **2003**, *19*, 4351-4357.

(28) Wishart, D. S.; Jewison, T.; Guo, A. C.; Wilson, M.; Knox, C.; Liu, Y. F.; Djoumbou, Y.; Mandal, R.; Aziat, F.; Dong, E.; Bouatra, S.; Sinelnikov, I.; Arndt, D.; Xia, J. G.; Liu, P.; Yallou, F.; Bjorndahl, T.; Perez-Pineiro, R.; Eisner, R.; Allen, F.; Neveu, V.; Greiner, R.; Scalbert, A. *Nucleic Acids Res.* **2013**, *41*, D801-D807.

Chapter 6 Conclusions and Future Outlook

6.1 Chapter Conclusions

Small-molecule metabolite is becoming a significant type of biomarkers, thanks to the emergence and rapid development of metabolomics. Quite a variety of metabolites were reported to be associated with certain diseases and medical conditions. To this regard, the drive towards sensing from a single metabolite to multiple metabolites was the primary motivation to the work conducted in this thesis on surface plasmon resonance sensing (SPR) of metabolites. However, a common challenge associated with the detection of small molecules using SPR is the sensitivity issue. To tackle this issue, a series of indirect sensing strategies involving gold nanoparticles or relatively large antibody molecules have been developed in Chapter 2, 3, and 4, using different metabolites as targets. Chapter 5 demonstrated for the first time the use of SPR imaging (SPRi) as a promising platform to detect multiple metabolites simultaneously on a single SPR chip. This thesis has shown the great power of SPR in sensing a single metabolite target to multiple targets simultaneously with proper design and choice of sensing strategy and detection format, providing new avenues and direction of SPR applications. Given the current situation of direct SPR sensing of small molecules, the distribution of which is sporadic, this thesis would provide insights to the SPR community and inspire more work to be done in terms of small molecule sensing, thus having more impact in the fields of medical diagnosis of small molecule biomarkers, therapeutic drug discovery, food safety control, and environmental monitoring.

Chapter 2 introduced the development of a competitive assay for folic acid (FA), which combines a periplasmic binding protein for recognition with target modified gold nanoparticles (AuNPs). Specifically, a SPR imaging substrate containing immobilized folate binding protein (FBP) is used to measure the adsorption of FA conjugated AuNPs (FA-AuNPs). The immobilization of the FBP and the binding of the FA conjugated AuNPs is characterized and optimized. It is shown that free FA in solution can be quantitatively measured by competition for the surface binding sites with the FA-AuNPs. We demonstrate that the dynamic range can be lowered from micromolar to nanomolar by decreasing the concentration of FA-AuNPs involved in the competition. More importantly, this type of competitive assay can be applied to other metabolites as well, as long as the metabolites can be conjugated to AuNPs.

In chapter 3, we utilized an indirect detection format and developed a inhibition immunosensor for sensitive and selective analysis of a sex hormone (17β-estradiol, E2) in the physiological concentration range using SPR imaging (SPRi). One competitor, BSA-E2 conjugate, was immobilized to the gold chip surface via the reaction between the primary amine group of the conjugate and the succinimide group (NHS) introduced by the formation of a thiol-NHS monolayer on gold surface. Free E2 molecules in solution compete with BSA-E2 conjugates on chip surface for binding sites provided by a monoclonal anti-E2 antibody (E2-Ab). It was found the binding affinity of E2 antibody to BSA-E2 conjugate increases with decreasing surface density of BSA-E2 conjugate. The surface coverage of BSA-E2 conjugate on chip surface and the concentration of E2-Ab were optimized to obtain the highest sensitivity. Under optimal conditions, a sigmoidal calibration curve with a negative slope and a dynamic range from 10 pM to 2 nM was

generated, showing good sensitivity and reproducibility. Moreover, the immunosensor exhibits high specificity for E2 detection when using estrone (E1) as a potential interference.

In chapter 4, we successfully developed a general strategy incorporating dopamine (DA) DNA aptamer (DAAPT) and gold nanoparticle (AuNP) for DA analysis using SPRi. The as-prepared 10 nm DAAPT-AuNP conjugate demonstrates strong binding affinity (K_d = 3.1 ± 1.4 nM) to the complementary DNA (cDNA) probe on the gold chip surface. The cDNA probe was immobilized to the chip surface via polydopamine surface chemistry, which allows the Michael addition of any primary amine-terminated biomolecules. Two calibration curves were generated with dynamic ranges from 100 μM to 2 mM, and from 200 fM to 20 nM, respectively. The calibration curves have negative slopes, showing good agreement to a dose-response curve in an enzyme inhibition assays. In addition, the inhibition strategy was evaluated to be specific for DA detection using a series of DA analogs and other metabolites as potential interferences.

Chapter 5 demonstrated the great multiplex potential of SPRi platform to detect multiple metabolites simultaneously on a single SPR chip. Small-molecule (micro)arrays were first developed to immobilized multiple metabolite targets onto our SPR chip surface. Dual signal amplification strategy by primary antibody and secondary antibody was employed to overcome the sensitivity challenge. The surface coverage for each target was optimized to give a higher signal response for the following corresponding antibody binding to the target. All the antibodies used have low cross-reactivity to other metabolites on chip surface, which is of great importance for the success of the

multiplexed detection. This work shows both inhibition and displacement formats are applicable to the multiplexed metabolites detection. To our knowledge, this is the first demonstration using SPR/SPRi technique to do multiplexed small-molecule metabolites detection.

6.2 Future Outlook

The development of sensing systems for the measurement of small molecules is an active area of research. A sensor based approach for the measurement of metabolites can potentially provide the simplicity and portability required for widespread use. Rapid detection and quantitation of small-molecule metabolites can potentially emerge as an effective way to link the metabolite profile to disease state. As the development of metabolomics, more and more metabolites are being and will be discovered as biomarkers related to certain diseases and medical conditions. Therefore, sensing strategies and sensors are highly required for the newly discovered metabolites biomarkers, either single or multiple targets. However, a big gap exists between the proof-of-principle sensing strategies and the real-world applications. To fulfill the translational purpose, any developed proof-of-principle strategies and/or assays should be validated in real-world samples before they can be used in clinical settings. To this end, a promising future direction can be the validation of the sensing strategies and/or assays developed in this thesis in real clinical samples such as plasma and urine samples. Another direction could be the combination of the developed assays after validation with compact SPR instrument[1], which enables the development of a point-of-care device for medical diagnostics. Last but not least, some of the sensing strategies developed here

could have value and find applications in pharmaceutical research, food safety control, as well as environmental monitoring.

6.3 References

(1) Charbonneau, D. M.; Breault-Turcot, J.; Sinnett, D.; Krajinovic, M.; Leclerc, J. M.; Masson, J. F.; Pelletier, J. N. *ACS Sens.* **2017**, 2, 1761-1766.

Bibliography/References

Chapter 1:

(1) Wood, R. W. *Philos. Mag.* **1902**, *4*, 396-402.

(2) Wood, R. W. *Philos. Mag.* **1912**, *23*, 310-317.

(3) Pick, H.; Raether, H.; Bennemann, K. H. *Springer Tracts in Modern Physics*, vol. 38; Springer-Verlag, 1965.

(4) Raether, H. *Excitation of Plasmons and Interband Transitions by Electrons*; Springer-Verlag, 1980.

(5) Otto, A. *Z. Phys.* **1968**, *216*, 398-410.

(6) Kretschmann, E.; Raether, H. *Z. Naturforsch., Teil A,* **1968**, *23*, 2135-2136.

(7) Ritchie, R.; Arakawa, E.; Cowan, J.; Hamm, R. *Phys. Rev. Lett.* **1968**, *21*, 1530-1533.

(8) Raether, H. *Surface Plasmons on Smooth and Rough Surfaces and on Gratings*; Springer-Verlag, 1986.

(9) Bruns, R.; Raether, H. *Z. Phys.* **1970**, *237*, 98-106.

(10) Cullen, D. C.; Brown, R. G. W.; Lowe, C. R. *Biosensors* **1987**, *3*, 211-225.

(11) Raether, H. *Thin Solid Films* **1975**, *28*, 119-124.

(12) Nylander, C.; Liedberg, B.; Lind, T. *Sens. Actuators* **1982**, *3*, 79-88.

(13) Liedberg, B.; Nylander, C.; Lundstrom, I. *Sens. Actuators* **1983**, *4*, 299-304.

(14) Flanagan, M. T.; Pantell, R. H. *Electron. Lett.* **1984**, *20*, 968-970.

(15) Zhang, L. M.; Uttamchandani, D. *Electron. Lett.* **1988**, *24*, 1469-1470.

(16) Daniels, P. B.; Deacon, J. K.; Eddowes, M. J.; Pedley, D. G. *Sens. Actuators* **1988**, *15*, 11-18.

(17) Kooyman, R. P. H.; Kolkman, H.; Vangent, J.; Greve, J. *Anal. Chim. Acta* **1988**, *213*, 35-45.

(18) Johnsson, B.; Lofas, S.; Lindquist, G. *Anal. Biochem.* **1991**, *198*, 268-277.

(19) Jonsson, U.; Fagerstam, L.; Ivarsson, B.; Johnsson, B.; Karlsson, R.; Lundh, K.; Lofas, S.; Persson, B.; Roos, H.; Ronnberg, I.; Sjolander, S.; Stenberg, E.; Stahlberg, R.; Urbaniczky, C.; Ostlin, H.; Malmqvist, M. *Biotechniques* **1991**, *11*, 620-627.

(20) Jost, J. P.; Munch, O.; Andersson, T. *Nucleic Acids Res.* **1991**, *19*, 2788-2788.

(21) Lofas, S.; Malmqvist, M.; Ronnberg, I.; Stenberg, E.; Liedberg, B.; Lundstrom, I. *Sens. Actuators, B.* **1991**, *5*, 79-84.

(22) Altschuh, D.; Dubs, M. C.; Weiss, E.; Zederlutz, G.; Vanregenmortel, M. H. V. *Biochemistry* **1992**, *31*, 6298-6304.

(23) Brighamburke, M.; Edwards, J. R.; Oshannessy, D. J. *Anal. Biochem.* **1992**, *205*, 125-131.

(24) Dubs, M. C.; Altschuh, D.; Vanregenmortel, M. H. V. *Immunol. Lett.* **1992**, *31*, 59-64.

(25) Hasegawa, Y.; Okazaki, I.; Endo, T.; Kawasaki, T.; Kobata, A. *Glycoconjugate J.* **1993**, *10*, 283-283.

(26) Terrettaz, S.; Stora, T.; Duschl, C.; Vogel, H. *Langmuir* **1993**, *9*, 1361-1369.

(27) Natsume, T.; Koide, T.; Yokota, S.; Hirayoshi, K.; Nagata, K. *J. Biol. Chem.* **1994**, *269*, 31224-31228.

(28) OConnorMcCourt, M. D.; Segarini, P.; Grothe, S.; Tsang, M. L. S.; Weatherbee, J. A. *Ann. N. Y. Acad. Sci.* **1995**, *766*, 300-302.

(29) Englebienne, P. *Analyst* **1998**, *123*, 1599-1603.

(30) Mayer, M.; Lederer, F.; Le, K. H. D. *J. Inorg. Biochem.* **1999**, *74*, 227-227.

(31) Saenko, E.; Sarafanov, A.; Greco, N.; Shima, M.; Loster, K.; Schwinn, H.; Josic, D. *J. Chromatogr. A* **1999**, *852*, 59-71.

(32) Zakhary, D. R.; Bond, M. *Biophys. J.* **1999**, *76*, 100-100.

(33) Bondeson, K.; Frostellkarlsson, A.; Fagerstam, L.; Magnusson, G. *Anal. Biochem.* **1993**, *214*, 245-251.

(34) Polymenis, M.; Stollar, B. D. *J Immunol.* **1995**, *154*, 2198-2208.

(35) Yang, W. P.; Wu, H.; Barbas, C. F. *J. Immunol. Methods* **1995**, *183*, 175-182.

(36) Seimiya, M.; Kurosawa, Y. *FEBS Lett.* **1996**, *398*, 279-284.

(37) Haruki, M.; Noguchi, E.; Kanaya, S.; Crouch, R. J. *J. Biol. Chem.* **1997**, *272*, 22015-22022.

(38) Hendrix, M.; Priestley, E. S.; Joyce, G. F.; Wong, C. H. *J. Am. Chem. Soc.* **1997**, *119*, 3641-3648.

(39) Vukusic, P. S.; Brown, G. P. B.; Sambles, J. R. *Sensors* **1991**, 145-149.

(40) Ideta, K.; Arakawa, T. *Sens. Actuators, B* **1993**, *13*, 384-386.

(41) Jorgenson, R. C.; Yee, S. S. *Sens. Actuators, B* **1993**, *12*, 213-220.

(42) Stenberg, E.; Persson, B.; Roos, H.; Urbaniczky, C. *J. Colloid Interface Sci.* **1991**, *143*, 513-526.

(43) Oshannessy, D. J.; Odonnell, K. C.; Martin, J.; Brighamburke, M. *Anal. Biochem.* **1995**, *229*, 119-124.

(44) Uda, T.; Hifumi, E.; Kubota, N.; Shimizu, K.; Ogino, K. *Denki Kagaku* **1995**, *63*, 1160-1166.

(45) Kunz, U.; Katerkamp, A.; Reinhard, R.; Spener, F.; Cammann, K. *Sens. Actuators, B* **1996**, *32*, 149-155.

(46) Saito, K.; Yokota, H.; Yanagida, T. *Biophys. J.* **1996**, *70*, 300-300.

(47) Salamon, Z.; Wang, Y.; Soulages, J. L.; Brown, M. F.; Tollin, G. *Biophys. J.* **1996**, *71*, 283-294.

(48) Sigal, G. B.; Bamdad, C.; Barberis, A.; Strominger, J.; Whitesides, G. M. *Anal. Chem.* **1996**, *68*, 490-497.

(49) Sota, H.; Hasegawa, Y.; Iwakura, M. *Anal. Chem.* **1998**, *70*, 2019-2024.

(50) Stockley, P. G.; Baron, A. J.; Wild, C. M.; Parsons, I. D.; Miller, C. M.; Holtham, C. A. M.; Baumberg, S. *Biosens. Bioelectron.* **1998**, *13*, 637-650.

(51) Wink, T.; van Zuilen, S. J.; Bult, A.; van Bennekom, W. P. *Anal. Chem.* **1998**, *70*, 827-832.

(52) Brockman, J. M.; Frutos, A. G.; Corn, R. M. *J. Am. Chem. Soc.* **1999**, *121*, 8044-8051.

(53) Caide, X.; Sui, S. F. *Eur. Biophys. J.* **1999**, *28*, 151-157.

(54) Green, R. J.; Davies, M. C.; Roberts, C. J.; Tendler, S. J. B. *Biomaterials* **1999**, *20*, 385-391.

(55) Rebois, R. V.; VanRyk, D.; Schuck, P. *Faseb J.* **1999**, *13*, 1510-1510.

(56) Schlereth, D. D. *J Electroanal. Chem.* **1999**, *464*, 198-207.

(57) Schwarz, T.; Yeung, D.; Hawkins, E.; Heaney, P.; Mcdougall, A. *Trends Biotechnol.* **1991**, *9*, 339-340.

(58) Devries, E. F. A.; Schasfoort, R. B. M.; Vanderplas, J.; Greve, J. *Biosens. Bioelectron.* **1994**, *9*, 509-514.

(59) Jordan, C. E.; Frutos, A. G.; Thiel, A. J.; Corn, R. M. *Anal. Chem.* **1997**, *69*, 4939-4947.

(60) Peterlinz, K. A.; Georgiadis, R. M.; Herne, T. M.; Tarlov, M. J. *J. Am. Chem. Soc.* **1997**, *119*, 3401-3402.

(61) Thiel, A. J.; Frutos, A. G.; Jordan, C. E.; Corn, R. M.; Smith, L. M. *Anal. Chem.* **1997**, *69*, 4948-4956.

(62) Kuhn, C.; Muller, F.; Melle, C.; Nasheuer, H. P.; Janus, F.; Deppert, W.; Grosse, F. *Oncogene* **1999**, *18*, 769-774.

(63) Kukanskis, K.; Elkind, J.; Melendez, J.; Murphy, T.; Miller, G.; Garner, H. *Anal. Biochem.* **1999**, *274*, 7-17.

(64) Wink, T.; de Beer, J.; Hennink, W. E.; Bult, A.; van Bennekom, W. P. *Anal. Chem.* **1999**, *71*, 801-805.

(65) Davis, T. M.; Wilson, W. D. *Anal. Biochem.* **2000**, *284*, 348-353.

(66) Hall, D. *Handbook of Surface Plasmon Resonance* **2008**, 81-122.

(67) Wilson, W. D. *Science* **2002**, *295*, 2103-2105.

(68) Al Mubarak, Z. H.; Ramesh, R.; Liu, L.; Krishnan, S. *J. Colloid Interface Sci.* **2015**, *460*, 209-213.

(69) Mehand, M. S.; Srinivasan, B.; De Crescenzo, G. *Sci. Rep.* **2015**, *5*.

(70) Myszka, D. G. *Anal. Biochem.* **2004**, *329*, 316-323.

(71) Yakes, B. J.; Kanyuck, K. M.; DeGrasse, S. L. *Anal. Chem.* **2014**, *86*, 9251-9255.

(72) Kennedy, A. E.; Sheffield, K. S.; Eibl, J. K.; Murphy, M. B.; Vohra, R.; Scott, J. A.; Ross, G. M. *J. Biomol. Screening* **2016**, *21*, 96-100.

(73) Munoz, E. M.; Lorenzo-Abalde, S.; Gonzalez-Fernandez, A.; Quintela, O.; Lopez-Rivadulla, M.; Riguera, R. *Biosens. Bioelectron.* **2011**, *26*, 4423-4428.

(74) Nakamoto, K.; Kurita, R.; Sekioka, N.; Niwa, O. *Chem. Lett.* **2008**, *37*, 698-699.

(75) Aizawa, H.; Tozuka, M.; Kurosawa, S.; Kobayashi, K.; Reddy, S. M.; Higuchi, M. *Anal. Chim. Acta* **2007**, *591*, 191-194.

(76) Kawazumi, H.; Gobi, K. V.; Ogino, K.; Maeda, H.; Miura, N. *Sens. Actuators, B* **2005**, *108*, 791-796.

(77) Keegan, J.; O'Kennedy, R.; Crooks, S.; Elliott, C.; Brandon, D.; Danaher, M. *Anal. Chim. Acta* **2011**, *700*, 41-48.

(78) Zuo, X. L.; Xiao, Y.; Plaxco, K. W. *J. Am. Chem. Soc.* **2009**, *131*, 6944-6945.

(79) Sharma, A. K.; Heemstra, J. M. *J. Am. Chem. Soc.* **2011**, *133*, 12426-12429.

(80) Ruscito, A.; DeRosa, M. C. *Front. Chem.* **2016**, *4*, 14.

(81) Yang, K. A.; Barbu, M.; Halim, M.; Pallavi, P.; Kim, B.; Kolpashchikov, D. M.; Pecic, S.; Taylor, S.; Worgall, T. S.; Stojanovic, M. N. *Nat. Chem.* **2014**, *6*, 1003-1008.

(82) Wang, J. L.; Munir, A.; Zhou, H. S. *Talanta* **2009**, *79*, 72-76.

(83) Wang, Q.; Huang, J. H.; Yang, X. H.; Wang, K. M.; He, L. L.; Li, X. P.; Xue, C. Y. *Sens. Actuators, B* **2011**, *156*, 893-898.

(84) Wang, J. L.; Zhou, H. S. *Anal. Chem.* **2008**, *80*, 7174-7178.

(85) Zou, F.; Wu, B. P.; Wang, X. X.; Chen, Y. Y.; Koh, K.; Wang, K. M.; Chen, H. X. *Sens. Actuators, B* **2017**, *241*, 160-167.

(86) Kim, S.; Lee, H. J. *Anal. Chem.* **2017**, *89*, 6624-6630.

(87) Wang, J. L.; Munir, A.; Zhu, Z. Z.; Zhou, H. S. *Anal. Chem.* **2010**, *82*, 6782-6789.

(88) Li, X. M.; Wang, Y.; Wang, L. L.; Wei, Q. L. *Chem. Commun.* **2014**, *50*, 5049-5052.

(89) Law, W. C.; Yong, K. T.; Baev, A.; Prasad, P. N. *ACS Nano* **2011**, *5*, 4858-4864.

(90) Lisi, S.; Scarano, S.; Fedeli, S.; Pascale, E.; Cicchi, S.; Ravelet, C.; Peyrin, E.; Minunni, M. *Biosens. Bioelectron.* **2017**, *93*, 289-292.

(91) Wang, Q.; Li, Q.; Yang, X. H.; Wang, K. M.; Du, S. S.; Zhang, H.; Nie, Y. J. *Biosens. Bioelectron.* **2016**, *77*, 1001-1007.

(92) Lee, E. G.; Park, K. M.; Jeong, J. Y.; Lee, S. H.; Baek, J. E.; Lee, H. W.; Jung, J. K.; Chung, B. H. *Anal. Biochem.* **2011**, *408*, 206-211.

(93) Zagorodko, O.; Spadavecchia, J.; Serrano, A. Y.; Larroulet, I.; Pesquera, A.; Zurutuza, A.; Boukherroub, R.; Szunerits, S. *Anal. Chem.* **2014**, *86*, 11211-11216.

(94) Singh, M.; Holzinger, M.; Tabrizian, M.; Winters, S.; Berner, N. C.; Cosnier, S.; Duesberg, G. S. *J. Am. Chem. Soc.* **2015**, *137*, 2800-2803.

(95) Ghrera, A. S.; Pandey, M. K.; Malhotra, B. D. *Biosens. Bioelectron.* **2016**, *80*, 477-482.

(96) Malic, L.; Sandros, M. G.; Tabrizian, M. *Anal. Chem.* **2011**, *83*, 5222-5229.

(97) Liang, R. P.; Yao, G. H.; Fan, L. X.; Qiu, J. D. *Anal. Chim. Acta* **2012**, *737*, 22-28.

(98) Fenzl, C.; Hirsch, T.; Baeumner, A. J. *Anal. Chem.* **2015**, *87*, 11157-11163.

(99) He, L.; Musick, M. D.; Nicewarner, S. R.; Salinas, F. G.; Benkovic, S. J.; Natan, M. J.; Keating, C. D. *J. Am. Chem. Soc.* **2000**, *122*, 9071-9077.

(100) Zeng, S.; Baillargeat, D.; Ho, H. P.; Yong, K. T. *Chem. Soc. Rev.* **2014**, *43*, 3426-3452.

(101) Hong, X.; Hall, E. A. H. *Analyst* **2012**, *137*, 4712-4719.

(102) Szunerits, S.; Spadavecchia, J.; Boukherroub, R. *Rev. Anal. Chem.* **2014**, *33*, 153-164.

(103) Yang, C. T.; Wu, L.; Bai, P.; Thierry, B. *J. Mater. Chem. C* **2016**, *4*, 9897-9904.

(104) Wang, J. L.; Wang, F.; Zou, X. Q.; Xu, Z. A.; Dong, S. J. *Electrochem. Commun.* **2007**, *9*, 343-347.

(105) Lai, E. P. C.; Fafara, A.; VanderNoot, V. A.; Kono, M.; Polsky, B. *Can. J. Chem.* **1998**, *76*, 265-273.

(106) Haupt, K.; Mosbach, K. *Chem. Rev.* **2000**, *100*, 2495-2504.

(107) Kugimiya, A.; Takeuchi, T. *Biosens. Bioelectron.* **2001**, *16*, 1059-1062.

(108) Matsui, J.; Akamatsu, K.; Hara, N.; Miyoshi, D.; Nawafune, H.; Tamaki, K.; Sugimoto, N. *Anal. Chem.* **2005**, *77*, 4282-4285.

(109) Zheng, R.; Cameron, B. D. *Proc. SPIE* **2010**, *7577*, 75770A.

(110) Xu, X. Y.; Tian, X. G.; Cai, L. G.; Xu, Z. L.; Lei, H. T.; Wang, H.; Sun, Y. M. *Anal. Methods* **2014**, *6*, 3751-3757.

(111) Cenci, L.; Andreetto, E.; Vestri, A.; Bovi, M.; Barozzi, M.; Iacob, E.; Busato, M.; Castagna, A.; Girelli, D.; Bossi, A. M. *J. Nanobiotechnol.* **2015**, *13*, 51.

(112) Gupta, B. D.; Shrivastav, A. M.; Usha, S. P. *Sensors* **2016**, *16*, 1381.

(113) Li, S. P.; Yang, M.; Zhou, W. F.; Johnston, T. G.; Wang, R.; Zhu, J. S. *Appl. Surf. Sci.* **2015**, *355*, 570-576.

(114) Ding, X. J.; Cheng, W.; Li, Y. J.; Wu, J. L.; Li, X. M.; Cheng, Q.; Ding, S. J. *Biosens. Bioelectron.* **2017**, *87*, 345-351.

Chapter 2:

(1) Homola, J. *Chem. Rev.* **2008**, *108*, 462-493.

(2) Long, F.; Zhu, A.; Shi, H. *Sensors* **2013**, *13*, 13928-13948.

(3) Lee, J. R.; Choi, J.; Shultz, T. O.; Wang, S. X. *Anal. Chem.* **2016**, *88*, 7457-7461.

(4) Hilvo, M.; de Santiago, I.; Gopalacharyulu, P.; Schmitt, W. D.; Budczies, J.; Kuhberg, M.; Dietel, M.; Aittokallio, T.; Markowetz, F.; Denkert, C.; Sehouli, J.; Frezza, C.; Darb-Esfahani, S.; Braicu, E. I. *Cancer Res.* **2016**, *76*, 796-804.

(5) Seviour, T.; Doyle, L. E.; Lauw, S. J.; Hinks, J.; Rice, S. A.; Nesatyy, V. J.; Webster, R. D.; Kjelleberg, S.; Marsili, E. *Chem. Commun.* **2015**, *51*, 3789-3792.

(6) Lam, C. W.; Law, C. Y.; Sze, K. H.; To, K. K. *Clin. Chim. Acta* **2015**, *438*, 24-28.

(7) Park, M. H.; Igarashi, K. *Biomol. Ther.* **2013**, *21*, 1-9.

(8) Fernie, A. R.; Trethewey, R. N.; Krotzky, A. J.; Willmitzer, L. *Nat. Rev. Mol. Cell Biol.* **2004**, *5*, 763-769.

(9) Ravanbakhsh, S.; Liu, P.; Bjorndahl, T. C.; Mandal, R.; Grant, J. R.; Wilson, M.; Eisner, R.; Sinelnikov, I.; Hu, X.; Luchinat, C.; Greiner, R.; Wishart, D. S. *PLoS One* **2015**, *10*, e0124219.

(10) Bouatra, S.; Aziat, F.; Mandal, R.; Guo, A. C.; Wilson, M. R.; Knox, C.; Bjorndahl, T. C.; Krishnamurthy, R.; Saleem, F.; Liu, P.; Dame, Z. T.; Poelzer, J.; Huynh, J.; Yallou, F. S.; Psychogios, N.; Dong, E.; Bogumil, R.; Roehring, C.; Wishart, D. S. *PLoS One* **2013**, *8*, e73076.

(11) Psychogios, N.; Hau, D. D.; Peng, J.; Guo, A. C.; Mandal, R.; Bouatra, S.; Sinelnikov, I.; Krishnamurthy, R.; Eisner, R.; Gautam, B.; Young, N.; Xia, J.; Knox, C.; Dong, E.; Huang, P.; Hollander, Z.; Pedersen, T. L.; Smith, S. R.; Bamforth, F.; Greiner, R.; McManus, B.; Newman, J. W.; Goodfriend, T.; Wishart, D. S. *PLoS One* **2011**, *6*, e16957.

(12) Larive, C. K.; Barding, G. A., Jr.; Dinges, M. M. *Anal. Chem.* **2015**, *87*, 133-146.

(13) Chen, D.; Su, X.; Wang, N.; Li, Y.; Yin, H.; Li, L.; Li, L. *Sci. Rep.* **2017**, *7*, 40543.

(14) Zhao, S.; Luo, X.; Li, L. *Anal. Chem.* **2016**, *88*, 10617-10623.

(15) Couture, M.; Zhao, S. S.; Masson, J. F. *Phys. Chem. Chem. Phys.* **2013**, *15*, 11190-11216.

(16) Wu, B.; Jiang, R.; Wang, Q.; Huang, J.; Yang, X.; Wang, K.; Li, W.; Chen, N.; Li, Q. *Chem. Commun.* **2016**, *52*, 3568-3571.

(17) Patra, A.; Ding, T.; Engudar, G.; Wang, Y.; Dykas, M. M.; Liedberg, B.; Kah, J. C.; Venkatesan, T.; Drum, C. L. *Small* **2016**, *12*, 1174-1182.

(18) Bockova, M.; Chadtova Song, X.; Gedeonova, E.; Levova, K.; Kalousova, M.; Zima, T.; Homola, J. *Anal. Bioanal. Chem.* **2016**, *408*, 7265-7269.

(19) Jang, H. R.; Wark, A. W.; Baek, S. H.; Chung, B. H.; Lee, H. J. *Anal. Chem.* **2014**, *86*, 814-819.

(20) Maisonneuve, M.; Valsecchi, C.; Wang, C.; Brolo, A. G.; Meunier, M. *Biosensors & Bioelectronics* **2015**, *63*, 80-85.

(21) Martinez-Perdiguero, J.; Retolaza, A.; Bujanda, L.; Merino, S. *Talanta* **2014**, *119*, 492-497.

(22) Zagorodko, O.; Spadavecchia, J.; Serrano, A. Y.; Larroulet, I.; Pesquera, A.; Zurutuza, A.; Boukherroub, R.; Szunerits, S. *Anal. Chem.* **2014**, *86*, 11211-11216.

(23) Zhou, W. J.; Chen, Y.; Corn, R. M. *Anal. Chem.* **2011**, *83*, 3897-3902.

(24) Scarano, S.; Ermini, M. L.; Spiriti, M. M.; Mascini, M.; Bogani, P.; Minunni, M. *Anal. Chem.* **2011**, *83*, 6245-6253.

(25) He, L.; Musick, M. D.; Nicewarner, S. R.; Salinas, F. G.; Benkovic, S. J.; Natan, M. J.; Keating, C. D. *J. Am. Chem. Soc.* **2000**, *122*, 9071-9077.

(26) Li, S.; Yang, M.; Zhou, W.; Johnston, T. G.; Wang, R.; Zhu, J. *Appl. Surf. Sci.* **2015**, *355*, 570-576.

(27) Liang, W.; Wang, S.; Festa, F.; Wiktor, P.; Wang, W.; Magee, M.; LaBaer, J.; Tao, N. *Anal. Chem.* **2014**, *86*, 9860-9865.

(28) Zeng, S.; Baillargeat, D.; Ho, H. P.; Yong, K. T. *Chem. Soc. Rev.* **2014**, *43*, 3426-3452.

(29) Bolduc, O. R.; Masson, J. F. *Anal. Chem.* **2011**, *83*, 8057-8062.

(30) Jain, P. K.; Huang, X.; El-Sayed, I. H.; El-Sayad, M. A. *Plasmonics* **2007**, *2*, 107-118.

(31) Liang, R. P.; Yao, G. H.; Fan, L. X.; Qiu, J. D. *Anal. Chim. Acta* **2012**, *737*, 22-28.

(32) Wang, J.; Munir, A.; Zhu, Z.; Zhou, H. S. *Anal. Chem.* **2010**, *82*, 6782-6789.

(33) Malic, L.; Sandros, M. G.; Tabrizian, M. *Anal. Chem.* **2011**, *83*, 5222-5229.

(34) Singh, M.; Holzinger, M.; Tabrizian, M.; Winters, S.; Berner, N. C.; Cosnier, S.; Duesberg, G. S. *J. Am. Chem. Soc.* **2015**, *137*, 2800-2803.

(35) Mitchell, J. *Sensors* **2010**, *10*, 7323-7346.

(36) Wang, J.; Zhou, H. S. *Anal. Chem.* **2008**, *80*, 7174-7178.

(37) Yockell-Lelievre, H.; Bukar, N.; McKeating, K. S.; Arnaud, M.; Cosin, P.; Guo, Y.; Dupret-Carruel, J.; Mougin, B.; Masson, J. F. *Analyst* **2015**, *140*, 5105-5111.

(38) Miyashita, M.; Shimada, T.; Miyagawa, H.; Akamatsu, M. *Anal. Bioanal. Chem.* **2005**, *381*, 667-673.

(39) Meneely, J. P.; Sulyok, M.; Baumgartner, S.; Krska, R.; Elliott, C. T. *Talanta* **2010**, *81*, 630-636.

(40) Zhao, S. S.; Bukar, N.; Toulouse, J. L.; Pelechacz, D.; Robitaille, R.; Pelletier, J. N.; Masson, J. F. *Biosens. Bioelectron.* **2015**, *64*, 664-670.

(41) Shankaran, D. R.; Kawaguchi, T.; Kim, S. J.; Matsumoto, K.; Toko, K.; Miura, N. *Anal. Bioanal. Chem.* **2006**, *386*, 1313-1320.

(42) Greenberg, J. A.; Bell, S. J.; Guan, Y.; Yu, Y. H. *Rev. Obstet. Gynecol.* **2011**, *4*, 52-59.

(43) Akbar, S.; Anwar, A.; Kanwal, Q. *Anal. Biochem.* **2016**, *510*, 98-105.

(44) Ren, W.; Fang, Y. X.; Wang, E. K. *ACS Nano* **2011**, *5*, 6425-6433.

(45) Caselunghe, M. B.; Lindeberg, J. *Food Chem.* **2000**, *70*, 523-532.

(46) Lermo, A.; Fabiano, S.; Hernandez, S.; Galve, R.; Marco, M. P.; Alegret, S.; Pividori, M. I. *Biosens. Bioelectron.* **2009**, *24*, 2057-2063.

(47) Mock, J. J.; Hill, R. T.; Degiron, A.; Zauscher, S.; Chilkoti, A.; Smith, D. R. *Nano Lett.* **2008**, *8*, 2245-2252.

(48) Lyon, L. A.; Musick, M. D.; Natan, M. J. *Anal. Chem.* **1998**, *70*, 5177-5183.

(49) Sambrook, J.; Russell, D. W. *Molecular Cloning: A Laboratory Manual*; Cold Spring Harbor Laboratories Press: Cold Spring Harbor, New York, 2001.

(50) Nelson, B. P.; Frutos, A. G.; Brockman, J. M.; Corn, R. M. *Anal. Chem.* **1999**, *71*, 3928-3934.

(51) Kanda, V.; Kariuki, J. K.; Harrison, D. J.; McDermott, M. T. *Anal. Chem.* **2004**, *76*, 7257-7262.

(52) Campbell, I. G.; Jones, T. A.; Foulkes, W. D.; Trowsdale, J. *Cancer Res.* **1991**, *51*, 5329-5338.

(53) Elwood, P. C. *J. Biol. Chem.* **1989**, *264*, 14893-14901.

(54) Sadasivan, E.; Rothenberg, S. P. *J. Biol. Chem.* **1989**, *264*, 5806-5811.

(55) Knecht, S.; Ricklin, D.; Eberle, A. N.; Ernst, B. *J. Mol. Recognit.* **2009**, *22*, 270-279.

(56) Wang, G.; Lipert, R. J.; Jain, M.; Kaur, S.; Chakraboty, S.; Torres, M. P.; Batra, S. K.; Brand, R. E.; Porter, M. D. *Anal. Chem.* **2011**, *83*, 2554-2561.

(57) Stella, B.; Arpicco, S.; Peracchia, M. T.; Desmaele, D.; Hoebeke, J.; Renoir, M.; D'Angelo, J.; Cattel, L.; Couvreur, P. *J. Pharm. Sci.* **2000**, *89*, 1452-1464.

(58) Auld, D. S.; Farmen, M. W.; Kahl, S. D.; Kriauciunas, A.; McKnight, K. L.; Montrose, C.; Weidner, J. R. In *Assay Guidance Manual*, Sittampalam, G. S.; Coussens, N. P.; Brimacombe, K.; Grossman, A.; Arkin, M.; Auld, D.; Austin, C.; Baell, J.; Bejcek, B.; Chung, T. D. Y.; Dahlin, J. L.; Devanaryan, V.; Foley, T. L.; Glicksman, M.; Hall, M. D.; Hass, J. V.; Inglese, J.; Iversen, P. W.; Lal-Nag, M.; Li, Z.; McGee, J.; McManus, O.; Riss, T.; Trask, O. J., Jr.; Weidner, J. R.; Xia, M.; Xu, X., Eds.: Bethesda (MD), 2004; pp 129-154.

(59) McManus, O. B.; Garcia, M. L.; Weaver, D.; Bryant, M.; Titus, S.; Herrington, J. B. In *Assay Guidance Manual*, Sittampalam, G. S.; Coussens, N. P.; Brimacombe, K.; Grossman, A.; Arkin, M.; Auld, D.; Austin, C.; Baell, J.; Bejcek, B.; Chung, T. D. Y.; Dahlin, J. L.; Devanaryan, V.; Foley, T. L.; Glicksman, M.; Hall, M. D.; Hass, J. V.; Inglese, J.; Iversen, P. W.; Lal-Nag, M.; Li, Z.; McGee, J.; McManus, O.; Riss, T.; Trask, O. J., Jr.; Weidner, J. R.; Xia, M.; Xu, X., Eds.: Bethesda (MD), 2004; pp 413-426.

(60) Bee, C.; Abdiche, Y. N.; Stone, D. M.; Collier, S.; Lindquist, K. C.; Pinkerton, A. C.; Pons, J.; Rajpal, A. *PLoS One* **2012**, *7*, e36261.

Chapter 3:

(1) Hilvo, M.; de Santiago, I.; Gopalacharyulu, P.; Schmitt, W. D.; Budczies, J.; Kuhberg, M.; Dietel, M.; Aittokallio, T.; Markowetz, F.; Denkert, C.; Sehouli, J.; Frezza, C.; Darb-Esfahani, S.; Braicu, E. I. *Cancer Res.* **2016**, *76*, 796-804.

(2) Park, M. H.; Igarashi, K. *Biomol. Ther.* **2013**, *21*, 1-9.

(3) Johnson, C. H.; Ivanisevic, J.; Siuzdak, G. *Nat. Rev. Mol. Cell Biol.* **2016**, *17*, 451-459.

(4) Fernie, A. R.; Trethewey, R. N.; Krotzky, A. J.; Willmitzer, L. *Nat. Rev. Mol. Cell Biol.* **2004**. 5, 763-769.

(5) Wishart, D. S.; Mandal, R.; Stanislaus, A.; Ramirez-Gaona, M. *Metabolites* **2016**, *6*, 10.

(6) Wishart, D. S. *Nat. Rev. Drug Discovery* **2016**, *15*, 473-484.

(7) Bouatra, S.; Aziat, F.; Mandal, R.; Guo, A. C.; Wilson, M. R.; Knox, C.; Bjorndahl, T. C.; Krishnamurthy, R.; Saleem, F.; Liu, P.; Dame, Z. T.; Poelzer, J.; Huynh, J.; Yallou, F. S.; Psychogios, N.; Dong, E.; Bogumil, R.; Roehring, C.; Wishart, D. S. *PLoS One* **2013**, *8*, e73076.

(8) Psychogios, N.; Hau, D. D.; Peng, J.; Guo, A. C.; Mandal, R.; Bouatra, S.; Sinelnikov, I.; Krishnamurthy, R.; Eisner, R.; Gautam, B.; Young, N.; Xia, J.; Knox, C.; Dong, E.; Huang, P.; Hollander, Z.; Pedersen, T. L.; Smith, S. R.; Bamforth, F.; Greiner, R.; McManus, B.; Newman, J. W.; Goodfriend, T.; Wishart, D. S. *PLoS One* **2011**, *6*, e16957.

(9) Homola, J. *Chem. Rev.* **2008**, *108*, 462-493.

(10) McKeating, K. S.; Couture, M.; Dinel, M. P.; Garneau-Tsodikova, S.; Masson, J. F. *Analyst* **2016**, 141, 5120-5126.

(11) Zhao, S. S.; Bichelberger, M. A.; Colin, D. Y.; Robitaille, R.; Pelletier, J. N.; Masson, J. F. *Analyst* **2012**, *137*, 4742-4750.

(12) Bockova, M.; Chadtova Song, X.; Gedeonova, E.; Levova, K.; Kalousova, M.; Zima, T.; Homola, J. *Anal. Bioanal. Chem.* **2016**, 408, 7265-7269.

(13) Rebe Raz, S.; Haasnoot, W. *Trends Anal. Chem.* **2011**, *30*, 1526-1537.

(14) Rodriguez-Mozaz, S.; Marco, M. P.; Lopez de Alda, M. J.; Barcelo, D. *Anal. Bioanal. Chem.* **2004**, *378*, 588-598.

(15) Li, M.; Cushing, S. K.; Wu, N. *Analyst* **2015**, *140*, 386-406.

(16) Rosenfeldt, E. J.; Linden, K. G. *Environ. Sci. Technol.* **2004**, *38*, 5476-5483.

(17) Shanle, E. K.; Xu, W. *Chem. Res. Toxicol.* **2011**, *24*, 6-19.

(18) Ryan, K. J. *Cancer Res.* **1982**, *42*, 3342s-3344s.

(19) Stricker, R.; Eberhart, R.; Chevailler, M. C.; Quinn, F. A.; Bischof, P.; Stricker, R. *Clin. Chem. Lab. Med.* **2006**, *44*, 883-887.

(20) Han, Q.; Shen, X.; Zhu, W.; Zhu, C.; Zhou, X.; Jiang, H. *Biosens. Bioelectron.* **2016**, *79*, 180-186.

(21) Zhu, B.; Alsager, O. A.; Kumar, S.; Hodgkiss, J. M.; Travas-Sejdic, J. *Biosens. Bioelectron.* **2015**, *70*, 398-403.

(22) Kanso, H.; Inguimbert, N.; Barthelmebs, L.; Istamboulie, G.; Thomas, F.; Calas-Blanchard, C.; Noguer, T. *Chem. Commun.* **2014**, *50*, 1658-1661.

(23) Alsager, O. A.; Kumar, S.; Zhu, B.; Travas-Sejdic, J.; McNatty, K. P.; Hodgkiss, J. M. *Anal. Chem.* **2015**, *87*, 4201-4209.

(24) Liu, J.; Bai, W.; Niu, S.; Zhu, C.; Yang, S.; Chen, A. *Sci. Rep.* **2014**, *4*, 7571.

(25) Du, L.; Ji, W.; Zhang, Y.; Zhang, C.; Liu, G.; Wang, S. *Analyst* **2015**, *140*, 2001-2007.

(26) Nelson, B. P.; Frutos, A. G.; Brockman, J. M.; Corn, R. M. *Anal. Chem.* **1999**, *71*, 3928-3934.

(27) Kanda, V.; Kariuki, J. K.; Harrison, D. J.; McDermott, M. T. *Anal. Chem.* **2004**, *76*, 7257-7262.

(28) Bain, C. D.; Troughton, E. B.; Tao, Y. T.; Evall, J.; Whitesides, G. M.; Nuzzo, R. G. *J. Am. Chem. Soc.* **1989**, *111*, 321-335.

(29) Jadzinsky, P. D.; Calero, G.; Ackerson, C. J.; Bushnell, D. A.; Kornberg, R. D. *Science* **2007**, *318*, 430-433.

(30) Lee, J. W.; Sim, S. J.; Cho, S. M.; Lee, J. *Biosens. Bioelectron.* **2005**, *20*, 1422-1427.

(31) Ostuni, E.; Yan, L.; Whitesides, G. M. *Colloids Surf., B* **1999**, *15*, 3-30.

(32) Rhoden, J. J.; Dyas, G. L.; Wroblewski, V. J. *J. Biol. Chem.* **2016**, *291*, 11337-11347.

(33) Lamminmaki, U.; Westerlund-Karlsson, A.; Toivola, M.; Saviranta, P. *Protein Sci.* **2003**, *12*, 2549-2558.

(34) Monnet, C.; Bettsworth, F.; Stura, E. A.; Le Du, M. H.; Menez, R.; Derrien, L.; Zinn-Justin, S.; Gilquin, B.; Sibai, G.; Battail-Poirot, N.; Jolivet, M.; Menez, A.; Arnaud, M.; Ducancel, F.; Charbonnier, J. B. *J. Mol. Biol.* **2002**, *315*, 699-712.

(35) Auld, D. S.; Farmen, M. W.; Kahl, S. D.; Kriauciunas, A.; McKnight, K. L.; Montrose, C.; Weidner, J. R. In *Assay Guidance Manual*, Sittampalam, G. S.; Coussens, N. P.; Brimacombe, K.; Grossman, A.; Arkin, M.; Auld, D.; Austin, C.; Baell, J.; Bejcek, B.; Chung, T. D. Y.; Dahlin, J. L.; Devanaryan, V.; Foley, T. L.; Glicksman, M.; Hall, M.

D.; Hass, J. V.; Inglese, J.; Iversen, P. W.; Lal-Nag, M.; Li, Z.; McGee, J.; McManus, O.; Riss, T.; Trask, O. J., Jr.; Weidner, J. R.; Xia, M.; Xu, X., Eds.: Bethesda (MD), 2004; pp 129-154.

Chapter 4:

(1) Hilvo, M.; de Santiago, I.; Gopalacharyulu, P.; Schmitt, W. D.; Budczies, J.; Kuhberg, M.; Dietel, M.; Aittokallio, T.; Markowetz, F.; Denkert, C.; Sehouli, J.; Frezza, C.; Darb-Esfahani, S.; Braicu, E. I. *Cancer Res.* **2016**, *76*, 796-804.

(2) Park, M. H.; Igarashi, K. *Biomol. Ther.* **2013**, *21*, 1-9.

(3) Wang, P. C.; Kuchel, O.; Buu, N. T.; Genest, J. *J. Neurochem.* **1983**, *40*, 1435-1440.

(4) Cohen, J. Y. *Science* **2015**, *350*, 47-48.

(5) Meek, S.; Thomson, A. J.; Sutherland, L.; Sharp, M. G.; Thomson, J.; Bishop, V.; Meddle, S. L.; Gloaguen, Y.; Weidt, S.; Singh-Dolt, K.; Buehr, M.; Brown, H. K.; Gill, A. C.; Burdon, T. *Sci. Rep.* **2016**, *6*, 25592.

(6) Homola, J. *Chem. Rev.* **2008**, *108*, 462-493.

(7) McKeating, K. S.; Aube, A.; Masson, J. F. *Analyst* **2016**, *141*, 429-449.

(8) Zhao, S. S.; Bukar, N.; Toulouse, J. L.; Pelechacz, D.; Robitaille, R.; Pelletier, J. N.; Masson, J. F. *Biosens. Bioelectron.* **2015**, *64*, 664-670.

(9) Bockova, M.; Chadtova Song, X.; Gedeonova, E.; Levova, K.; Kalousova, M.; Zima, T.; Homola, J. *Anal. Bioanal. Chem.* **2016**, *408*, 7265-7269.

(10) Rebe Raz, S.; Haasnoot, W. *Trends Anal. Chem.* **2011**, *30*, 1526-1537.

(11) Rodriguez-Mozaz, S.; Marco, M. P.; Lopez de Alda, M. J.; Barcelo, D. *Anal. Bioanal. Chem.* **2004**, *378*, 588-598.

(12) Li, M.; Cushing, S. K.; Wu, N. *Analyst* **2015**, *140*, 386-406.

(13) Maisonneuve, M.; Valsecchi, C.; Wang, C.; Brolo, A. G.; Meunier, M. *Biosens. Bioelectron.* **2015**, *63*, 80-85.

(14) Martinez-Perdiguero, J.; Retolaza, A.; Bujanda, L.; Merino, S. *Talanta* **2014**, *119*, 492-497.

(15) Jang, H. R.; Wark, A. W.; Baek, S. H.; Chung, B. H.; Lee, H. J. *Anal. Chem.* **2014**, *86*, 814-819.

(16) Mousavi, M. Z.; Chen, H. Y.; Lee, K. L.; Lin, H.; Chen, H. H.; Lin, Y. F.; Wong, C. S.; Li, H. F.; Wei, P. K.; Cheng, J. Y. *Analyst* **2015**, *140*, 4097-4104.

(17) Li, S.; Yang, M.; Zhou, W.; Johnston, T. G.; Wang, R.; Zhu, J. *Appl. Surf. Sci.* **2015**, *355*, 570-576.

(18) Liang, W.; Wang, S.; Festa, F.; Wiktor, P.; Wang, W.; Magee, M.; LaBaer, J.; Tao, N. *Anal. Chem.* **2014**, *86*, 9860-9865.

(19) Zeng, S.; Baillargeat, D.; Ho, H. P.; Yong, K. T. *Chem. Soc. Rev.* **2014**, *43*, 3426-3452.

(20) Bolduc, O. R.; Masson, J. F. *Anal. Chem.* **2011**, *83*, 8057-8062.

(21) Wu, B.; Jiang, R.; Wang, Q.; Huang, J.; Yang, X.; Wang, K.; Li, W.; Chen, N.; Li, Q. *Chem. Commun.* **2016**, *52*, 3568-3571.

(22) He, L.; Musick, M. D.; Nicewarner, S. R.; Salinas, F. G.; Benkovic, S. J.; Natan, M. J.; Keating, C. D. *J. Am. Chem. Soc.* **2000**, *122*, 9071-9077.

(23) Jain, P. K.; Huang, X.; El-Sayed, I. H.; El-Sayad, M. A. *Plasmonics* **2007**, *2*, 107-118.

(24) Wang, J. L.; Munir, A.; Zhu, Z. Z.; Zhou, H. S. *Anal. Chem.* **2010**, *82*, 6782-6789.

(25) Malic, L.; Sandros, M. G.; Tabrizian, M. *Anal. Chem.* **2011**, *83*, 5222-5229.

(26) Singh, M.; Holzinger, M.; Tabrizian, M.; Winters, S.; Berner, N. C.; Cosnier, S.; Duesberg, G. S. *J. Am. Chem. Soc.* **2015**, *137*, 2800-2803.

(27) Zagorodko, O.; Spadavecchia, J.; Serrano, A. Y.; Larroulet, I.; Pesquera, A.; Zurutuza, A.; Boukherroub, R.; Szunerits, S. *Anal. Chem.* **2014**, *86*, 11211-11216.

(28) Walsh, R.; DeRosa, M. C. *Biochem. Biophys. Res. Commun.* **2009**, *388*, 732-735.

(29) Mannironi, C.; Di Nardo, A.; Fruscoloni, P.; Tocchini-Valentini, G. P. *Biochemistry* **1997**, *36*, 9726-9734.

(30) Wood, J. B.; Szyndler, M. W.; Halpern, A. R.; Cho, K.; Corn, R. M. *Langmuir* **2013**, *29*, 10868-10873.

(31) Kanda, V.; Kariuki, J. K.; Harrison, D. J.; McDermott, M. T. *Anal. Chem.* **2004**, *76*, 7257-7262.

(32) Nelson, B. P.; Frutos, A. G.; Brockman, J. M.; Corn, R. M. *Anal. Chem.* **1999**, *71*, 3928-3934.

(33) Bain, C. D.; Troughton, E. B.; Tao, Y. T.; Evall, J.; Whitesides, G. M.; Nuzzo, R. G. *J. Am. Chem. Soc.* **1989**, *111*, 321-335.

(34) Jadzinsky, P. D.; Calero, G.; Ackerson, C. J.; Bushnell, D. A.; Kornberg, R. D. *Science* **2007**, *318*, 430-433.

(35) Cutler, J. I.; Auyeung, E.; Mirkin, C. A. *J. Am. Chem. Soc.* **2012**, *134*, 1376-1391.

(36) Rosi, N. L.; Giljohann, D. A.; Thaxton, C. S.; Lytton-Jean, A. K. R.; Han, M. S.; Mirkin, C. A. *Science* **2006**, *312*, 1027-1030.

(37) Liu, Y.; Ai, K.; Lu, L. *Chem. Rev.* **2014**, *114*, 5057-5115.

(38) Loget, G.; Wood, J. B.; Cho, K.; Halpern, A. R.; Corn, R. M. *Anal. Chem.* **2013**, *85*, 9991-9995.

(39) Lytton-Jean, A. K. R.; Mirkin, C. A. *J. Am. Chem. Soc.* **2005**, *127*, 12754-12755.

(40) Randeria, P. S.; Jones, M. R.; Kohlstedt, K. L.; Banga, R. J.; Olvera de la Cruz, M.; Schatz, G. C.; Mirkin, C. A. *J. Am. Chem. Soc.* **2015**, *137*, 3486-3489.

(41) Youdim, M. B.; Edmondson, D.; Tipton, K. F. *Nat. Rev. Neurosci.* **2006**, *7*, 295-309.

(42) Weinshenker, D. *Nat. Med.* **2010**, *16*, 969-970.

Chapter 5:

(1) Donia, M. S.; Fischbach, M. A. *Science* **2015**, *349*, 1254766.

(2) Li, X. J.; Hu, B. Y.; Jones, S. A.; Zhang, Y. S.; Lavaute, T.; Du, Z. W.; Zhang, S. C. *Stem Cells* **2008**, *26*, 886-893.

(3) Akki, S. U.; Werth, C. J.; Silverman, S. K. *Environ. Sci. Technol.* **2015**, *49*, 9905-9913.

(4) Guan, Y.; Shan, X.; Zhang, F.; Wang, S.; Chen, H. Y.; Tao, N. *Sci. Adv.* **2015**, *1*, e1500633.

(5) McKeating, K. S.; Aube, A.; Masson, J. F. *Analyst* **2016**, *141*, 429-449.

(6) Johnson, C. H.; Ivanisevic, J.; Siuzdak, G. *Nat. Rev. Mol. Cell Biol.* **2016**, *17*, 451-459.

(7) Larive, C. K.; Barding, G. A.; Dinges, M. M. *Anal. Chem.* **2015**, *87*, 133-146.

(8) Clendinen, C. S.; Pasquel, C.; Ajredini, R.; Edison, A. S. *Anal. Chem.* **2015**, *87*, 5698-5706.

(9) Guennec, A. L.; Giraudeau, P.; Caldarelli, S. *Anal. Chem.* **2014**, *86*, 5946-5954.

(10) Huan, T.; Troyer, D. A.; Li, L. *Sci. Rep.* **2016**, *6*, 32272.

(11) Nelson, B. P.; Frutos, A. G.; Brockman, J. M.; Corn, R. M. *Anal. Chem.* **1999**, *71*, 3928-3934.

(12) Spoto, G.; Minunni, M. *J. Phys. Chem. Lett.* **2012**, *3*, 2682-2691.

(13) Homola, J. *Chem. Rev.* **2008**, *108*, 462-493.

(14) Chen, Y.; Nakamoto, K.; Niwa, O.; Corn, R. M. *Langmuir* **2012**, *28*, 8281-8285.

(15) Maisonneuve, M.; Valsecchi, C.; Wang, C.; Brolo, A. G.; Meunier, M. *Biosens. Bioelectron.* **2015**, *63*, 80-85.

(16) Wu, B.; Jiang, R.; Wang, Q.; Huang, J.; Yang, X.; Wang, K.; Li, W.; Chen, N.; Li, Q. *Chem. Commun.* **2016**, *52*, 3568-3571.

(17) Li, X. M.; Wang, Y.; Wang, L. L.; Wei, Q. L. *Chem. Commun.* **2014**, *50*, 5049-5052.

(18) Wang, J.; Zhou, H. S. *Anal. Chem.* **2008**, *80*, 7174-7178.

(19) Zhao, S. S.; Bichelberger, M. A.; Colin, D. Y.; Robitaille, R.; Pelletier, J. N.; Masson, J. F. *Analyst* **2012**, *137*, 4742-4750.

(20) Hergenrother, P. J.; Depew, K. M.; Schreiber, S. L. *J. Am. Chem. Soc.* **2000**, *122*, 7849-7850.

(21) MacBeath, G.; Koehler, A. N.; Schreiber, S. L. *J. Am. Chem. Soc.* **1999**, *121*, 7967-7968.

(22) Kuruvilla, F. G.; Shamji, A. F.; Sternson, S. M.; Hergenrother, P. J.; Schreiber, S. L. *Nature* **2002**, *416*, 653-657.

(23) Winssinger, N.; Ficarro, S.; Schultz, P. G.; Harris, J. L. *Proc. Natl. Acad. Sci. U. S. A.* **2002**, *99*, 11139-11144.

(24) Bradner, J. E.; McPherson, O. M.; Koehler, A. N. *Nat. Protoc.* **2006**, *1*, 2344-2352.

(25) Bain, C. D.; Troughton, E. B.; Tao, Y. T.; Evall, J.; Whitesides, G. M.; Nuzzo, R. G. *J. Am. Chem. Soc.* **1989**, *111*, 321-335.

(26) Lim, C. Y.; Owens, N. A.; Wampler, R. D.; Ying, Y.; Granger, J. H.; Porter, M. D.; Takahashi, M.; Shimazu, K. *Langmuir* **2014**, *30*, 12868-12878.

(27) Frederix, F.; Bonroy, K.; Laureyn, W.; Reekmans, G.; Campitelli, A.; Dehaen, W.; Maes, G. *Langmuir* **2003**, *19*, 4351-4357.

(28) Wishart, D. S.; Jewison, T.; Guo, A. C.; Wilson, M.; Knox, C.; Liu, Y. F.; Djoumbou, Y.; Mandal, R.; Aziat, F.; Dong, E.; Bouatra, S.; Sinelnikov, I.; Arndt, D.; Xia, J. G.; Liu, P.; Yallou, F.; Bjorndahl, T.; Perez-Pineiro, R.; Eisner, R.; Allen, F.; Neveu, V.; Greiner, R.; Scalbert, A. *Nucleic Acids Res.* **2013**, *41*, D801-D807.

Chapter 6:

(1) Charbonneau, D. M.; Breault-Turcot, J.; Sinnett, D.; Krajinovic, M.; Leclerc, J. M.; Masson, J. F.; Pelletier, J. N. *ACS Sens.* **2017**, 2, 1761-1766.